DIAGNOSTIC VALUE OF DYNAMIC ULTRASOUND IN SUPINATION-EXTERNAL ROTATION INJURIES

DISSERTATION

Presented to the Graduate Council of the

Graduate School of Biomedical Sciences

University of North Texas

Health Science Center at Fort Worth

In Partial Fulfillment of the Requirements

For the Degree of

DOCTOR OF PHILOSOPHY

By

Cara L. Fisher, B.S., M.S.

Fort Worth, Texas

July 2018

Fisher, Cara L., Diagnostic Value of Dynamic Ultrasound Evaluation of Supination-External Rotation Ankle Injuries. Doctor of Philosophy (Biomedical Sciences), July, 2018, 157pp., 8 tables, 70 figures, references, 78 titles

Ankle syndesmosis injuries are common and range in severity from subclinical to grossly unstable. Definitive diagnosis of these injuries can be made with plain film radiographs if the injury is severe enough, but often is missed when severity or image quality is low. Computed tomography (CT) and magnetic resonance imaging (MRI) can provide early definitive diagnosis regardless of severity, but are costly and introduce the patient to radiation when CT is used. Ultrasound diagnosis may circumvent many of these disadvantages by being inexpensive, efficient, and able to detect subtle injuries without radiation exposure. This study evaluates the ability of ultrasound to detect subtle supination-external rotation (SER) ankle syndesmosis injuries with a dynamic external rotational stress test.

Nine all male fresh frozen specimens were secured to an ankle rig and stress tested to 10 Nm of external rotational torque with ultrasound monitoring at the tibiofibular clear space. The ankles were subjected to syndesmosis ligament sectioning and repeat stress measurements of the tibiofibular clear space at peak torque. Stress tests and measurements were repeated three times and averaged. Data was analyzed using a two-way repeated measures ANOVA.

Ankle Phases Examined:

1. Normal (baseline)

2. 75% of anterior inferior tibiofibular ligament (AITFL) cut

3. 100% of AITFL cut

4. Fibula fracture (Fx) - cut 8 cm proximal to lateral malleolus

5. 75% posterior inferior tibiofibular ligament (PITFL) cut

6. 100% PITFL cut

Dynamic external rotation stress evaluation using ultrasound was able to detect a significant difference between the uninjured ankle tibiofibular clear space of 4.5 mm and the injured ankle with 100% of anterior inferior tibiofibular ligament cut 6.0 mm. Additionally, this method was able to detect significant differences between the uninjured ankle and the injured states. Dynamic external rotational stress evaluation using ultrasound was able to detect stage 1 Lauge-Hansen SER injuries with statistical significance and corroborates criteria for diagnosing a syndesmosis injury at ≥ 6.0 mm of tibiofibular clear space widening.

TABLE OF CONTENTS

LIST OF TABLES

LIST OF FIGURES

APPENDIX FIGURES

CHAPTER 1

INTRODUCTION

This chapter provides a brief description of the background to the problem under investigation, followed by a discussion on the focus of the research. Finally, the aim and hypothesis are presented.

1.1 Background Description

While the tibiofibular syndesmosis is an extremely strong articulation, injury can occur if the talus is externally rotated within the mortise. This external rotation forces the talus to rotate laterally, which pushes the fibula away from the tibia causing the bones to separate (diastasis), thus increasing the tibiofibular clear space. This injury is referred to as an ankle syndesmosis injury or high ankle sprain. In addition to ligament damage, fracturing of the fibula proximal to the syndesmosis ligaments may also occur if the external rotational force continues.[1] Physicians rely upon imaging and stress examination to properly diagnose and treat syndesmotic injuries. Failure to diagnose a syndesmotic injury does occur and can lead to longer recovery times, early osteoarthritis, and poor outcomes.[1,2] Post-traumatic arthritis is the most common type of arthritis at the talocrural joint.[3]

Even with prompt diagnosis and treatment the time to return to full function can range from four weeks in minor injuries to several months with more severe injuries. Delaying this process only adds to the already long recovery time of typical ankle injuries.

1.2 Research Focus

This research focuses on the diagnosis of the Lauge-Hansen supination-external rotation (SER) syndesmotic injury pattern predictions. The Lauge-Hansen classification system provides stages for different types of ankle injuries based on the mechanism of injury (Table 1.1). An external rotational stress test in an in vitro model utilizing fresh frozen specimens was done to evaluate the tibiofibular clear space, the space between the tibia and fibula, 1cm proximal to the tibial plafond at the level of the anterior inferior tibiofibular ligament (AITFL). This was done via ultrasound and fluoroscopy as an examiner applied an external rotational torque to the ankle at pre-injury and incremental levels of ligament damage at each stage of an SER ankle injury. This comparative data can allow physicians to choose the appropriate imaging based upon the severity of injury and clinical suspicion thereby increasing the positive predictive value of the tests and decreasing missed diagnosis and malreductions (failure to return structures to anatomical position).

Table 1.1. Lauge-Hansen Stages and Injury Patterns.

Stage 1	Anterior inferior tibiofibular ligament (AITFL) injury
Stage 2	Fibula fracture (Fx)
Stage 3	Posterior inferior tibiofibular ligament (PITFL) injury or posterior malleolar Fx
Stage 4	Deltoid ligament injury or medial malleolar Fx

1.3 Aim and Hypothesis

The central hypothesis of the proposed work is that dynamic ultrasound is superior to fluoroscopy evaluation at subtle stage 1-2 injuries and equivalent to fluoroscopy evaluation with detecting unstable syndesmotic injuries of stage 3-4 (Table 1.1). Specific Aim 1: Determine the minimum level of syndesmotic injury detectable by dynamic ultrasound examination of the tibiofibular clear space. Hypothesis: Dynamic ultrasound evaluation can detect all stages of SER injury. Specific Aim 2: Determine the minimum level of syndesmotic injury detectable by stress fluoroscopy examination of the tibiofibular clear space. Hypothesis: Stress fluoroscopy maintains diagnostic fidelity at SER injury stage 2 and above.

CHAPTER 2

ANATOMY REVIEW

This chapter covers anatomical terminology, movements, and anatomy of the leg, ankle, and foot. A review of the motions, planes, and axes of the ankle and foot will be discussed first, followed by a thorough description anatomy of the leg, including the tibiofibular joints. This is followed by a description of the ankle joint and ligaments. Lastly, the anatomy of the foot and its joints are presented.

2.1 Motion of the Ankle and Foot

The purpose of the muscles of the leg and foot is to pull on their bony attachments to produce different movements. A thorough description of these movements is essential for understanding their function. Descriptions of motion in the ankle and foot are based upon the body when it is in anatomical position. Anatomical position refers to a person standing erect, facing forward, feet close together pointing anteriorly, and arms at the side with palms facing forward as well (Figure 2.1). This gives a standard reference point for movements and directional descriptions. From this description, one can then divide the body into different axes and planes (Figures 2.2 and 2.3). The median plane is a longitudinal plane that divides the body into equal right and left halves, and as such, there is only one median plane. A sagittal plane is similar to

the median plane in that it is longitudinal, but it divides the body into unequal right and left parts. The coronal plane is a vertical plane that divides the body into anterior and posterior parts and the transverse plane is a horizontal plane that divides the body into superior and inferior parts. There are unlimited sagittal, coronal, and transverse planes. Typically, these planes occur around cardinal axes.[4] The axes of the ankle (talocrural) and foot joints are complicated because they do not follow traditional planes and axes of movement. Commonly, the joint axes are oblique and cross sagittal, transverse, and coronal planes.[4] The cardinal axes for motions of the ankle/foot complex are coronal, vertical, and longitudinal. The coronal axis passes through from lateral to medial through the talocrural joint and the movements of dorsiflexion/plantarflexion occur around this axis in a sagittal plane (Figure 2.4). The movement of dorsiflexion brings the toes superiorly and depresses the heel, decreasing the angle between the leg and the dorsum of the foot. During dorsiflexion, the wide part of the wedge-shaped talus slides between the two malleoli. In order to accommodate the widened portion, the fibula moves proximally (superiorly), translates posterolaterally, and externally rotates. External rotation of the foot causes medial translation, posterior displacement, and external rotation of the fibula through the syndesmosis.[1] The limiting factor to the amount of dorsiflexion possible is soft tissue restraint, namely the muscles of the posterior compartment of the leg. Plantarflexion, a very strong movement necessary for heel and toe off, points the toes towards the floor and raises the heel, increasing the angle between the leg and the dorsum of the foot. During plantarflexion, the fibula moves distally (inferiorly), translates anteromedially, and internally rotates.[1] Limiting factors to plantarflexion are also soft tissue related, being the muscles of the anterior compartment of the leg.

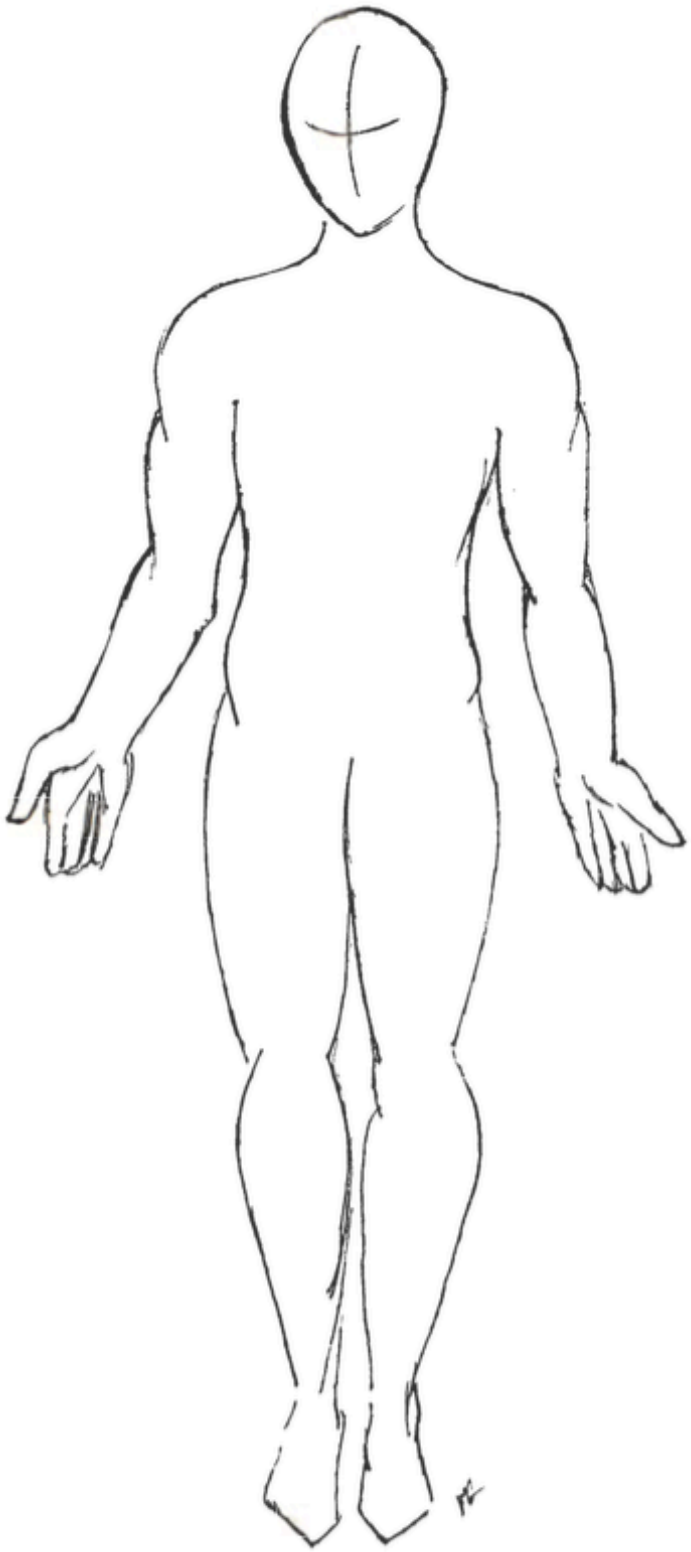

Figure 2.1. Anatomical position. (Drawing credit: Vaughna Galvin)

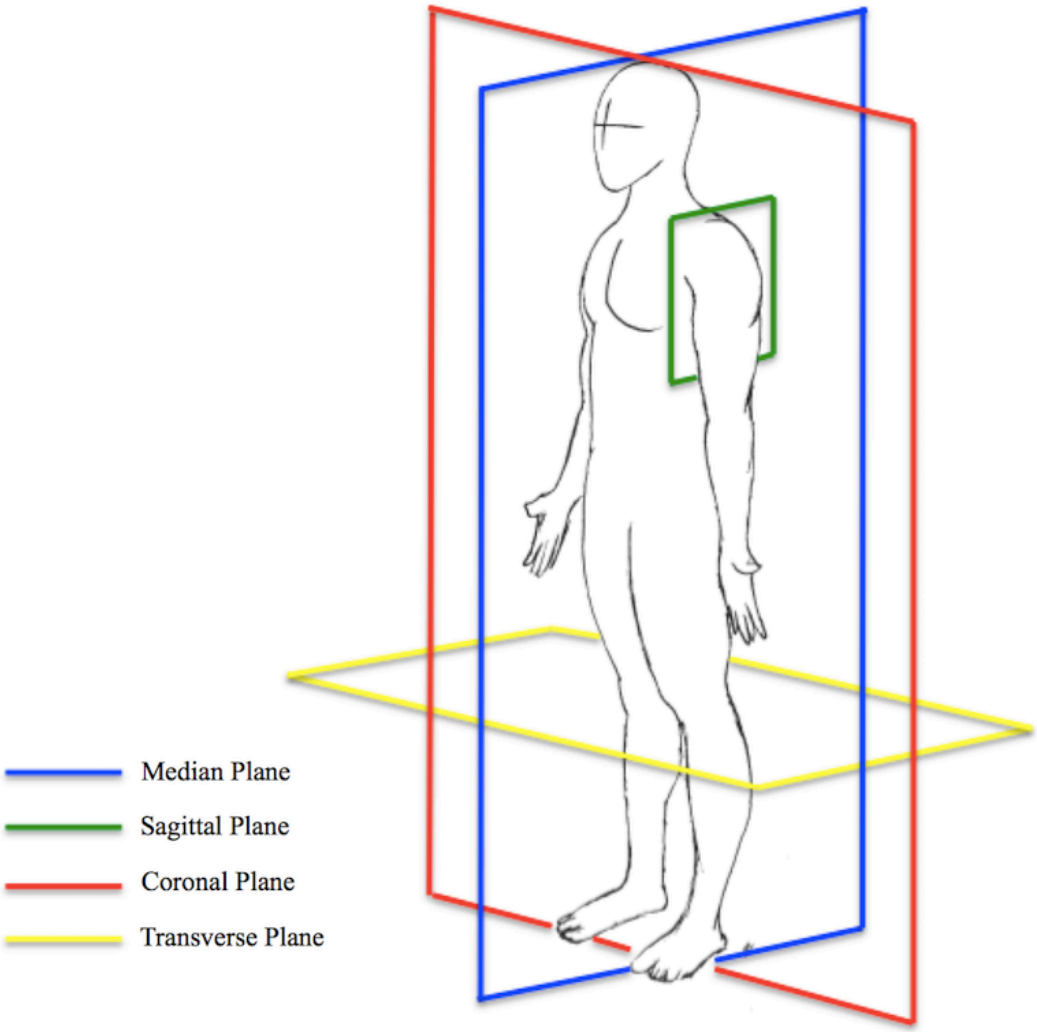

Figure 2.2. Lateral view of the body showing anatomical planes. (Drawing credit: Vaughna Galvin)

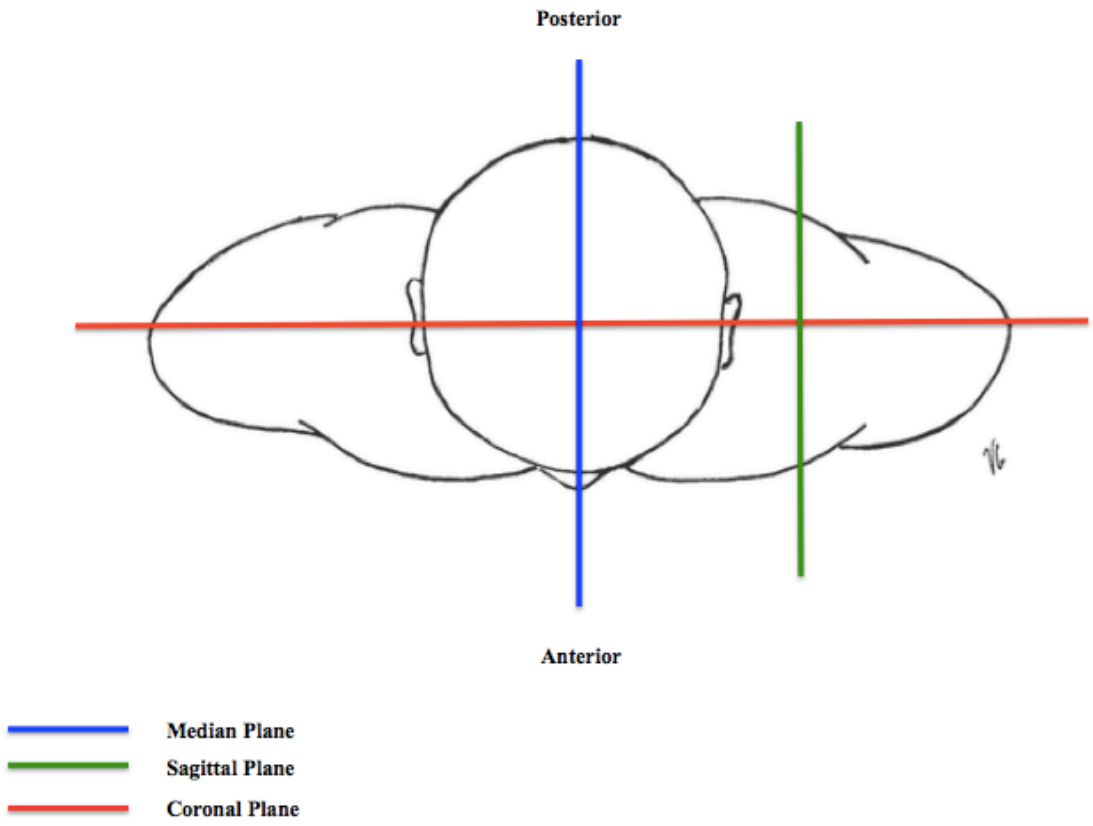

Figure 2.3. Superior view showing anatomical planes. (Drawing credit: Vaughna Galvin)

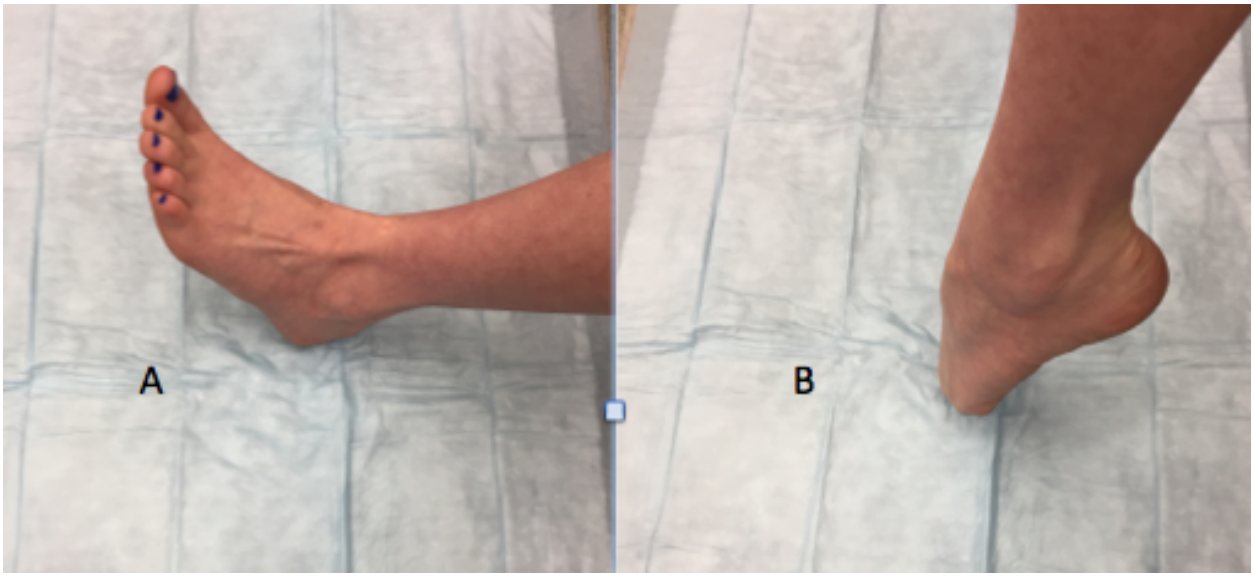

Figure 2.4. A - dorsiflexion. B - plantarflexion. (Photo credit: Cara Fisher)

The vertical axis of the ankle/foot complex passes from superior to inferior through the tibia, talus, and calcaneus. The motions of abduction/adduction occur here. Abduction moves a structure away from the midline of the body, while adduction brings structures closer to the midline. These movements occur in the coronal plane. The longitudinal axis passes from anterior to posterior through the length of the foot and the motions of inversion/eversion (Figure 2.5) occur around this axis in a transverse plane. Inversion and eversion occur at the subtalar and transverse tarsal joints simultaneously. Inversion brings the plantar aspect (sole) of the foot medially and eversion brings it laterally. Inversion and eversion are sometimes referred to as supination and pronation respectively, but these movements are more complex and, in reality, are combinations of two movements. Pronation is the combination of abduction and eversion and supination of adduction and inversion.[5] The subtalar axis is obliquely oriented between longitudinal and vertical axes. This means that the movements of pronation/supination are about equal combinations of eversion/inversion and abduction/adduction.

Internal and external rotation, otherwise known as medial and lateral rotation, refers to bringing a structure either closer to or further away from the midline using a rotary movement. Individual bones may rotate, as may entire structures.

Commonly, the fibula, talus, and calcaneus will rotate to create the complex movements needed for ambulation at the talocrural and foot joints. Varus and valgus are also used to describe motions occurring at the ankle/foot complex. Context is important when using these terms, as they can also be used to describe clinical presentations. Generally, they are used to describe a decrease or increase of the medial angle between two bones. Valgus refers to an increase in the medial angle, and varus refers to a decrease in the medial angle.

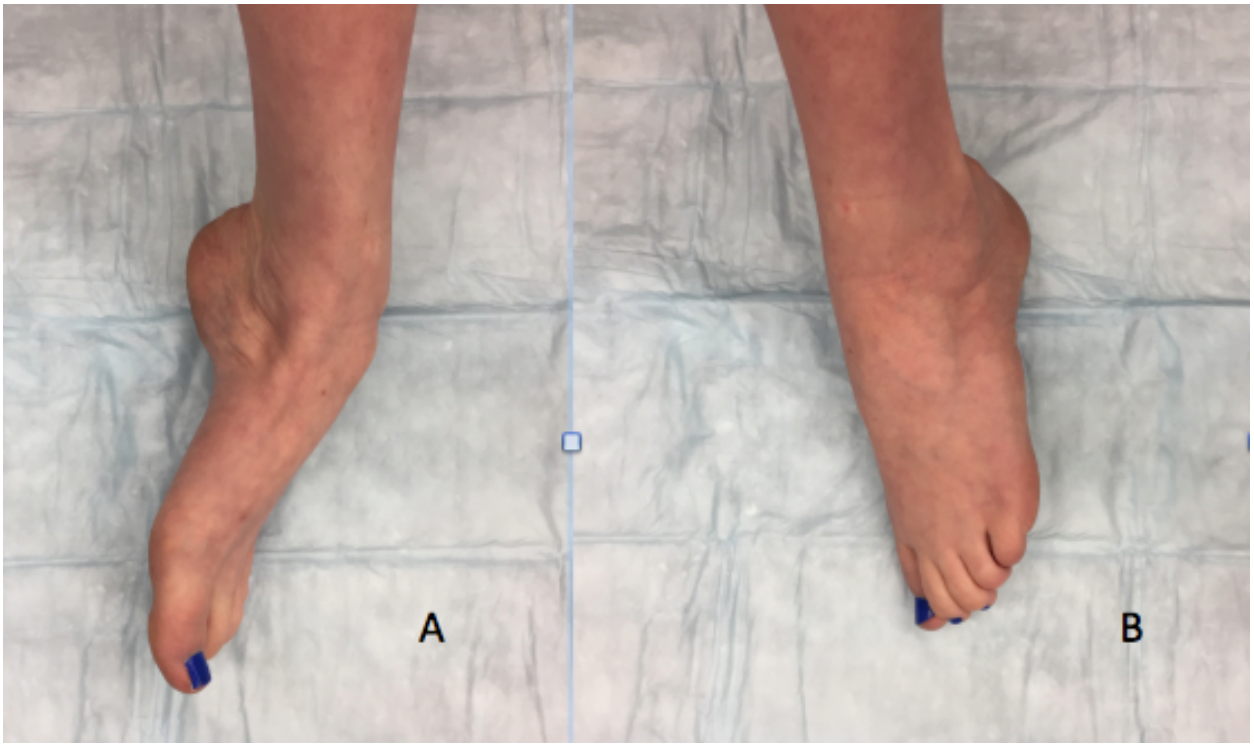

Figure 2.5. A - inversion. B - eversion. (Photo credit: Cara Fisher)

2.2 Leg Anatomy Overview

In order to understand all the structures that cross or interact with the ankle/foot complex, it is important to cover the anatomy of the leg and foot. Most muscles found in the leg will cross the talocrural and other joints as they pass to their attachment points in the foot. Arteries and nerves in the leg will also cross these joints, providing articular branches as they go. Because the joints of the body function as a chain, problems with the foot or ankle will translate to problems further up the chain like the knee, hip, or spine. Therefore, thorough coverage of the anatomy is essential.

The leg is the area of the lower extremity that lies between the knee and the talocrural joint. The leg includes most of the tibia and fibula. Deep to the superficial fascia, the muscles of the leg are wrapped in deep fascia called crural fascia (crus means leg). The crural fascia limits the amount of outward expansion the muscles can do when contracting, which allows them to be more efficient at compressing vasculature and assisting with venous return to the heart. Proximally, the crural fascia is continuous with the fascia lata of the thigh and distally it forms the superior and inferior extensor retinacula above and below the talocrural joint, the flexor retinaculum on the medial aspect of the talocrural joint, and the superior and inferior fibular retinacula on the lateral aspect of the talocrural joint. When crural fascia contacts bone, in areas around the knee, tibia (shin), and ankle, it becomes continuous with the periosteum. This fascia is thick proximally and helps provide attachment points for some of the muscles of the leg. The leg is divided into three compartments by the tibia, fibula, interosseous membrane, and the anterior and posterior intermuscular septa, which are deep extensions of the crural fascia. These septa extend towards the bone and attach to the tibia and fibula forming the anterior, lateral, and posterior compartments. The posterior compartment is further divided into superficial and deep

subcompartments by the transverse intermuscular septum, a deep extension of the crural fascia. This septum continues inferiorly, getting thicker as it goes, to become the flexor retinaculum. The muscles of the leg and their neurovascular bundles are divided up amongst these three compartments. Typically, muscles within a compartment share common functions and innervations.

Retinacula

Retinacula are thickenings of deep fascia, found around joints, which act to hold tendons down to prevent them from bowstringing. In doing so they act as a pulley, which helps the muscles perform their actions. Some retinacula also provide support to the ligaments of the talocrural and subtalar joints. The superior extensor retinaculum is located superior to the talocrural joint, attaching to the tibia and fibula proximal to the malleoli. This retinaculum is thin and sometimes poorly defined. The inferior extensor retinaculum is a Y-shaped band that has its stem located laterally, attaching to the anterosuperior surface of the calcaneus in an area known as the sinus tarsi. One part of the Y then passes superomedially to attach to the medial malleolus. The other part of the Y passes inferomedially and attaches to the plantar aponeurosis and other fascia in the foot. These retinacula hold down the tendons of the anterior compartment of the leg (Figure 2.6). The superior and inferior fibular retinacula are found above and below the lateral malleolus. The superior attaches to the tip of the lateral malleolus and then passes posteroinferior to the calcaneus. The inferior attaches to the calcaneus only. Both retinacula cover the fibularis longus and brevis tendons. The flexor retinaculum covers the tendons of the deep posterior compartment as they pass posterior to the medial malleolus. The flexor retinaculum attaches to the medial malleolus and passes posteroinferiorly to the calcaneus.

The deep surface of this retinaculum forms individual tunnels for the tendons of the deep posterior compartment along with the posterior tibial artery and veins, and the tibial nerve.

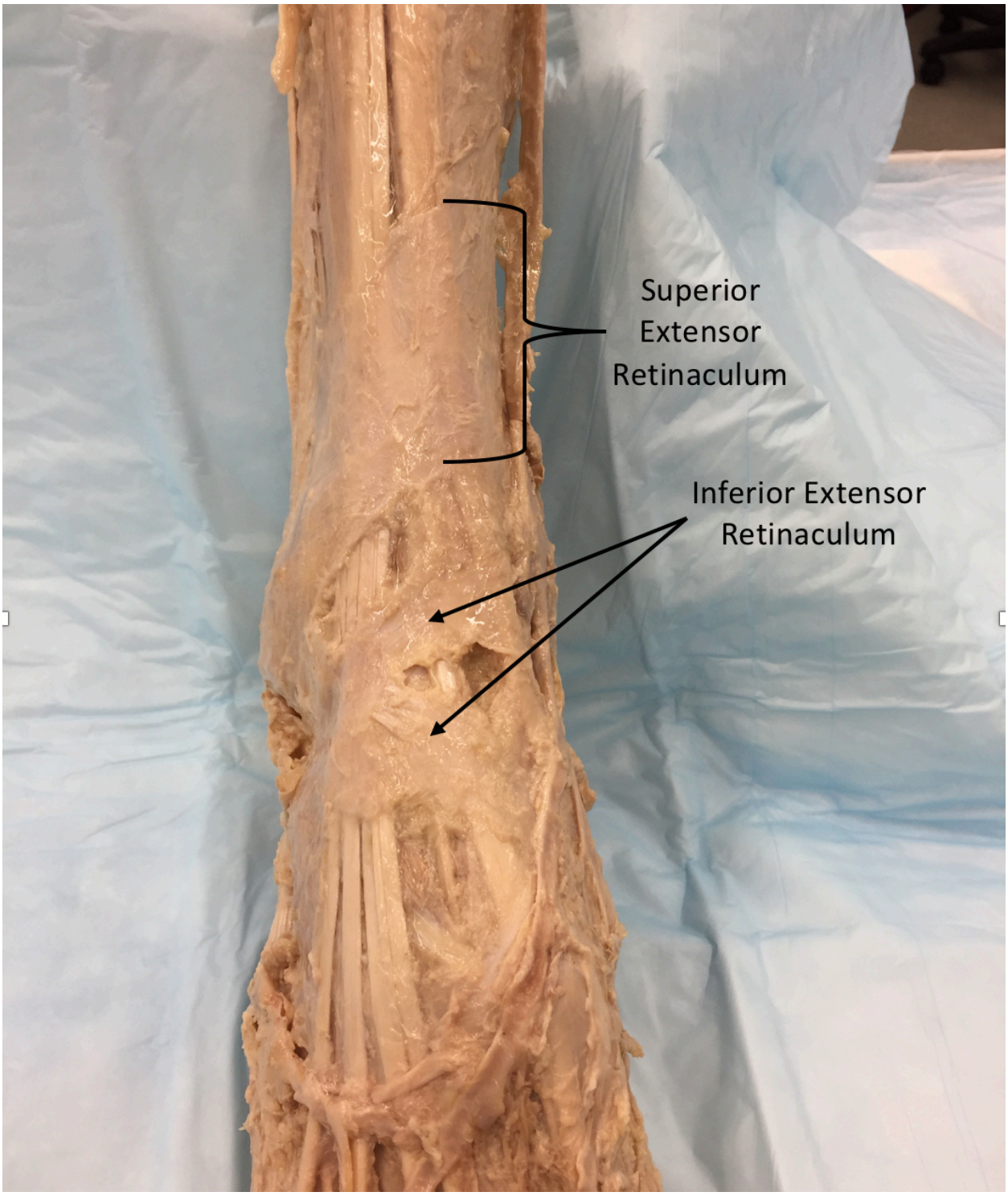

Figure 2.6. Superior and inferior extensor retinacula. (Photo credit: Cara Fisher)

2.3 Osteology of the Leg

There are two bones in the leg, the tibia and fibula, located medially and laterally respectively. The tibia is a triangular-shaped, weight-bearing bone that transmits body weight from the femur down to the talus. The tibia has three surfaces – medial, posterior, and lateral and three borders – anterior, medial, and interosseous. Proximally, the tibia articulates (forms a joint) with the femoral condyles at the tibial plateau, forming the knee, and the head of the fibula posterolaterally. The tibial plateau is formed by the medial and lateral tibial condyles, which are separated by the intercondylar eminence. The intercondylar eminence consists of medial and lateral tubercles and anterior and posterior intercondylar areas. Distally, the tibial plafond and medial malleolus articulate with the talus.

The fibula is also triangular-shaped, but is usually considered to be a non-weight-bearing bone. One study by Takabe et al., found that the fibula transmits no more than 10% of body weight forces, but this is dependent on positioning. [6] Greater forces are transmitted through the fibula when the foot is in the everted position, as the lateral malleolus contacts the lateral aspect of the foot.[7] The fibula articulates proximally with the tibia and the talus distally. The fibula has three surfaces – medial, posterior, and lateral and three borders – anterior, interosseous, and posterior. The head of the fibula is found proximally. The head has a pointy part that extends superiorly which is the apex. The neck of the fibula sits below the head and transitions into the shaft, which becomes the lateral malleolus at its distal end. The lateral malleolus is longer than the medial malleolus, extending 1 cm further than the medial and it articulates with the talus.[8]

2.4 Arthrology of the Leg

The head of the fibula and the posterolateral aspect of the lateral tibial condyle form the proximal tibiofibular joint, a plane-type synovial joint, which is bound by the anterior and posterior tibiofibular ligaments. This joint allows for a small amount of gliding motion when movement at the distal tibiofibular joint occurs in response to movement at the ankle, such as dorsiflexion. The distal tibiofibular joint is a syndesmotic, fibrous joint formed between the lateral aspect of the tibia, an area known as the incisura, and the lateral malleolus. Although the syndesmosis is stable, there is movement present during ambulation. One study by Beumer et al., showed that an intact syndesmosis may rotate as many as 2-5 degrees under rotational stress and translate 1-3 mm posteriorly.[9] The space between the tibia and fibula at this level is known as the tibiofibular clear space, which is what this research was measuring. The anterior inferior tibiofibular ligament (AITFL), posterior inferior tibiofibular ligament (PITFL), and interosseous ligament (IOL) are the primary ligaments responsible for the stability of the distal tibiofibular joint.[4,10] These ligaments keep the talus well seated between the tibia and fibula, thus maintaining mortise integrity. The AITFL is usually composed of 2-3 bands and does not have much variability. The inferior transverse ligament is often classified as a separate ligament, but it is the deepest, most distal part of the PITFL and they are often considered as a unit. The deltoid ligament, while not one of the ligaments primarily responsible for the stability of the syndesmosis, is often involved in supination-external rotation (SER) ankle injuries. Injuries to the syndesmosis are commonly concomitant in up to 23% of all ankle fractures and involved in up to 10% of all ankle sprains.[1] When the syndesmosis is injured, it allows greater movement of the talus within the mortise and decreases the contact surface area in the ankle.[11] This can cause decreased function due to pain and instability, which may lead to accelerated degradation of

cartilage and formation of osteoarthritis.[12] The IOL, which extends superiorly as the interosseous membrane, also provides support for the proximal tibiofibular joint. The interosseous membrane is a fibrous union between the tibia and fibula. Its fibers are oriented obliquely from tibia to fibula. This orientation helps the fibula resist the downward pull of eight of the nine muscles that attach to it. Because the tibia, fibula, and associated tibiofibular joints are part of a closed chain, all the ligaments that attach to the tibia and fibula support both tibiofibular joints. Table 2.2 is a summary of these and other ligaments discussed in this chapter and Figures 2.7-2.9 show the AITFL and PITFL.

2.5 Myology of the Leg

The anterior compartment of the leg consists of four muscles that generally dorsiflex the ankle and extend the digits. The posterior compartment consists of muscles that generally plantarflex the ankle and flex the digits, and the lateral compartment consists of muscles that generally evert the foot. It is important to note that all muscles that cross the ankle joint contribute to its stability. Especially those muscles that pass anterior or posterior to the joint, as this is where the joint capsule is the weakest.

Anterior Compartment of the Leg

Tibialis anterior, extensor hallucis longus, extensor digitorum longus, and fibularis tertius are the muscles that comprise the anterior compartment of the leg. The tibialis anterior is the most medially located and also has the largest muscle belly. Its proximal attachment is to the lateral aspect of the proximal tibia and the tendon passes deep to the extensor retinacula on its way to the foot. Distally, the tibialis anterior attaches to the medial cuneiform and base of the first metatarsal. In addition to dorsiflexion, the tibialis anterior also inverts the foot. The extensor

hallucis longus muscle, which lies deep proximally, attaches to the fibula and interosseous membrane. As it descends through the leg it becomes more superficial, to a point where its tendon is palpable proximal to the superior extensor retinaculum. The extensor hallucis longus muscle passes deep to the extensor retinacula and attaches distally to the base of the distal phalanx of the great toe, which it extends. The extensor digitorum longus muscle arises proximally from the tibia, fibula, and interosseous membrane, passes deep to the extensor retinacula, and attaches distally to the middle and distal phalanges of digits 2-5. It is responsible for extending these digits. The fibularis tertius, a detached part of extensor digitorum longus, is not always present. When it is, its tendon passes deep to the extensor retinacula and attaches distally to the base of the dorsum of the fifth metatarsal. While the fibularis tertius does weakly dorsiflex the foot, it primarily assists the lateral compartment muscles with eversion of the foot.

Lateral Compartment of the Leg

The lateral compartment has just two muscles present, fibularis longus and fibularis brevis. Both of these muscles will pass posterior to the PITFL, providing support, as they go behind the lateral malleolus. The fibularis longus attaches proximally to the head and shaft of the fibula. It passes posterior to the lateral malleolus, posterior to the tendon of fibularis brevis, and deep to the superior and inferior fibular retinacula. The fibularis longus tendon goes inferior to the fibular trochlea of the calcaneus and then passes through a groove on the plantar surface of the cuboid. The fibularis longus attaches distally on the medial cuneiform and base of first metatarsal. This muscle is primarily an evertor of the foot, the purpose of which is to pull the medial longitudinal arch into closer contact with the ground to help steady the leg on the foot while standing. It is also a weak plantarflexor. The fibularis brevis lies deep to the fibularis longus and has its proximal attachment more distally in location on the lateral surface of the

fibula. The fibularis brevis also runs posterior to the lateral malleolus and deep to the fibular retinacula, but passes superiorly to the fibular trochlea of the calcaneus. It attaches distally onto the tuberosity at the base of the fifth metatarsal. This muscle primarily everts the foot, but will also do weak plantarflexion. Hatch et al., investigated the fibularis longus and brevis muscles' role in static support of the talocrural joint. They found that sectioning of the fibularis tendons and superior fibular retinaculum, while exerting a 150 N anterior force on the talus, caused an increased 15% anterior displacement of the talus compared to the ankles that were left intact.[13] Clearly these structures are important to the stability of the talocrural joint and limiting displacement of the talus.

Posterior Compartment of the Leg

Bear in mind that the posterior compartment of the leg is broken into superficial and deep subcompartments by the transverse intermuscular septum. The superficial compartment contains three muscles and the deep four. All three of the superficial muscles will cross the ankle joint. Only three of the four deep muscles from the posterior compartment cross the ankle joint.

Superficial Posterior Compartment

The plantaris, gastrocnemius, and soleus muscles comprise the superficial compartment with both the plantaris and gastrocnemius muscles crossing the knee and ankle joints. The triceps surae, composed of the two heads of the gastrocnemius and the soleus, comprises the strongest plantarflexor of the ankle. The plantaris muscle has a small muscle belly and a long skinny tendon. This muscle is absent about 5-10% of the time.[8] When the plantaris muscle is present, it attaches proximally to the lateral femur. Its tendon passes medially between the gastrocnemius and soleus muscles to attach distally to the posterior calcaneus. The plantaris muscle acts as a flexor of the knee and a plantarflexor of the foot, although the contribution is minimal. Because

it does have a large number of muscle spindles, this muscle is thought to help with proprioception. The gastrocnemius muscle is a two-headed muscle located most superficial in the posterior compartment. Proximally this muscle attaches to the lateral and posteromedial femur as two separate heads. The two heads of the gastrocnemius merge in the posterior leg and descend to a common distal attachment on the posterior calcaneus. The gastrocnemius muscle flexes the knee and plantarflex the foot. Because this muscle crosses the knee and ankle joints, its ability to plantarflex the foot is dependent upon the position of the knee. If the knee if fully flexed, it is limited in the amount of plantarflexion it can do. The gastrocnemius is a strong plantarflexor of the foot when the knee is extended. Deep to the gastrocnemius, lies the soleus muscle. This muscle has a tendinous attachment proximally to the fibula and tibia, forming an upside down U known as the tendinous arch of the soleus. There is a gap in the superior part of this arch where the neurovascular bundle from the popliteal fossa passes into the deep posterior compartment. The tendon of the soleus joins with that of the gastrocnemius forming the calcaneal tendon (Achille's tendon), which attaches distally to the calcaneus. The soleus muscle also plantarflexes the foot, but because it does not cross the knee joint, it does plantarflexion regardless of knee position.

Deep Posterior Compartment

The deep posterior compartment of the leg contains the popliteus, flexor hallucis longus, tibialis posterior, and flexor digitorum longus muscles. These deep muscles, with the exception of the popliteus, will pass over the deltoid ligament medially on their way to the foot. They help stabilize this medial collateral ligament complex. The popliteus muscle lies deep in the popliteal fossa, the area posterior to the knee, forming part of its floor. Proximally, this muscle attaches to the lateral femoral condyle within the joint capsule of the knee. The tendon of the popliteus exits

the joint capsule posteriorly and attaches distally to the posterior surface of the tibia proximal to the soleus. The popliteus is considered a weak flexor of the knee with its primary function being rotation. It will medially or laterally rotate, depending on the position of the knee. If the knee is extended and weight bearing, the popliteus muscle will rotate the femur approximately five degrees laterally on the tibia to unlock it, thus allowing flexion of the knee to occur. In a flexed, non-weight bearing knee, the popliteus will medially rotate the tibia on the femur. This is the only muscle in the deep posterior compartment that does not cross the talocrural joint. The flexor hallucis longus muscle is located laterally in the deep posterior compartment. It attaches proximally to the fibula and interosseous membrane and descends through the posterior leg. The flexor hallucis longus tendon passes posterior to the medial malleolus through the groove between the medial and lateral tubercles of the posterior process of the talus, posterior to the tibial nerve. As the tendon of the flexor hallucis longus passes deep to the flexor retinaculum and abductor hallucis muscle, it passes under the sustentaculum tali, which it uses as a pulley. The tendon then passes through the medial aspect of the plantar foot, deep to the tendon of flexor digitorum longus, between the two sesamoid bones at the base of the first metatarsal, to attach distally at the distal phalanx of the great toe. The flexor hallucis longus muscle helps with plantarflexion of the foot and with toe off during the pre-swing phase of gait. The tibialis posterior muscle lies in the middle of the deep posterior compartment and is the largest of the extrinsic foot muscles next to the triceps surae. Most of its proximal attachment is to the interosseous membrane, with some attachment to the surrounding tibia and fibula. The tibialis posterior muscle descends through the posterior leg and its tendon passes immediately posterior to the medial malleolus deep to the flexor retinaculum. The tendon of the tibialis posterior passes

deep to the abductor hallucis muscle to enter the plantar foot. Here the tendon attaches to all the bones of the foot with the exceptions of the talus, first and fifth metatarsals, and the phalanges.

A strong plantarflexor, the tibialis posterior will also invert the foot. Because it is large and crosses so many joints, the tibialis posterior will have a long moment arm for supination at both the subtalar and transverse tarsal joints.[14] The tendon of the tibialis posterior also plays an important role in supporting the talar head, which is the keystone of the medial longitudinal arch of the foot. The flexor digitorum longus muscle arises from the posterior tibia and interosseous membrane. Its tendon passes laterally so it crosses over that of tibialis posterior. This places the flexor digitorum longus tendon between the tendon of the tibialis posterior and the posterior tibial artery when it passes posterior to the medial malleolus, deep to the flexor retinaculum. The tendon of the flexor digitorum longus then dives deep to the abductor hallucis muscle and enters the plantar surface of the foot. Its tendon crosses the tendon of flexor hallucis longus and angles laterally to attach to digits 2-5. The flexor digitorum longus muscle is a plantarflexor of the foot and also flexes digits 2-4.

2.6 Angiology of the Leg

The blood supply to the leg is derived from the popliteal artery, which is a direct continuation of the femoral artery as it descends through the adductor hiatus. The popliteal artery passes through the popliteal fossa, deep to the popliteal vein, and terminates as the anterior tibial artery and posterior tibial artery at the inferior border of the popliteus muscle. The anterior tibial artery passes through a gap in the superior part of the interosseous membrane to enter the anterior compartment of the leg. Here it will supply the muscles of the anterior compartment as it descends between tibialis anterior and extensor digitorum longus muscles. As the anterior tibial

artery continues to descend through the anterior compartment, it gives rise to perforating branches that are essential to helping supply the lateral compartment. The anterior tibial artery terminates as the dorsalis pedis artery distal to the inferior border of the inferior extensor retinaculum. The posterior tibial artery continues to run through the posterior compartment of the leg with the tibial nerve, deep to the transverse intermuscular septum. It supplies the muscles of the posterior compartment and gives rise to the fibular artery. At the distal end of the leg, the posterior tibial artery passes posterior to the medial malleolus between the flexor digitorum longus tendon and the tibial nerve, giving rise to its terminal medial and lateral plantar arteries deep to the flexor retinaculum. These terminal branches then dive deep to the abductor hallucis muscle and enter the plantar aspect of the foot. The fibular artery dives deep to the flexor hallucis longus muscle in the deep posterior compartment of the leg. It runs deep to the flexor hallucis longus muscle through most of the leg, also supplying essential perforating branches to the lateral compartment as it descends. Distally the fibular artery gives rise to a perforating branch that passes through the interosseous membrane onto the dorsum of the foot where it will anastomose with the arcuate artery. The fibular artery terminates as lateral calcaneal and lateral malleolar branches, which help form the periarticular anastomosis around the ankle. McKeon, et al., looked at the vascular supply of the tibiofibular syndesmosis and found that in 86% of their specimens, the fibular artery predominantly supplied the AITFL and IOL. In 63%, the fibular artery was the only artery supplying the anterior syndesmotic structures. In 100% of the specimens, the fibular artery provided blood supply to the PITFL.[15] Damage to this vessel during SER ankle injuries is highly likely. If structures need to be surgically repaired, the fibular artery could also be injured during posterolateral surgical approaches to the fibula because of its proximity to the PITFL.[16]

Venous drainage of the leg is plentiful and done via superficial and deep veins, both of which communicate with each other through perforating veins. The great and small saphenous veins provide superficial venous drainage of the leg. The great saphenous vein is formed on the medial aspect of the dorsum of the foot and ascends anterior to the medial malleolus, crossing the ankle, and up the medial aspect of the leg. From there it passes posterior to the medial aspect of the knee and up the medial thigh. The great saphenous vein terminates as it drains into the femoral vein in the femoral triangle. The small saphenous vein is formed on the lateral aspect of the dorsum of the foot and ascends posterior to the lateral malleolus. It passes between the two heads of the gastrocnemius muscle and terminates by draining into the popliteal vein in the popliteal fossa. Deep venous drainage of the leg is done by the anterior and posterior venae comitantes, companion veins, which surround their respective arteries. They ascend through the leg and just distal to the popliteal fossa, they join together and form the popliteal vein. The popliteal vein terminates as the femoral vein as it passes through the adductor hiatus.

2.7 Neurology of the Leg

Innervation to the muscles of the leg, regardless of their compartment, comes from branches of the sciatic nerve. The sciatic nerve originates from the lumbosacral plexus, L4-S3. In addition to supplying the motor innervation to the leg and foot, it also supplies the majority of the sensation to the leg and foot as well. The sciatic nerve passes through the gluteal region deep to the gluteus maximus and enters the posterior thigh, where it descends deep to the long head of the biceps femoris muscle. Typically, the sciatic nerve separates into the tibial and common fibular nerves just proximal to the popliteal fossa. The tibial nerve descends into the posterior compartment of the leg deep to the soleus muscle and supplies all muscles in the superficial and

deep posterior compartments. The tibial nerve passes posterior to the medial malleolus between the posterior tibial artery and flexor hallucis longus tendon, giving rise to its terminal medial and lateral plantar nerves deep to the flexor retinaculum. The terminal branches then pass deep to the abductor hallucis muscle and enter the plantar aspect of the foot.

The common fibular nerve passes laterally and wraps around the neck of the fibula. Deep to the fibularis longus muscle and the fibular neck, the common fibular nerve divides into superficial and deep fibular nerves. The superficial fibular nerve supplies the muscles of the lateral compartment and then emerges about 2/3 of the way down to provide sensation to the anterolateral leg. The superficial fibular nerve then splits into its two terminal branches, the intermediate and medial dorsal cutaneous nerves, which travel superficial to the superior and inferior extensor retinacula onto the dorsum of the foot. Because of the close relationship of the superficial fibular nerve to the tibiofibular syndesmosis, this nerve may be injured during surgical repairs of the syndesmosis. The deep fibular nerve enters the anterior compartment of the leg and descends between the extensor digitorum longus and tibialis anterior muscles on the interosseous membrane. As the deep fibular nerve descends, it eventually comes to settle between the tibialis anterior and extensor hallucis longus muscles. This nerve then passes deep to the superior and inferior extensor retinacula onto the dorsum of the foot. The deep fibular nerve terminates as the lateral and medial branches of the deep fibular nerve.

Sensation to the leg is provided by the saphenous, lateral sural cutaneous, sural, and superficial fibular nerves. The saphenous nerve branches from the femoral nerve in the femoral triangle. It descends through the thigh in the adductor canal, passes medial at the knee, and then runs with the great saphenous vein through the leg. The saphenous nerve supplies sensation to the anteromedial leg and then passes into the medial foot. The lateral sural cutaneous nerve

supplies the proximal posterolateral aspect of the leg, with the sural nerve handling the distal posterolateral leg. The superficial fibular nerve supplies the skin of the distal anterior leg. The sural, saphenous, and superficial fibular nerves also supply the skin surrounding the ankle. Because of their close relationship with the medial and lateral malleoli, all of the above nerves are at risk of damage during surgical repairs of the ankle.[4]

2.8 Ankle Anatomy

The talocrural joint, a hinge-type synovial joint, is formed by the tibial plafond, the medial and lateral malleoli, and the talus. For the most part, this joint is considered to uniaxial with one degree of freedom around which movements of dorsiflexion and plantarflexion occur.[4,16] The ankle joint is at its most vulnerable when the foot is plantarflexed, or loose-packed, as the narrow part of the talus is between the malleoli and there is room for it to wobble.

The joint capsule is relatively weak anteriorly and posteriorly because it is thinner in these areas. In addition to surrounding musculature, this joint is strengthened by numerous ligaments. The ligaments supporting the proximal and distal tibiofibular joints help maintain the stability of the mortis, which in turn support the ankle joint. Lumped together, the ligaments immediately surrounding the ankle joint are referred to as the medial and lateral collateral ligaments of the ankle and they function to regulate medial/lateral joint stability.[16] These ligaments are also under constant tension when the ankle is being dorsiflexed or plantarflexed, which helps keep the joint stable.[17] As many of these ligaments cross the subtalar joint, they will also contribute to its stability. To better understand their attachments, it is best to look at them individually.

Laterally, the anterior talofibular (ATFL), calcaneofibular (CFL), and posterior talofibular (PTFL) ligaments make up the lateral collateral ligament complex (Figures 2.7 and 2.9). The anterior talofibular ligament extends as two bands from the anterior aspect of the lateral malleolus onto the neck of the talus. It is possible that a third band might be present. This ligament is relatively weak and commonly torn during inversion ankle injuries. A round, cord-like ligament, the calcaneofibular ligament, extends from the tip of the lateral malleolus to the posterolateral surface of the calcaneus. Static reinforcement for the calcaneofibular ligament comes from the superior fibular retinaculum.[13] The posterior talofibular ligament runs posteromedially from the lateral malleolar fossa to the lateral tubercle of the talus. It is the strongest ligament in this complex. The lateral collateral ligament complex is weaker as a whole than its medial counterpart and is more commonly injured. Its purpose is to control inversion/supination of the ankle and talus and is injured most commonly during inversion ankle sprains.[18,19]

The medial collateral ligament, or deltoid ligament, of the ankle shown in Figures 2.10 and 2.11, varies in composition based on the source. Most sources agree on four parts – the anterior tibiotalar, tibionavicular, tibiocalcaneal, and posterior tibiotalar ligaments. However, Cromeens and Fisher et al., documented that there are anterior and posterior deep tibiotalar ligaments as well.[20,21] In this case, the aforementioned posterior tibiotalar ligament is referred to as the superficial posterior tibiotalar ligament to distinguish it from the deep. The medial collateral ligament complex attaches to the medial malleolus and fans out its distal attachments between the navicular, talus, and calcaneus. This ligament complex is strong, so strong that it may avulse, or tear off, part of the medial malleolus rather than tear itself. Again, it is important to note that while this ligament is not one that primarily supports the syndesmosis, it is often

injured with SER injuries. This is largely due to the ankle being unstable in dorsiflexion when external rotational forces are applied and explains the observation by Fujii et al., that the deltoid ligament is usually injured when the foot is in the dorsiflexed position.[18] The purpose of the deltoid ligament is to control eversion of the ankle and talus. Sensory innervation to the ankle is provided by articular branches of the nerves that cross it, mainly the tibial, superficial fibular, deep fibular, saphenous, and sural nerves.[22] When ankle injuries occur, it is the above nerves that carry the somatic afferents for the sensation of pain. Blood supply to the ankle comes from the arteries that cross it, namely the anterior tibial, posterior tibial, and fibular arteries. Small branches from these arteries that supply the ankle (articular branches) will be the ones that bleed, causing swelling and bruising, with ankle injuries.

2.9 Foot Anatomy Overview

The foot consists of dorsal and plantar surfaces. It contains seven tarsals, five metatarsals, and fourteen phalanges, which are subdivided into hindfoot, midfoot, and forefoot respectively. The hindfoot is formed by the talus and calcaneus, the midfoot by the cuboid, navicular, and cuneiforms, and the forefoot by the metatarsals and phalanges.

The deep fascia of the foot is thin on the dorsal aspect and covers the tendons from the anterior compartment of the leg as they pass into the foot. On the plantar aspect, this fascia thickens considerably, especially centrally where it forms the plantar aponeurosis. This aponeurosis has a strong attachment to the calcaneus and fans out to the plantar plates on the tendinous sheaths of the five digits. This aponeurosis functions like a superficial ligament, helping to hold the parts of the foot together and supporting the longitudinal arches of the foot, especially during the stance phase of gait. During the late stance phase, maximum tension on the

plantar aponeurosis can reach up to 96% of body weight, transferring these forces between hindfoot and forefoot.[23]

The plantar fascia has septa that extend inward to create three compartments in the plantar aspect foot – medial, lateral, and central. A fourth plantar compartment, the interosseous compartment, exists between the plantar and dorsal interosseous fascias. These compartments contain the muscles, bones, and neurovasculature of the foot.

2.10 Osteology of the Foot

The hindfoot is formed by the talus and calcaneus. The talus is a wedge-shaped bone that is wider anteriorly than it is posteriorly. It is unique in that it has no muscular or tendinous attachment. The dome, or trochlea, of the talus is the uppermost portion of the body that articulates with the tibial plafond. On either side of the dome are the smaller medial malleolar facet and the larger lateral malleolar facet, which are covered with articular cartilage that is continuous with that on the dome. These facets contact the medial and lateral malleoli respectively. Extending anteriorly from the body of the talus is the neck and head. The head is covered with articular cartilage and forms a joint with the posterior aspect of the navicular. Extending posteriorly from the body is the posterior process of the talus. This structure is formed by medial and lateral tubercles with a groove in between. The groove holds the flexor hallucis longus tendon. Inferiorly, the talus articulates with the calcaneus.

The calcaneus distributes the majority of the body weight from the talus to the ground. The superior surface of the calcaneus has three articular facets, anterior, medial, and posterior, which articulate with the inferior surface of the talus. Wang et al., found that the posterior facet transmitted 75% of the force through the subtalar joint.[24] These calcaneal facets have been

classified by Bunning and Barnett into three types: Type A has three separate articular facets, in Type B the anterior and medial facets are confluent, and in Type C all facets are confluent.[25] The anterior surface of the calcaneus articulates with the cuboid. On the lateral surface of the calcaneus is the fibular trochlea. The fibularis brevis and longus tendons pass superior and inferior respectively, using the trochlea as a pulley to accomplish eversion of the foot. On the superomedial aspect of the calcaneus is the sustentaculum tali, or talar shelf. This projection supports the head of the talus superiorly and acts as a pulley for the tendon of the flexor hallucis longus muscle after it passes posterior to the medial malleolus. The calcaneal tuberosity is found posteriorly. It has medial, lateral, and anterior tubercles, which act as attachment points for different muscles and ligaments. During weight bearing, the medial tubercle is the only one to touch the ground.

The midfoot is composed of the cuboid, navicular, and three cuneiforms. The cuboid sits most lateral. Posteriorly, it articulates with the calcaneus, medially with the lateral cuneiform, and anteriorly with the lateral two metatarsals at their base. It has a tuberosity on its lateral aspect and a groove inferiorly that contains the tendon of the fibularis longus muscle. The navicular, a boat-shaped bone, sits anterior to the talar head. It articulates anteriorly with the three cuneiforms. Inferiorly, it has a projection called the navicular tuberosity, which helps form part of the medial longitudinal arch. The navicular tuberosity is an important site for ligamentous and tendinous attachment. The three cuneiforms, medial, intermediate, and lateral, are wedge-shaped bones that sit distal to the navicular, medial to the cuboid, and proximal to the medial three metatarsals. The medial cuneiform is the largest of the three cuneiforms and the lateral cuneiform is the smallest. The tarsometatarsal joint is formed where the tarsals articulate with the bases of the metatarsals.

The forefoot is composed of the metatarsals and phalanges. There are five metatarsals. The first metatarsal is found medially and is the largest. It has a large tuberosity at its base on the plantar surface, as well as two sesamoid bones found in tendons by the head. Each metatarsal has a base, located proximally, a shaft, and a head. The second metatarsal is the longest, and the fifth metatarsal has a large tuberosity at its base that is an important attachment site for the fibularis brevis muscle. This attachment is so strong that it is possible to avulse the tuberosity from the metatarsal during inversion ankle sprains. There are fourteen phalanges total in the foot. Digits 2-4 have proximal, middle, and distal phalanges, while the first digit, the great toe, has only proximal and distal. Each phalanx has a proximal base, a shaft, and a distal head.

2.11 Arthrology of the Foot

Subtalar Joint

The subtalar joint, a joint that is rarely dislocated due to its osteological congruency and strong ligamentous attachments, is between the inferior surface of the talus and the superior surface of the calcaneus. It is here that the majority of inversion and eversion occur around an oblique axis. The subtalar joint has anatomical and clinical descriptions, both of which are correct depending on whether one looks at anatomical structure or strictly function. The anatomical subtalar joint is a synovial joint between the concave posterior calcaneal articular surface of the talus and the convex posterior articular facet of the calcaneus.[8] Medial, lateral, posterior, and interosseous talocalcaneal, calcaneofibular (Figures 2.7-2.9), and cervical ligaments reinforce the weak joint capsule. The cervical ligament is the strongest ligament for this joint.[26,27] The cervical ligament is found anteriorly in the sinus tarsi, passing between the neck of the talus and the neck of the calcaneus. The interosseous talocalcaneal ligament is also

found within the sinus tarsi and serves to separate the subtalar and talocalcaneonavicular joints. As anatomical descriptions go, this is correct as, structurally, the subtalar joint is a separate joint that has its own joint capsule and articular surfaces. The clinical description of this joint includes the anatomical subtalar joint as well as the talocalcaneal part of the talocalcaneonavicular joint. The two parts of the clinical subtalar joint straddle the interosseous talocalcaneal ligament.[8] Functionally this is correct, as both parts of the joint in the clinical description function as a unit.

Calcaneocuboid Joint

The calcaneocuboid joint, formed by the anterior surface of the calcaneus and the posterior surface of the cuboid, has its own joint capsule that is strengthened by several ligaments. Laterally, the bifurcate ligament (calcaneocuboid ligament), dorsally, the dorsal calcaneocuboid ligament, and inferiorly, the short and long plantar ligaments all contribute to the integrity of this joint (Figures 2.8 and 2.12). The most important would be the long plantar ligament, as it spans from the calcaneus, to cuboid, and on to the bases of metatarsals 2-4. Because of this path, it supports the transverse tarsal joint and lateral longitudinal arch.[28] Cromeens and Fisher et al., found that tears in the bifurcate and dorsal calcaneocuboid ligaments caused a higher incidence of osteochondral lesions at the talocrural joint.[29] It might be practical to look for ligament injury here when investigating syndesmosis injuries to ensure the best fix for the talocrural joint and decrease the risk of osteoarthritis development down the road.

Talonavicular Joint

The talonavicular joint is a ball-and-socket joint between the head of the talus and the posterior part of the navicular. The joint capsule surrounds the talonavicular joint facets and the anterior and medial facets of the subtalar joint. Inferiorly, the capsule is formed by the spring ligament, which spans the space between the calcaneus and the navicular, supporting the talar

head. The talonavicular joint is reinforced laterally by the bifurcate ligament, and dorsally by the dorsal talonavicular ligament (Figure 2.8). Support also comes from the medial and lateral collateral ligament complexes, both parts of the inferior extensor retinaculum, and the talocalcaneal ligaments.

The ligaments of the calcaneocuboid joint also contribute support to this joint, which makes sense as it is helps form the remainder of the transverse tarsal joint and they are functionally linked.[4]

Transverse Tarsal joint

The transverse tarsal joint is a compound S-shaped joint comprised of the talonavicular and calcaneocuboid joints. It separates the hindfoot from the midfoot and forefoot, both of which will rotate on a longitudinal axis around the hindfoot. The motions of inversion and eversion, occurring at the subtalar joint, occur at the same time at this joint, as they share a mechanical link.[30] During weightbearing, the navicular and cuboid are considered relatively immobile with the talus and calcaneus moving on them.[4]

Metatarsophalangeal and Interphalangeal Joints

The distal heads of the metatarsals articulate with the phalanges forming the metatarsophalangeal (MTP) joints. The joints between the proximal and middle phalanx are called the proximal interphalangeal joints (PIP) and the ones between the middle and distal phalanges are the distal interphalangeal (DIP) joints. In cases where there are only two phalanges, there is a single interphalangeal (IP) joint. The talocalcaneonavicular joint in particular receives articular branches from the main nerves in the leg, the tibial, superficial and deep fibular, sural, and saphenous. It is interesting to note that many of these articular branches arise quite high in the leg, sometimes about 2/3 of the way down.[22] Damage at the level of the

ankle could possibly denervate the joints supplied by those nerves. The other numerous joints of the foot receive their blood supply and innervation via articular branches from the arteries and nerves that cross those joints.

2.12 Arches of the Foot

The foot has two primary arches, longitudinal and transverse, with the longitudinal being broken down into medial and lateral counterparts. These arches work together to support the integrity of the foot as well as provide cushion with each step by distributing weight throughout the foot, either through the heel or the ball.

The medial longitudinal arch is typically the highest arch and is functionally more important. It extends from the calcaneus posteriorly to the heads of the first three metatarsals anteriorly.[16] The medial longitudinal arch includes the talus, calcaneus, navicular, cuneiforms, and medial three metatarsals. The head of the talus is considered the "keystone" of the medial longitudinal arch.[4,8] In other words, it is the talus that receives all the body weight transferred down through the tibia and then distributes it to either the calcaneus or the forefoot. If the head of the talus falls, pes planus, or flat-foot deformity will result. Muscular support comes from the tibialis anterior and posterior muscles and the tendon of the fibularis longus. The most important ligamentous structure for support of the medial longitudinal arch is the plantar aponeurosis.[31] The tibialis posterior has been shown to have the most important muscular role in supporting the medial longitudinal arch, most likely because of its attachments that support the talar head.[32]

The lateral longitudinal arch is considerably flatter than the medial and lies on the ground when standing. It includes the calcaneus, cuboid, and lateral two metatarsals with the cuboid acting as the keystone of this arch. Three major ligaments help support the longitudinal arches of

the foot. They are the plantar calcaneonavicular ligament (spring ligament), the long plantar ligament, and the plantar calcaneocuboid ligament (short plantar ligament), which can be seen in Figures 2.10 and 2.12. The plantar calcaneonavicular ligament spans between the sustentaculum tali of the calcaneus and the posteroinferior navicular. It helps support the talar head and thus the medial longitudinal arch. The long plantar ligament passes from the plantar aspect of the calcaneus to the cuboid and metatarsals. The tendon of the fibularis longus passes through the groove in the cuboid deep to this ligament. The plantar calcaneocuboid ligament sits between the spring and long plantar ligaments. It attaches to the anterior inferior calcaneus and the cuboid. The cuboid, cuneiforms, and bases of all five metatarsals form the transverse arch of the foot. The transverse arch spans the medial and longitudinal arches, using them as pillars. Muscular support comes primarily from the tendons of the tibialis posterior and fibularis longus muscles. To a lesser extent the transverse head of adductor hallucis will help by holding the bases of the metatarsals together. Passive and dynamic support is responsible for maintaining all of these arches. Passive support comes from the shape of the articulated bones, which contribute minimally, and bowstringing of the longitudinal arches by the following structures: the plantar aponeurosis, the long plantar, plantar calcaneocuboid, and plantar calcaneonavicular ligaments. It was long thought that intrinsic muscles, particularly abductor hallucis, flexor hallucis brevis, flexor digitorum brevis, abductor digiti minimi, and the dorsal interossei, played little role in arch support in the static foot, but recent research suggests that these intrinsic muscles of the foot play a substantial role in arch support when standing.[33,34]

Dynamic support comes from intrinsic muscles of the foot as they reflexively contract as well as active contraction of the flexor hallucis longus, flexor digitorum longus, fibularis longus, and tibialis posterior muscles. Of all the structures listed providing passive and dynamic support, the plantar structures, providing passive support, carry the lion's share of the work.

2.13 Myology of the Foot

The plantar surface of the foot is divided into four layers with the first layer being superficial and the fourth layer being deep. While the muscles of the plantar surface of the foot are assigned individual functions, their main purpose is to function as a unit during the stance phase to support the longitudinal arches as weight is transferred from the heel to the toe, to support the transverse arch during toe off, and to help the foot accommodate to uneven ground. When referring to independent actions of foot muscles, the second digit is used as the axis for the foot.

First Layer

The first layer of the foot contains the abductor hallucis, flexor digitorum brevis, and the abductor digiti minimi. All three muscles attach proximally to the calcaneus and plantar aponeurosis. Abductor hallucis acts to abduct the great toe, the first digit, by bringing it medially, flexor digitorum brevis flexes digits 2-4, and abductor digiti minimi abducts the fifth digit by bringing it laterally away from the second digit.

Second Layer

The second layer of the foot contains six muscles, the quadratus plantae and the four lumbricals. The quadratus plantae attaches proximally to the calcaneus and distally to the posterior aspect of the flexor digitorum longus muscle. It functions to realign the pull of the

flexor digitorum longus as it passes through the plantar aspect of the foot obliquely and will assist with flexion of the lateral four digits. The four lumbricals arise from the four tendons of the flexor digitorum longus and attach distally to the extensor expansions of the lateral four digits. They will flex the MTP joints and extend the IP joints.

Third Layer

The third layer of the foot contains flexor hallucis brevis, adductor hallucis, and flexor digiti minimi brevis. The flexor hallucis brevis arises from the cuneiforms and the cuboid. It attaches distally to either side of the proximal phalanx of the great toe. The two sesamoid bones sit in the two tendons of the flexor hallucis brevis and create a trough for the tendon of flexor hallucis longus. The flexor hallucis brevis muscle acts on the MTP joint and flexes the proximal phalanx of the first digit. The adductor hallucis muscle has two heads, an oblique head that arises from the bases of metatarsals 2-4 and a transverse head that arises from the plantar ligaments of the MTP joints. Both heads attach on the lateral aspect of the proximal phalanx of the great toe and will pull the great toe laterally towards the second digit. The flexor digiti minimi brevis attaches to the base of the fifth metatarsal and the proximal phalanx of the fifth digit. It acts on the MTP joint when flexing the proximal phalanx.

Fourth Layer

The fourth layer contains the plantar and dorsal interosseous muscles. There are three plantar interosseous muscles and four dorsal. The plantar interossei attach proximally to the metatarsals and distally to the bases of digits 3-5 on the medial sides. They adduct digits 3-5 toward the second digit and help flex the MTP joints. The dorsal interossei arise from the metatarsal shafts of digits 1-5.

Distally, they attach to the medial side of the second digit and the lateral sides of digits 2-4. They abduct these digits away from the midline and help flex the MTP joint as well.[8]

Unlike the hand, there are two intrinsic muscles found on the dorsum of the foot. These muscles lie deep to the deep fascia and extensor tendons. The extensor hallucis brevis muscle attaches proximally to the calcaneus and surrounding fascia. It traverses medially as it passes to the base of the proximal phalanx of the great toe. Here the extensor hallucis brevis will assist the extensor hallucis longus with extension of the great toe. The extensor digitorum brevis shares a common proximal attachment with the extensor hallucis brevis. Unlike extensor digitorum longus, the brevis only gives rise to three tendons that attach to the long extensor tendons of digits 2-4. It will assist with extension of digits 2-4. The lateral branch of the deep fibular nerve supplies both of these muscles.

2.14 Angiology of the Foot

The blood supply to the foot is from branches of the anterior and posterior tibial arteries. The dorsalis pedis artery is the direct continuation of the anterior tibial artery inferior to the extensor retinaculum. As the dorsalis pedis artery crosses the talocrural joint, it gives rise to anterior medial and lateral malleolar branches, which help supply the joint. The dorsalis pedis continues distally down the dorsum of the foot and gives rise to the lateral tarsal artery, which then runs deep to the extensor digitorum brevis muscle. It will supply it and the underlying joints and tarsals, then continuing on to anastomose with the arcuate artery. One to two medial tarsal arteries arise shortly after and supply the tarsals and joints of the medial midfoot. The arcuate artery arises from the dorsalis pedis shortly before it terminates. The arcuate artery passes laterally and gives rise to metatarsal arteries to digits 2-5 and also receives perforating branches

from the deep plantar arch. The dorsalis pedis artery terminates by splitting into the first dorsal metatarsal artery and the deep plantar artery between the great and second toes. The deep plantar artery provides an important anastomosis in the foot by diving deep through the first dorsal interosseous muscle and joining up with the lateral plantar artery in the plantar aspect of the foot to form the deep plantar arch. This anastomosis is used when one stands for a long period of time and the plantar arteries are compressed. The medial and lateral plantar arteries are the terminal branches of the posterior tibial artery arising deep to the flexor retinaculum. The medial plantar artery is the smaller terminal branch and supplies mainly the great toe, the skin on the medial side of the plantar aspect of the foot, and has digital branches that will accompany the digital branches of the medial plantar nerve. The lateral plantar artery runs laterally and distally with the lateral plantar nerve. The lateral plantar artery arches medially across the foot to form the deep plantar arch, which is completed by the deep plantar artery from dorsalis pedis. Four plantar metatarsal arteries arise from this arch and extend out to supply the digits. The deep plantar arch also gives rise to three perforating branches, which travel towards the dorsum of the foot and anastomose with the arcuate artery.

There are plantar and dorsal venous networks in the foot. Like the leg, there are superficial and deep veins, the deep accompanying arteries of the same name. Deep venous drainage of the foot is primarily to the superficial veins of the foot. Plantar veins drain into dorsal digital and metatarsal veins, which form the dorsal venous network (arch). Arising from the medial side of the dorsal venous arch is the great saphenous vein and from the lateral side, the small saphenous vein. Perforating veins from both of these large superficial veins continually push blood to the deep veins of the leg to take advantage of the musculovenous pump that is provided by muscular contraction and the crural fascia surrounding those muscles.

2.15 Neurology of the Foot

The medial and lateral plantar nerves are the terminal branches of the tibial nerve and, as their name implies, they are found on the plantar surface of the foot. Because the tibial nerve is closely associated with the medial malleolus of the ankle, damage to the nerve at that point would denervate the intrinsic plantar muscles of the foot. The medial plantar nerve courses distally between the abductor hallucis and flexor hallucis brevis muscles, which it innervates. The medial plantar nerve will supply the first lumbrical muscle and flexor hallucis brevis as well before terminating into three common plantar digital nerves. The lateral plantar nerve runs distally and laterally between the first and second layers of the foot. The lateral plantar nerve innervates the quadratus plantae, abductor digiti minimi, and all interosseous muscles before terminating into a superficial and deep branch. The superficial branch innervates the flexor digiti minimi brevis before it terminates by giving rise to common and proper digital branches. The deep branch runs with the plantar arch between the third and fourth layers of the foot. The deep branch innervates the adductor hallucis muscle.

Sensation to the foot is derived from numerous nerves. The majority of the dorsum of the foot receives its cutaneous innervation from the intermediate and medial dorsal cutaneous nerves, branches of the superficial fibular nerve. The medial branch of the deep fibular nerve innervates a small area of skin between the great and second toes. The saphenous nerve supplies sensation to the medial aspect of the foot to the base of the great toe. Laterally, the sural nerve supplies the hindfoot and midfoot as the lateral dorsal cutaneous nerve. Again, because the sural, saphenous, and superficial fibular nerves pass in close association to the malleoli at the ankle, the dorsum of the foot is at risk for being denervated if these nerves are damaged during SER injuries or orthopedic repairs. Numerous nerves also supply sensation to the plantar aspect of the

foot. The medial plantar nerve provides sensation to the sole of the foot proximal to the medial three digits and via its terminal common plantar digital nerves, the skin of digits 1-3 and half of digit four, including skin on the dorsum of the distal phalanges of these digits. Sensation to the fifth digit and other half of the fourth is by the common and proper digital branches of the superficial branch.[8] Calcaneal branches from the tibial and sural nerves supply sensation to the calcaneus.

Table 2.1. Summary of the ligaments around the tibiofibular syndesmosis, the ankle, and the foot.

Joint	Ligament	Attachment Points	Function(s)
Proximal tibiofibular	Anterior tibiofibular	Anterior head of fibula to anterior lateral tibial condyle	Restrains movement at proximal tibiofibular joint
	Posterior tibiofibular	Posterior head of fibular to posterior lateral tibial condyle	Restrains movement at proximal tibiofibular joint
Distal tibiofibular (syndesmosis)	Anterior inferior tibiofibular (AITFL)	Anterolateral tubercle of tibia of anterior tubercle of fibula	Maintains integrity between tibia and fibula
	Posterior inferior tibiofibular (PITFL)	Posterior tubercle of tibia to posterior part of lateral malleolus	Strongest component of syndesmosis
	Interosseous (IOL)	Distal tibia and fibula – lies deep to PITFL; continuation of interosseous membrane	Primary restraint to proximal migration of talus; limits spreading of tibia and fibula

Talocrural	**Lateral collateral ligament**		
	Anterior talofibular (ATFL)	Anterior lateral malleolus to neck of talus; usually as two bands, possible three	During plantarflexion, is primary restraint to inversion; resists anterolateral translation of talus in mortise
	Calcaneofibular (CFL)	Tip of lateral malleolus to posterolateral surface of calcaneus	Primary restraint to inversion when foot is neutral or dorsiflexed; restrains subtalar inversion
	Posterior talofibular (PTFL)	Lateral malleolar fossa to lateral tubercle of talus	Restricts internal and external rotation, talar tilt and dorsiflexion when ATFL and CFL are incompetent
	Medial collateral ligament		
	Anterior tibiotalar	Medial malleolus to neck of talus	Primary restraint to valgus tilting of talus; superficial and deep ligaments resist eversion of hindfoot; stabilization of ankle against plantarflexion, external rotation, and pronation
	Tibionavicular	Medial malleolus to dorsum of navicular	
	Tibiocalcaneal	Medial malleolus to sustentaculum tali	
	Superficial posterior tibiotalar	Medial malleolus to posterior process of talus	
	Deep anterior tibiotalar	Inferoposterior medial malleolus to posteromedial talus	
	Deep posterior tibiotalar	Inferoposterior medial malleolus to posteromedial talus	

Subtalar	Medial talocalcaneal	Posterior medial process of talus to posterior part of sustentaculum tali	Stabilization of talocalcaneal joint
	Lateral talocalcaneal	Lateral process of talus to lateral surface of calcaneus	Stabilization of talocalcaneal joint
	Posterior talocalcaneal	Lateral process of talus to upper medial part of calcaneus	Stabilization of talocalcaneal joint
	Interosseous talocalcaneal	Between articular facets of talus to corresponding depression on superior surface of calcaneus	Helps unite talocalcaneonavicular and talocalcaneal joints; binds talus and calcaneus firmly together
	Cervical	Sinus tarsi to neck of talus and neck of calcaneus	Resists inversion
Calcaneocuboid	Bifurcate	Anterior process of calcaneus to cuboid and navicular	Y-shaped ligament; divides into calcaneocuboid and calcaneonavicular; stabilization of transverse tarsal joint
	Dorsal calcaneocuboid	Dorsum of calcaneus to dorsum of cuboid	Stabilization of transverse tarsal joint
	Plantar calcaneocuboid (short plantar)	Anterior tubercle on plantar surface of calcaneus to plantar surface of cuboid posterior to groove	Helps maintain integrity of lateral longitudinal arch of foot
	Long plantar	Plantar surface of calcaneus anterior to tuberosity to cuboid and bases of 2nd, 3rd, and 4th metatarsals	Stabilization of transverse tarsal joint and helps maintain integrity of lateral longitudinal arch

Talonavicular	Plantar calcaneonavicular (spring)	Sustentaculum tali to inferior aspect of navicular	Stabilizes medial longitudinal arch and head of talus
	Bifurcate	Anterior process of calcaneus to cuboid and navicular	Y-shaped ligament; divides into calcaneocuboid and calcaneonavicular; stabilization of transverse tarsal joint
	Dorsal talonavicular	Neck of talus to dorsum of navicular	Stabilization of transverse tarsal joint
Transverse Tarsal	Please refer to calcaneocuboid and talonavicular joints as together they form this joint		

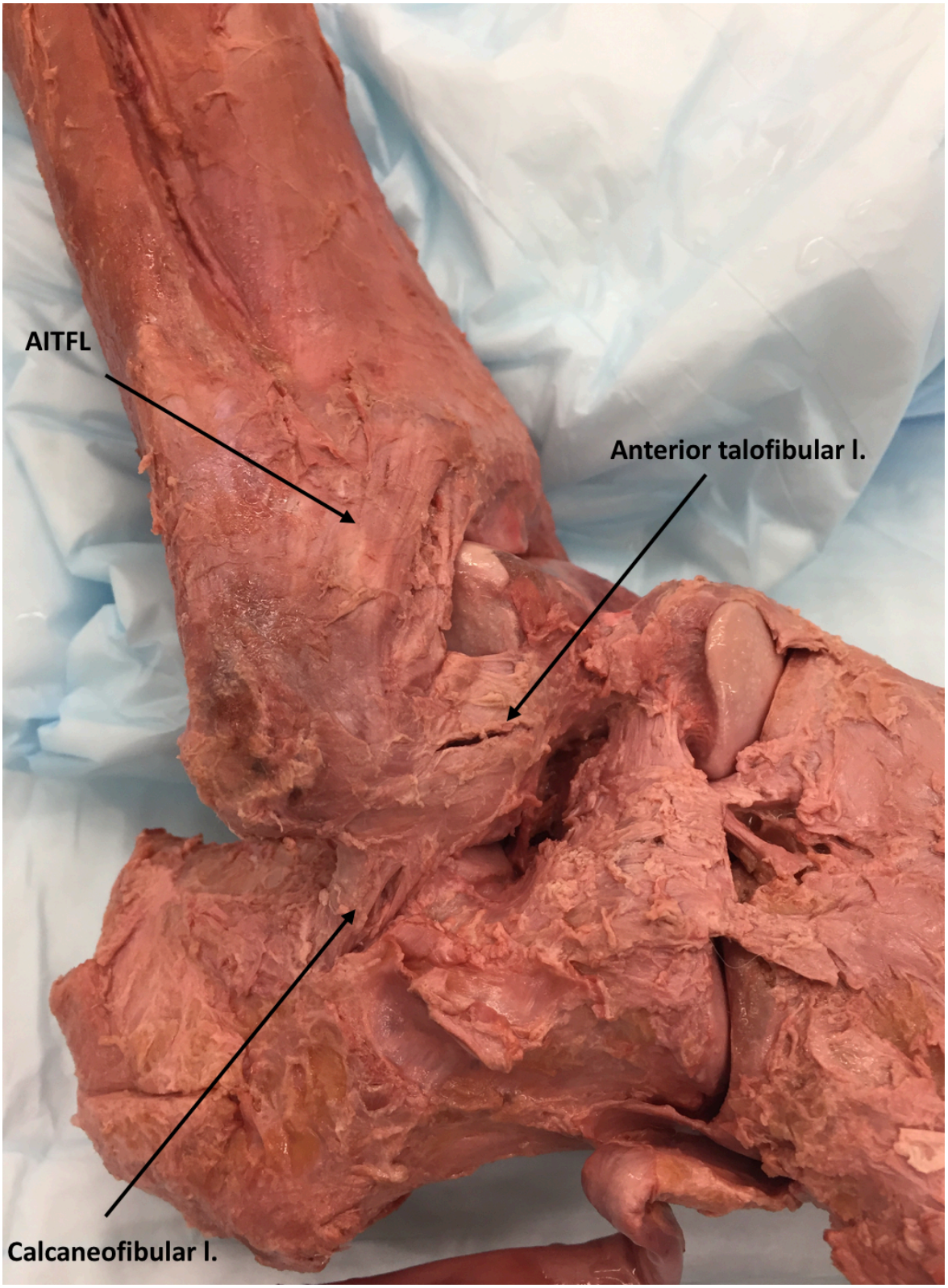

Figure 2.7. Lateral view of ankle and foot showing parts of the lateral collateral ligament (l.) complex. The anterior inferior tibiofibular ligament (AITFL) covers the syndesmosis and tibiofibular clear space, which was the focus of this study. (Photo credit: Cara Fisher)

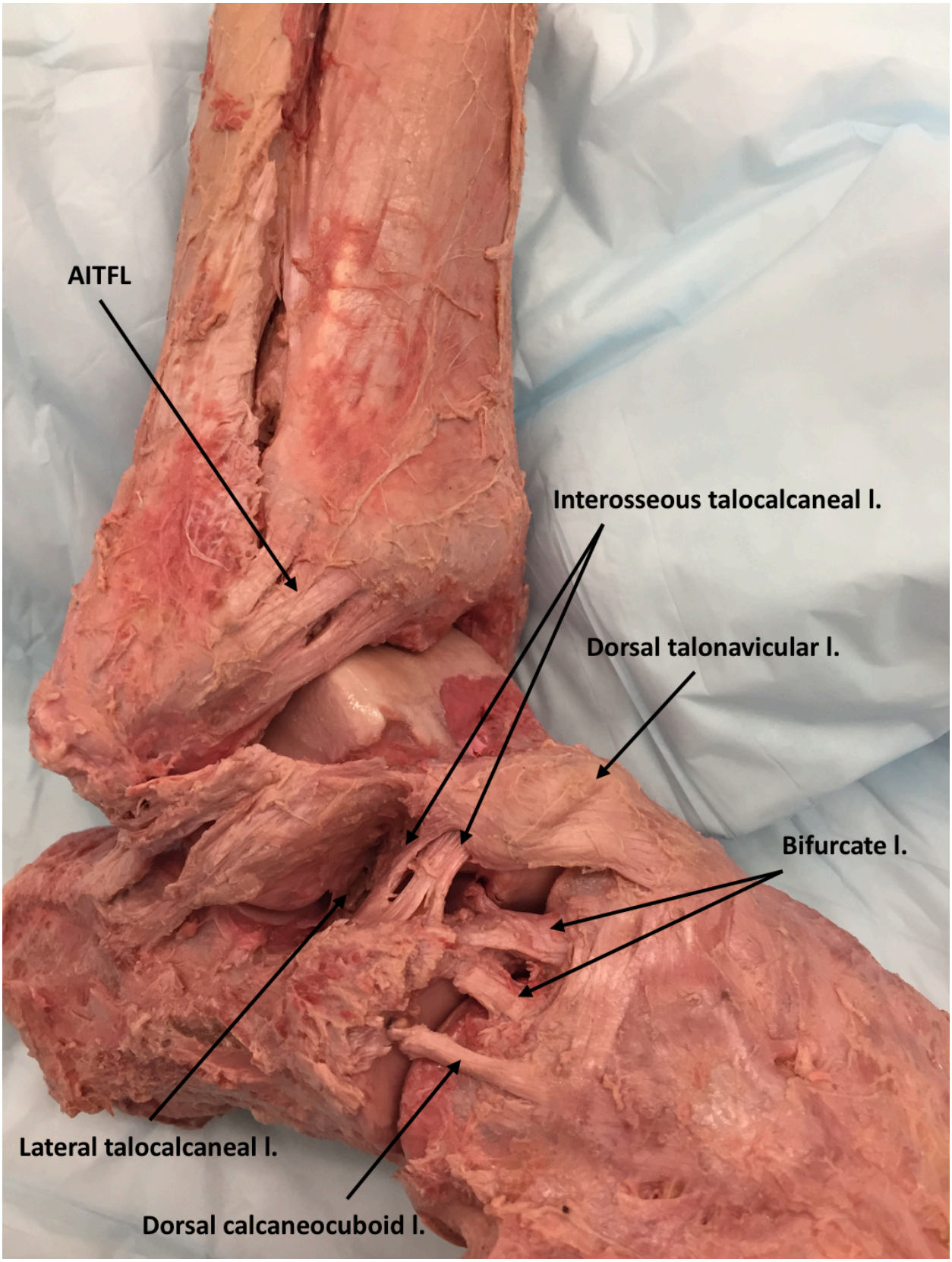

Figure 2.8. Lateral view of ankle and foot showing ligaments (l.). (Photo credit: Cara Fisher)

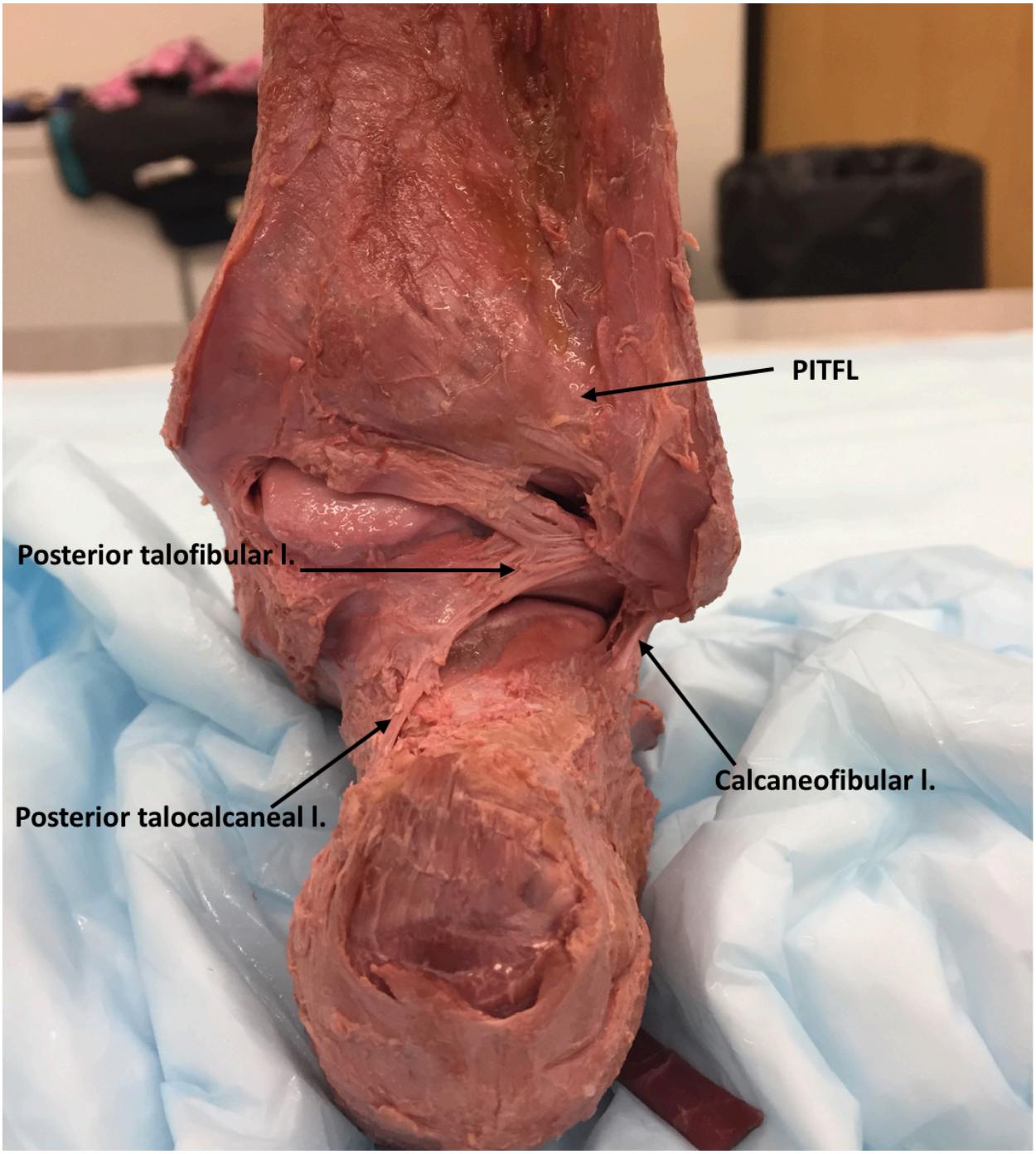

Figure 2.9. Posterior view of ankle showing posterior and lateral ankle ligaments (l.). The posterior inferior tibiofibular ligament (PITFL) covers the syndesmosis and tibiofibular clear space which was the focus of this study. (Photo credit: Cara Fisher)

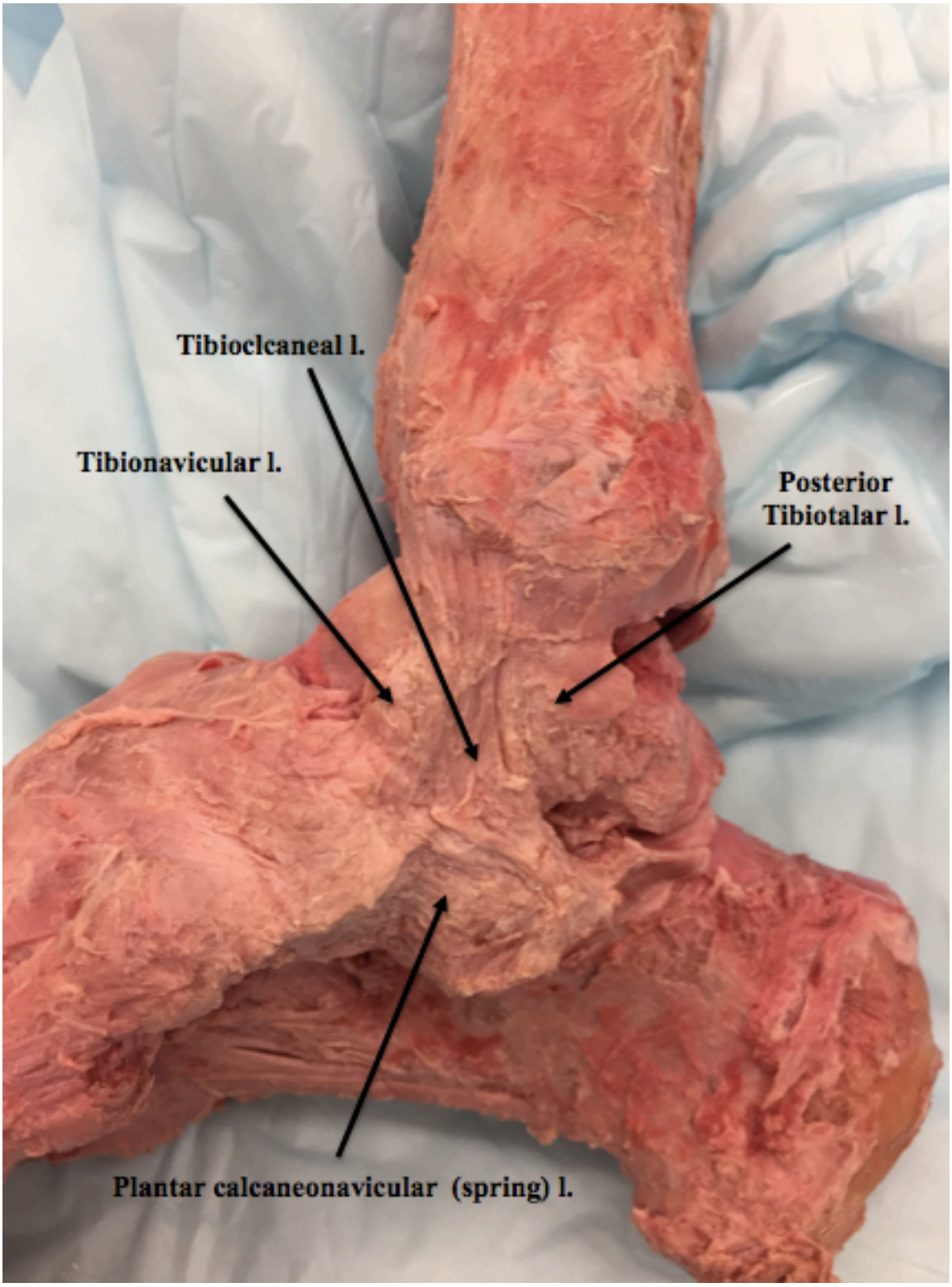

Figure 2.10. Medial view of ankle showing medial collateral ligament complex (l. ligament). (Photo credit: Cara Fisher)

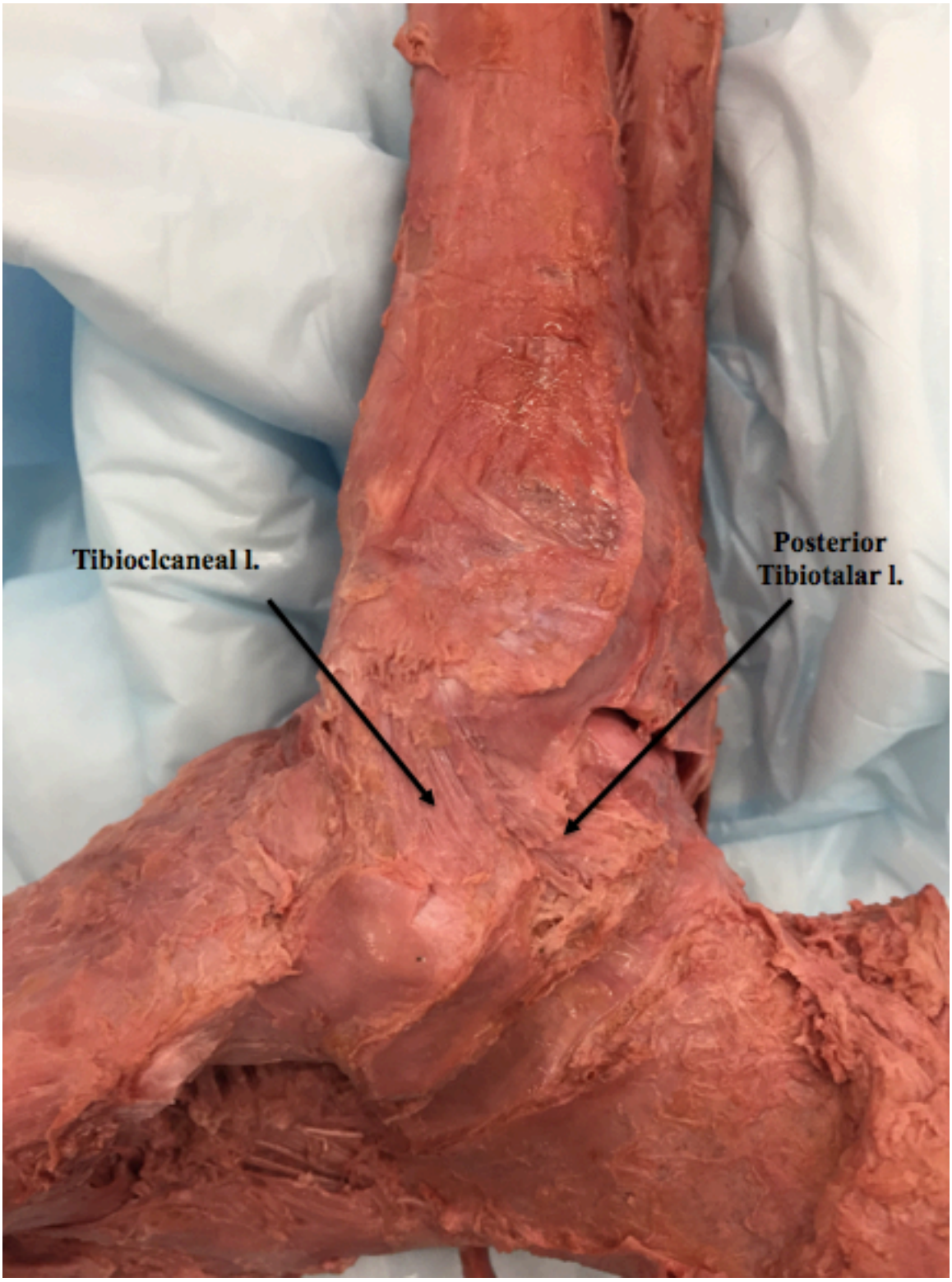

Figure 2.11. Medial view of ankle showing parts of the medial collateral ligament complex or deltoid ligament (l. ligament). (Photo credit: Cara Fisher)

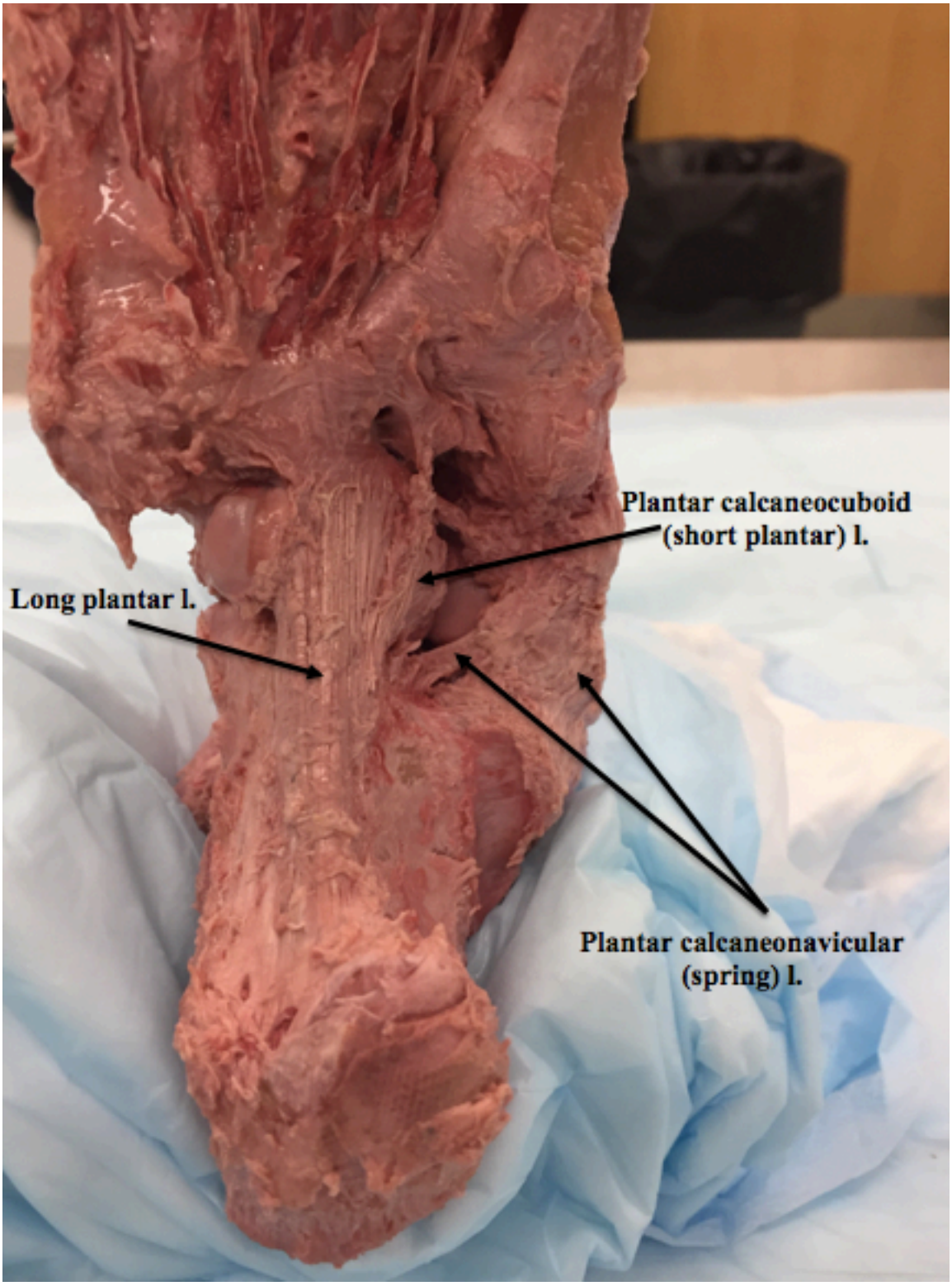

Figure 2.12. Plantar view of foot showing ligaments (l.). (Photo credit: Cara Fisher)

CHAPTER 3

BACKGROUND OF ANKLE INJURIES

This chapter covers the epidemiology, kinematics, classification system, presentation and diagnosis, and literature review of syndesmotic injuries. A review of the epidemiology of ankle injuries is discussed first, followed by a brief discussion of the kinematics of the syndesmotic ligaments. A short overview of the background of the Lauge-Hansen classification system is discussed next, followed by a discussion of syndesmotic injuries and diagnostic modalities. Finally, a review of previous research on syndesmotic injury diagnosis is presented.

3.1 Epidemiology of Ankle Injuries and Healthcare

Ankle syndesmosis and tibiotalar joint injuries are very common and are typically acute which can lead to chronic dysfunction. Ankle sprains account for 4% of all injury related visits in the United States. These patients also frequently visit the emergency room, with approximately 1.1 million visits each year.[35] The incidence of ankle sprains is approximately 210 per 100,000 annually in the United States.[36,37] Ankle fractures are equally as important to consider as the ankle is the most commonly fractured portion of the lower extremity with an estimated incidence ranging from 49-150 per 100,000 people and foot fractures having an estimated incidence of 125 per 100,000 people.[38,39] The large socioeconomic effects of these injuries are easy to foresee when you combine the essential role of the foot and ankle in musculoskeletal function and high

incidence of injury. Productive members of society typically require bipedal movement. This is especially true with working class Americans, as it is essential to perform tasks with their upper and lower extremities that require the full support of the foot and ankle to stabilize their bodies or mobilize for physical tasks. Ankle sprains alone cost the United States approximately 3.65 billion dollars in annual healthcare costs.[40,41] This large figure does not include the indirect loss of productivity to society. These indirect losses are hard to quantify, but for many patients result in a significant impact in productivity and may trigger a series of events leading to profound changes in a person's life. The combined direct and indirect costs for ankle sprain treatments were estimated between $1800 and $5270 per person. The direct costs for ankle sprains were estimated to account for between $292 and $2268 in non-hospitalized patients in the same study.[42] Unstable ankle fractures cost of treatment per patient ranged between $2860 and $19555 in direct costs, with the overall costs estimated between $8688 and $20414 per patient.[42] Clearly, foot and ankle injuries are common and place a large burden on patients and the healthcare system. The focus of the work of this dissertation is on foot and ankle structural anatomy and the use of ultrasound in ankle fractures and syndesmosis injury diagnosis.

Structural anatomy education for health professionals encompasses the entire human body, but the foot and ankle are unique in the amount of overlap of their use in multiple fields of healthcare. Physicians, physician assistants, nurse practitioners, and surgeons are all integral to lower extremity health. They must know how to diagnose, treat, and prevent foot and ankle injuries and coordinate care for their patients. Similarly, the podiatrist's entire focus is on the diagnosis and treatment of foot and ankle injuries and disease. Physical therapists are called upon to rehabilitate patients from foot and ankle injuries and evaluate patient safety and ability to perform functional tasks, which rely upon a strong base of support provided by the lower

extremity. There are approximately 20,000 physicians, 23,000 nurse practitioners, 6700 physician assistants, 9700 physical therapists, and 560 podiatrists that graduate each year with an overall approximate total of 60,000 students annually requiring foot and ankle anatomy education to become competent healthcare providers. This education includes and expands beyond the standard blood supply, innervation, origin, and insertion that are typical with musculoskeletal anatomy. The motion of the foot and ankle is one of most complicated in the body and requires thorough knowledge of the osteology and ligamentous restraints to fully grasp. Additionally, health profession schools of multiple disciplines have begun integrating ultrasound technology into their curriculums to match a rising trend in its use in practice. There has been an increasing trend towards the use of ultrasound for peripheral nerve injections, abdominal diagnostics, vascular evaluation, and a multitude of other functions where ultrasound has become essentially standard of care. Musculoskeletal ultrasound gained popularity over the past 5-10 years as insurance paid a significantly more amount of money to healthcare providers when used to guide joint and extremity injections. The use of ultrasound diagnosis of musculoskeletal injuries has been applied to rotator cuff tears, tenosynovitis, ligament tears, and several other soft tissue injuries that were traditionally diagnosed with physical exam findings and magnetic resonance imaging (MRI). Dynamic stress ultrasound evaluation of the ankle syndesmosis is another example of the expansion of ultrasound utility in healthcare.

3.2 Kinematics of the Syndesmotic Ligaments

Locomotion and function depend on a series of open and closed kinematic chains to enable performance of tasks that range from simply standing to the complexity of kicking a soccer ball. At the base of support for nearly all human functions are the foot and ankle.

The foot and ankle work in concert with the other joints in the musculoskeletal system by transmitting forces from the body to the base of support and vice versa to provide fluid movement and force. The foot and ankle have multiple centers of rotations, lever arms, and joints that enable such wide varying functions to be performed. When one of these components is disrupted it will influence all elements of motion and force proximal to the site of disruption. Common acute injuries to the foot and ankle are ligamentous sprains and fractures. These injuries disrupt the ability to transmit force and therefore motion through the kinematic chain whether open or closed. Ankle syndesmosis injury literature has focused on the contributions of the anterior inferior tibiofibular ligament (AITFL), posterior inferior tibiofibular ligament (PITFL), and interosseous ligament (IOL) to mortise stability. Classically, the most often quoted study determined the AITFL contributed 35%, PITFL 43%, and the IOL 22% to general syndesmosis stability, but only examined stability under one loading condition.[43] A recent study by Clanton et al., 2017 found that ligament contribution to syndesmosis stability is largely dependent upon the vector of loading. They found the PITFL to be the primary restraint with internal rotation and the AITFL to be the primary restraint to external rotation.[44] A simple method for predicting which vector is a ligaments principal direction of resistance to load is to draw a vector in parallel with the fibers. This method inevitably gives a simplified view of its primary role in restraining motion. However, this method does not take into account multiple ligaments working together to resist load at the same time. Jointly, the syndesmosis has three main components that act to resist translation and rotation with six degrees of freedom. The AITFL is the primary anterior restraint resisting external rotation. There are two different bone fragments that are avulsion injuries associated with the AITFL. The Wagstaff fragment is an avulsion of the AITFL from the fibula and the Chaput fragment is an avulsion from the tibia. The

PITFL is the primary posterior restraint resisting internal rotation. When there is an avulsion involving the posterior malleolus of the tibia that has a PITFL attachment it is called a Volkmann fragment. The IOL is the primary restraint to lateral translation. The three ligaments work in concert to keep the fibula well seated within the concavity of the incisura of the tibia.

3.3 Lauge-Hansen Classification

As mentioned in the introduction, the different stages of ankle syndesmotic injuries are determined using the Lauge-Hansen classification system. This system was developed using radiographs as the basis for identifying the different stages of ligamentous and fracture injury patterns. This classification system categorizes injuries based off their mechanism of injury and starting position of the ankle when the injury occurs. It also delineates the direction of force and order of ligamentous or bone injury that can help assess possible syndesmosis injury. There are four Lauge-Hansen classifications and their accompanying injury predictions.[45-47] Stage 1 supination-adduction (SA) injury typically results in talofibular ligament sprain or avulsion of the distal fibula while stage 2 a vertical fracture of the medial malleolus or impaction of the anteromedial part of the distal tibia. Supination-external rotation (SER) stages and injuries have been summarized in Table 1.1. Pronation-abduction (PA) injuries have three stages. Stage 1 will either result in a transverse medial malleolar fracture or rupture the deltoid ligament. Stage 2 will sprain the AITFL and Stage 3 injury constitutes transverse comminuted fracture of the fibula, proximal to the syndesmosis. Lastly is the pronation-external rotation (PER) classification. This classification has four stages. Stage 1 is similar to stage 1 of the PA injury. Stage 2 results in the disruption of the AITFL. Stage 3 results in a lateral short oblique or spiral fracture of the fibula. This fracture goes from anterosuperior to posteroinferior and occurs proximal to the

syndesmosis. Stage 4 will rupture the PITFL or result in a posterior malleolar fracture. Gardner et al., found that 49 of 59 ankle fractures, diagnosed utilizing radiograph and MRI, could be fit into the Lauge-Hansen classification system. However, 53% of those did not have ligamentous or fracture injury patterns that fit Lauge-Hansen predictions.[48] Even with these limitations, this system of prediction is still widely used.

3.4 Presentation and Diagnosis of Syndesmotic Injuries

Syndesmotic injuries can be subtle with only soft tissue injury or present frankly with concomitant fracture. Tenderness upon palpation over the anterior and posterior tibiofibular ligaments and the tibiofibular clear space is common with this type of injury.[49] During the acute phase, swelling might also be palpable proximal to the ankle joint[49,50] or at/above the AITFL.[51-53] Ankle injuries are not always prone to severe swelling because it is possible to have extracapsular tissue damage.[49]

Even though syndesmosis injuries are common, they are difficult to diagnose and treat. Assessing ankle syndesmosis injuries involves provocative testing and imaging. The primary measurements for assessment of syndesmosis injury are a tibiofibular clear space < 6 mm and the medial clear space < 4 mm for normal values. This is typically measured when the ankle is in dorsiflexion as the anterior talus is slightly wider than the posterior portion leading to a slight widening of the syndesmosis.

The most common clinical situation involved with syndesmosis injuries is ankle fractures. Clinical suspicion of a syndesmosis injury is high when a fracture is found on plain radiographs. Initial provocative tests performed clinically may lead a physician to more thoroughly investigate a syndesmosis injury, but the reliability of these tests (Table 3.1) is

frequently called into question.[54,55] Proper treatment of syndesmosis injuries requires prompt and accurate diagnosis to prevent the long-term sequelae of osteoarthritis and decreased function due to biomechanical changes and pain. The ligaments of the ankle syndesmosis prevent diastasis and contribute some stability to the ankle joint as a whole. The ligaments that comprise the syndesmosis are the AITFL (Figures 2.7 and 2.8), IOL, and the PITFL (Figure 2.9). The diagnosis and treatment of the syndesmosis injuries are typically focused on the AITFL and PITFL, as they are the major contributors to syndesmosis integrity.[2-5] Plain film radiographs and stress fluoroscopy are the traditional diagnostic modalities of choice, but current literature have shown lower sensitivity and specificity than initially perceived.[6,7] Dynamic ultrasound examination of the ankle syndesmosis has recently grown in popularity due to its cost effectiveness and simple function. However, widespread adoption of dynamic ultrasound examination for the ankle has slowed due to a lack of training and research. For ankle syndesmosis injuries, proper reduction, returning the bone to its normal anatomy, of the fibula in the tibial incisura is essential to proper treatment and requires imaging or direct visualization to verify. Traditional plain film radiographs and stress fluoroscopy have shown to be inconsistent methods for accurate diagnosis and fibular reduction verification.[6-8] Most commonly, plain film radiographs and stress fluoroscopies are used to evaluate the ankle syndesmosis with advanced imaging being reserved for subtle cases with high clinical suspicion. However, current definitive diagnosis can be made with computed tomography (CT) and MRI that are costly and require the patient to receive radiation with the use of CT. Diagnostic capabilities must be refined to improve cost efficiency and diagnostic accuracy to avoid long-term sequelae of syndesmotic diastasis and improve outcomes by identifying malreductions.

Table 3.1. Description of provocative tests used to help diagnose supination-external rotation ankle injuries.

Test	Protocol	Positive Findings
1. Cotton Test[54]	Distal tibia stabilized, lateral force applied to calcaneus	Increased lateral translation of talus from medial to lateral compared to contralateral side
2. Intraoperative Cotton Test[56]	Distal fibula is grasped and pulled laterally	Syndesmosis and/or mortise are widened
3. Intraoperative Modified Cotton Test[57]	Fibula is pushed or pulled in the sagittal plane while lateral radiograph is obtained	Syndesmosis and/or mortise are widened
4. Squeeze Test[54]	Compression of fibula to tibia above midpoint of calf	Pain over area of syndesmosis
5. Cross Leg Test[54]	Injured leg crossed over uninjured leg while seated; gentle downward pressure on knee of injured leg	Pain over area of syndesmosis
6. External Rotation Test[58]	Knee bent at 90°; one hand stabilizes patient's leg, while the other applies an external rotational force to the foot in neutral position	Pain over AITFL, PITFL, and interosseous membrane
7. Dorsiflexion Compression Test[59]	Patient stands and actively dorsiflexes foot – should cause pain; examiner applies compression to both malleoli at the same time	Reduction of pain or increased range of motion, or both

3.5 Review of Previous Syndesmotic Research

Advances in ultrasonic equipment have led to an increased use of this technology in diagnosing lateral collateral and syndesmotic ligament injuries. Milz et al., (1998)[60] used high frequency ultrasound to diagnose injury to the lateral collateral ligaments and AITFL in twenty patients that were clinically suspected of having rupture and/or injury and compared their ultrasound results to MRI. Anterior talofibular ligament tears were diagnosed correctly in thirteen out of fourteen cases and five cases appeared to be intact according to both methods.

One case could not be diagnosed via MRI, but appeared to be an incomplete tear based on ultrasonography. Ultrasound correctly diagnosed the four cases that had an injured calcaneofibular ligament and the other sixteen cases, the calcaneofibular ligaments were found to be intact using both ultrasound and MRI. The AITFL was ruptured in nine of the cases and ultrasound was able to diagnose six of those, while three of the nine appeared to have no injury. An incomplete rupture was shown by ultrasound in one case, but was not able to be confirmed by MRI. The last ten cases had no injury to the AITFL and this was confirmed by both methods. Interestingly, in the sixty ligaments investigated in this study, there was disagreement between MRI and ultrasound in only six cases. The authors suggest confounding factors leading to these disagreements could include a divided ligament (a ligament with three bands and only one is ruptured for example), fluid buildup from minor injuries, which can alter the signal in an MRI, leading to a misdiagnosis of a ligament injury where ultrasound found none, and accessory fibers with the ligament itself.

Mei-Dan et al., (2009)[61] evaluated the use of dynamic ultrasound to diagnose syndesmotic injuries in professional athletes. Three different groups were evaluated: nine professional athletes with a recent syndesmotic injury, eighteen subjects with no history of ankle injury, and twenty subjects with lateral ankle sprain. The tibiofibular clear space appeared normal in all athletes when examined using a radiograph and ankle fractures were ruled out using radiography as well. All athletes with complete tears of the AITFL were confirmed by magnetic resonance imaging (MRI). They examined the syndesmosis under three different states: internal rotation, external rotation, and neutral utilizing dynamic ultrasound. The ultrasound probe was placed 1 cm proximal to the tibial plafond at the level of the AITFL. After completing the study protocol, there were statistically significant differences found between the control group and the

injured athletes in all three states. The authors concluded that dynamic ultrasound was successful in accurately diagnosing a complete tear in the AITFL (Stage 1 Lauge-Hansen Injury) and that damage to the lateral collateral ligament complex could not be correlated to AITFL injury using dynamic ultrasound.

Developing standard values for normal tibiofibular clear space width using ultrasound is necessary in order to better diagnose syndesmotic widening. The accepted value for normal tibiofibular clear space width is <5-6 mm.[62] Mei-Dan et al., (2013)[63] evaluated 110 healthy subjects to determine normal values for tibiofibular clear space measurements using dynamic ultrasound. There were fifty-nine males and fifty-one females, mean age 32 (range 16-60) as part of this study. Gender, height, age, activity level, calf length, and leg dominance were taken into account. Calf length was calculated by measuring from the tibial tuberosity to the medial malleolus (mean 35 cm, range 30-41 cm). Participants were divided into two groups: those over 40 years of age (42 participants), and those under 40 years of age (68 participants), with 66% of the subjects being involved in professional sports in some manner. The right leg was dominant in 83% of the cases. The clear space was measured using dynamic ultrasound at neutral (N), forced internal rotation (IR), and forced external rotation (ER) with the foot in 5-10 degrees of dorsiflexion. Functional mean position measurements were 3.7 mm for the N position, 3.6 mm with IR, and 4.0 mm with ER. It was found with younger participants, men and women, that the clear space was significantly wider in the neutral position. Young men and women had a 3.8mm widening with N, whereas older individuals widened to 3.4 mm. The same was true when rotational force was applied. Young men and women had a 4.1 mm widening, where as older men widened only to 3.6 mm and older women to 3.8 mm. Interestingly, there was no correlation between height, activity, or leg length and widening of the tibiofibular clear space.

Also interesting was that females tended to have a higher widening ratio under rotational stress compared to neutral than males did. This was most common in those subjects who were active. Overall, the study by Mei-Dan et al., (2013) helped confirm the long used standard of <5-6 mm for normal tibiofibular clear space measurements.

Separation of the tibia and fibula after syndesmotic rupture can be seen with anterior posterior (AP) and mortise views but is often missed if the injury is subtle. Beumer et al., (2003)[64] utilized lateral radiography (LAT) and radiostereometry (RSA) to diagnose syndesmotic injuries caused by external rotational stress (7.5 Nm) on ten cadaveric legs that had all collateral and syndesmotic ligaments intact. All soft tissue from the knee to the tarsometatarsal joints was removed with the exception of the ligaments. The specimen was then placed in a device that secured the tibia, but allowing free movement of the fibular and ankle. After placing the specimens through the study protocol, lateral and RSA radiographs were taken. All measurements were taken 1 cm superior and parallel to the tibiotalar joint. Rotation and translation of the fibula were measured twice by three different observers and the mean of all six measurements was calculated. It was concluded that translations and rotations of the fibula prior to sectioning of two or more ligaments was too small to be detected by RSA and that LAT radiographs found posterior displacement two to three times greater than RSA and similar to those found by Xenos et al.[65] Overall, they found it was not possible to distinguish between healthy and injured syndesmotic injuries using conventional radiography.

Challenging the idea that conventional radiography was not as reliable as stress views and CT was a study done by Croft et al., (2015).[62] Typically AP, lateral, and mortise views are required when ankle injury is suspected. Usually it is the AP and mortise views that are used to identify the injury to the ankle syndesmosis. The suggestion of this study was to add an

orthogonal component to the lateral view, which is underutilized, thus increasing diagnostic reliability. Three orthopedic surgeons reviewed 72 normal radiographs, 35 men and 37 women, mean age 44 years. They documented four different measurements: tibial and fibular width (TW and FW respectively), anterior tibiofibular interval (ATFL), and posterior tibiofibular interval (PTFL). Measurements were taken 1 cm proximal to the tibial plafond. Creating ratios that described the relationship of the tibia and fibula, PTFL:TW, ATFL:TW, PTFL:(PTFL+FW), and ATFL:(ATFL+FW), they developed a ratio that describes what a healthy syndesmosis should look like. The anterior tibiofibular ratio (ATFR) characterizes the ATFL:TW ratio listed above. Based on their results, about 40% of the tibia should be anterior to the anterior fibular cortex at the point 1 cm proximal to the tibial plafond. They found no significant differences with regards to age or sex. This ratio should be a tool to use with lateral radiographs to define the ankle syndesmosis and can be used to show what the normal relationship between the tibia and fibula should be. It should be noted that this study was not validated on ankles with syndesmosis injuries, so the diagnostic capabilities of radiography are still not reliable.

CHAPTER 4

MATERIALS AND METHODS

This chapter covers the specimens, equipment, and experimental methods utilized in this study. A review of the specimens used in the study, including the rationale for excluding female specimens is covered first, followed by a description of the equipment used. This is followed by a discussion of the methods used to prepare the specimens and a detailed description of the experimental protocols. Finally, image processing and statistical methods are discussed.

4.1 Materials

Eleven, all male, fresh frozen specimens (n=9), aged 41-81 years (mean 54) were used for this study. Sample size is consistent with other orthopedic studies of this type.[2,11,44,64,66] All had intact tibiofibular articulations and were free of any gross ankle pathological conditions. Each specimen was serology tested for HIV 1 & 2, and Hepatitis B and C, prior to use and personal protective equipment was worn at all times. Specimens were identified by their state anatomical board (SAB) number and whether the specimen was right (R) or left (L).

Specimen one was 69091L. He was a 5’7” 158lb 62-year-old Caucasian male with a body mass index (BMI) of 24.7. He had a hip replacement and suffered from early onset Alzheimer’s. The donor smoked one cigarette a day and had one glass of wine per day. Causes of death were

listed as end stage sepsis due to *E.coli*, urinary tract infection (UTI) with peritonitis, acute renal failure, and hypertension. This donor passed away in March of 2016. Specimen 69091L was received on March 30 2016 and it was immediately placed in the freezer. This specimen was thawed at room temperature 24 hours prior to its preparation and use in the research protocol on July 16, 2016.

Specimen two was 69071L. He was a 5'10" 160lb 70-year-old Caucasian male with a BMI of 23. This donor had a history of varicose veins, osteoporosis, arthritis, myocardial infarction (MI), stroke, and chest pain. He underwent angioplasty after his heart attack. The donor had a 61-year smoking history and a 28-year alcohol use history. This donor passed away from a MI, chronic obstructive pulmonary disease (COPD), and hypertension in March of 2016. Specimen 69071L was received on March 30, 2016 and it was immediately placed in the freezer. The specimen was thawed at room temperature 24 hours prior to its preparation and use in the research protocol on July 16, 2016.

Specimens three and nine were 69084L and 69084R respectively. This donor was a 5'10" 200lb 41-year-old Hispanic male with a BMI of 28.7. Further medical information is not available on this donor as he was unclaimed from the Dallas County Medical Examiner. He passed away from acute ethanol poisoning in March of 2016. These specimens were received on March 30, 2016 and they were immediately placed in the freezer. These specimens were thawed at room temperature 24 hours prior to preparation and use in the study. Specimen 69084L was put through the research protocol on July 17, 2016 and 69084R on July 23, 2016.

Specimens four and eight were 69102L and 69102R respectively. He was 6'0 174lb 63-year-old Caucasian male with a BMI of 23.6. This donor had a history of diabetes, stroke, gastroesophageal reflux disease (GERD), stage 2 chronic kidney disease, heart disease, eye

issues, gastrointestinal (GI) issues, and had a knee replacement in the 1980s. This donor passed away from diabetes and a stroke in March of 2016. The specimens were received on March 30, 2016 and they immediately placed in the freezer. The specimens were then thawed at room temperature 24 hours prior to preparation and use in the study. Specimen 69102L was put through the research protocol on July 17, 2016 and 69102R on July 22, 2016.

Specimens five and six were 69100L and 69100R respectively. This donor was a 6'0 150lb 49-year-old Caucasian male with a BMI of 20.3. He had a history of Schizophrenia, clinical depression, bi-polar disorder, and COPD. He had an index finger amputated due to snakebite. The donor had smoked marijuana, drank beer daily, and smoked cigarettes for 30 years. He passed away from COPD and MI in March of 2016. I received the specimens on March 30, 2016 and they were immediately placed in the freezer. The specimens were thawed at room temperature 24 hours prior to preparation and use in the study. Specimen 69100L was put through the research protocol on July 17, 2016 and 69100R on July 19, 2016.

Specimen ten was 67416L. He was a 224lb 81-year-old Caucasian male who passed away from septic shock, severe encephalopathy, and respiratory failure on November 7, 2016. This donor came from a different Willed Body Program and they did not collect an extensive personal and/or medical history. I received this specimen November 9 and immediately placed it into the freezer. This specimen was thawed at room temperature 24 hours prior to preparation and use in the study. This specimen was put through the research protocol on December 15, 2016.

Specimen eleven was 65499L. He was a 223lb 75-year-old male who passed away from end stage congestive heart failure and coronary artery disease on September 28, 2016. This donor came from a different Willed Body Program that did not collect extensive personal and/or medical history.

I received the specimen on October 1 and it was immediately placed in the freezer. The specimen was brought out to thaw at room temperature 24 hours prior to preparation and use in the study. This specimen was put through the research protocol on December 20, 2016.

Female specimens were excluded for several reasons. The top three most common risk factors for fragility fractures are age, female gender, and Caucasian race.[67] Most donor specimens are older in age, which predisposes the females to osteoporosis. As a result, their bones do not effectively resist rotational stress. A study by Friedman and Mendelson found that "the lifetime incidence of any osteoporotic fracture is estimated to be 40% to 50% in women and 13% to 22% in men."[67] Three intact female specimens were tried in another external rotational kinematic study that I participated in and all three had their fibulas fracture within the 30-50 N range (unpublished data). Female donor 65473R's fibula fractured on the first rotation at 30 N in the Normal phase. Because of this early failure, and the failures of the female specimens in the earlier study, I realized that female specimens would not make it through the necessary protocol. Thus female specimens were excluded from this research study. Studies by Clanton et al., and Hunt et al., also utilized all male specimens.[11,44] Even utilizing only male specimens resulted in some early fractures. Donor 65498L suffered a tibial fracture on the first rotation at 50 N in the Normal phase. The poor quality of 65498L's bone was apparent upon specimen preparation. When scraping the periosteum off the bone, his cortical bone was scraped away as well. The fibula fractured on donor 69071R at 70 N on the third rotation, also in the Normal phase. Again, this is most likely due to the age of the donors and disease processes they have undergone.

4.2 Equipment

In Vitro Simulation Ankle Rig

An ankle rig and foot-mounting block was designed in-house by Addison Wood D.O., Ph.D. to fix the tibia and allow free fibular movement. The design for the ankle rig and foot-mounting block is original, but was loosely based on research by Hunt et al.[11] Barrett Cromeens D.O., Ph.D., designed the moveable metal stand holding the foot-mounting block for use in a previous study that I participated in looking at specific ankle ligaments. The combination of ankle rig and foot-mounting block was used to perform a controlled external rotation stress test that holds the foot fixed in five degrees of freedom, while allowing rotation in the transverse plane (Figure 4.1). Torque was recorded via a torque sensor (TRT-200, Transducer Techniques, Temecula CA) that was embedded in the foot- mounting block. This torque sensor tracked internal/external forces placed on the ankle by the examiner during rotational stress. Ankle position and movements of the fibular were recorded using an electromagnetic tracking system (Polhemus, Liberty System). The tracking system was used solely for foot positioning by acting as an electronic goniometer. No muscle loads or axial forces were applied to the specimen.

Fluoroscopic C-Arm

The c-arm was manufactured by OEC; model number 9600 ESP. This model includes a 4/6/9" tri-mode image intensifier, dual hi-resolution monitors, and a rotating anode x-ray tube. It has a charge-coupled device (CCD) camera for digital imaging. The SAB number and L or R was entered as the patient information to allow easy tracking of images and corresponding specimens. This c-arm was utilized because it was owned by the department and was more affordable than renting.

A mini c-arm might have made positioning easier, but is expensive and does not have the penetration capabilities of a full sized c-arm. A radiology technician was not used for this project, as it was cost prohibitive. Lead aprons and thyroid collars were utilized anytime this equipment was in use.

Ultrasound

The ultrasound (US) unit used for this project was a GE Healthcare Venue 40 and a 4-13 MHz probe. Ultrasound gel was placed under the skin flap and over the tibiofibular clear space to fill in gaps in order to achieve the highest image quality possible. This ultrasound unit was utilized because it was owned by the department making it a cost effective option.

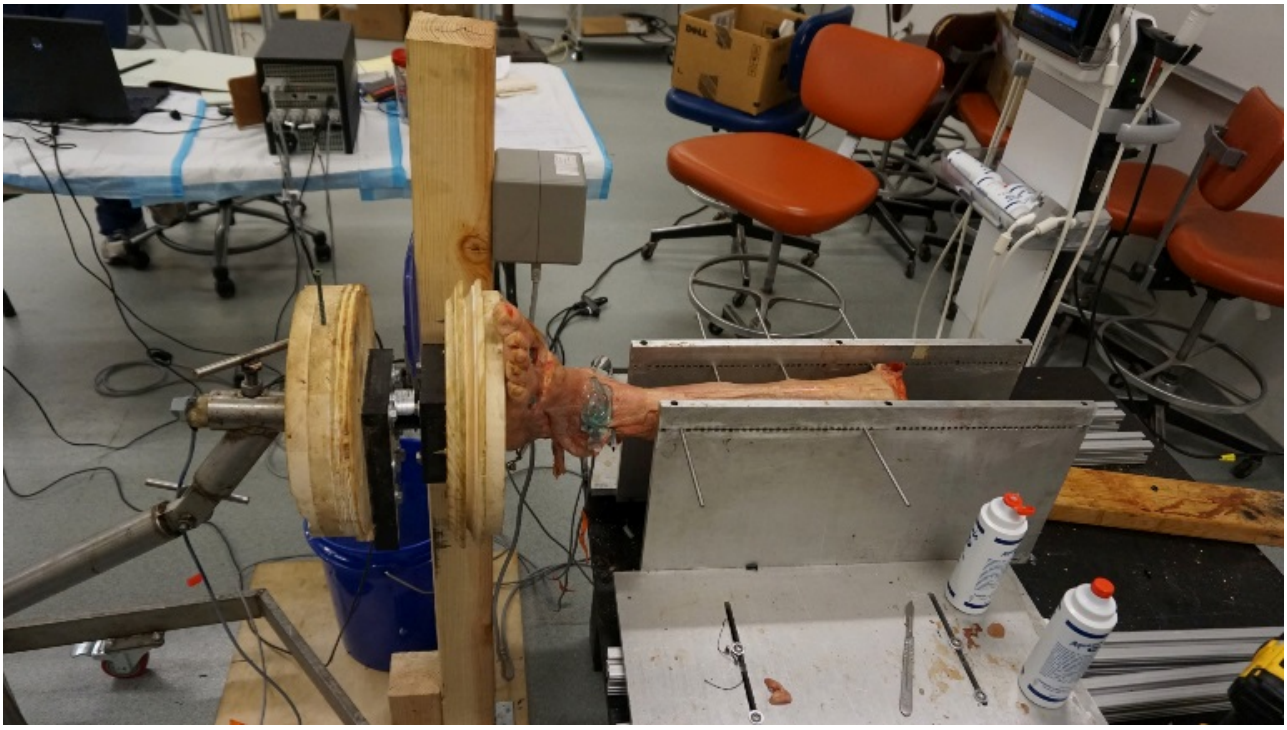

Figure 4.1. Image showing the set up for the ankle rig and foot-mounting block. (Photo credit: Addison Wood)

4.3 Methods

Preparatory Specimen Dissection

After thawing the specimens, dissection began with a lateral Kocher approach, done by incising the skin inferior and posterior to the fibula. The skin and superficial fascia was then reflected medially as a unit to expose the anterior inferior tibiofibular ligament (AITFL) and removed posteriorly to expose the posterior inferior tibiofibular ligament (PITFL). All musculature was kept intact around these ligaments and the inferior flexor retinaculum was released. Medially, the skin and superficial fascia was reflected away from the medial malleolus as a unit. The structures passing posterior to the medial malleolus were cut and reflected to expose the deltoid ligament (Figure 4.2). This ligament was cleaned so its borders were defined. All syndesmotic structures were directly inspected visually to ensure no prior trauma, surgery, or other confounding factor.

The periosteum was scraped off of the medial surface of the distal tibia and the posterior surface of the distal tibia. Two small holes, measured to fit the holes on the sensors, were then drilled in the medial surface of the distal tibia and the posterior surface of the distal fibula. These holes were then threaded (Figure 4.3) and cleaned using brake cleaning fluid to decrease adipocity in the area so the epoxy would set (Figure 4.4). Nylon screws were then placed into the holes and secured with epoxy (Figure 4.5). Once they had been allowed to dry for a few minutes, the screw heads were cut off (Figure 4.6).

Figure 4.2. Medial view of deltoid ligament in the process of being dissected. (Photo credit: Cara Fisher)

Figure 4.3. Threading the screw holes for the plastic sensor screws. (Photo credit: Cara Fisher)

Figure 4.4. Decreasing adipocity in the screw holes with brake cleaning fluid. (Photo credit: Cara Fisher)

Figure 4.5. Fixing nylon screws into holes with epoxy. (Photo credit: Cara Fisher)

Figure 4.6. Screws with tops cut off setting up after application of epoxy. (Photo credit: Cara Fisher)

Mounting to the Ankle Rig

To place the specimen into the ankle rig, the foot was first secured to a wooden wheel that would later be attached to the foot-mounting block. A large deck screw was placed through the center of the wooden wheel up through the calcaneus and into the center of the talus from the plantar aspect of the foot (Figure 4.7). This was done to create a subtalar fusion to limit or remove any midfoot or forefoot motion, thereby preventing erroneous measurement of subtalar motion. On the dorsum of the foot, 2-3 smaller deck screws were placed between the metatarsals to hold the foot onto the wheel (Figure 4.8). The tendons were cut surrounding the screws on the dorsum of the foot so they did not create pull on the tibia or fibula. Once the specimen was secured to the wheel, it was then placed into the ankle rig and secured using four Steinmann pins placed into the tibia using a drill. These pins were placed anterior to the fibula to ensure free movement of the fibula at all times (Figure 4.9). Electromagnetic tracking sensors were then placed on the screws in the tibia and fibula. The sensors were held in place on the screws with plastic tubing and small white nuts put onto the screws (Figure 4.10). Sensor one was always placed on the tibia and sensor two was always placed on the fibula. Once the specimen was securely in the ankle rig, the foot with wooden wheel was attached to the foot-mounting block using four large deck screws positioned at different points around the wheel. Care was taken to avoid contact with the torque sensor block. The foot-wheel-mounting block combination and the center of the talus were carefully aligned with the torque sensor's center of rotation. The third electromagnetic sensor was placed on the foot-mounting block in line with the second digit of the foot that was in alignment with the anterior border of the tibia (Figures 4.11 and 4.12).

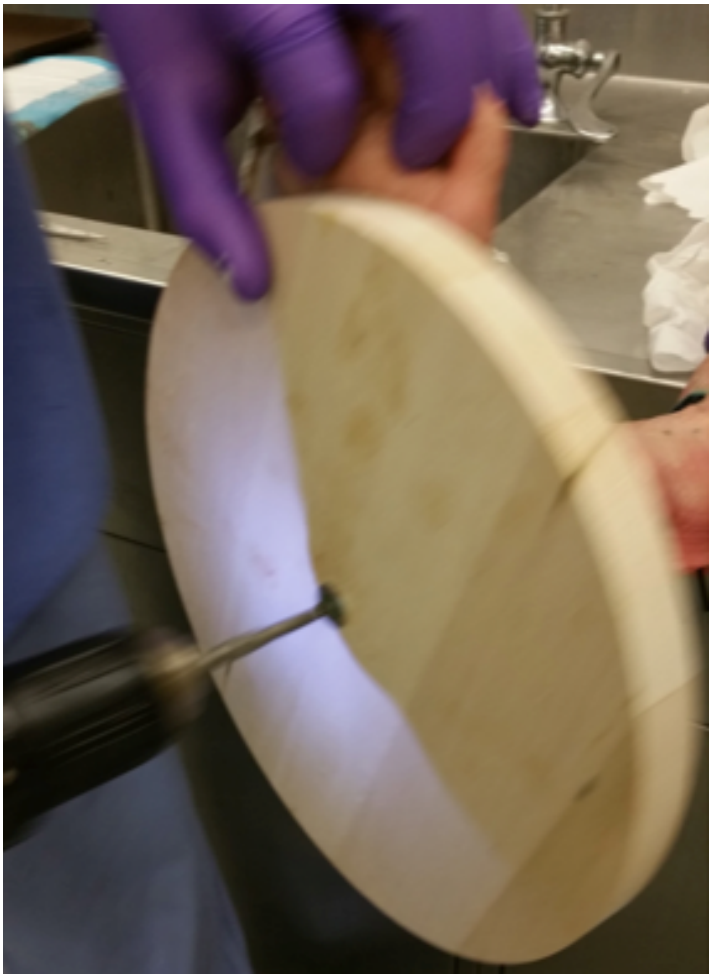

Figure 4.7. Drilling the large deck screw through the center of the wooden wheel, up through the calcaneus, and into the center of the talus. (Photo credit: Addison Wood)

Figure 4.8. Drilling smaller screws into the dorsum of the foot to secure it to the wooden wheel. (Photo credit: Addison Wood)

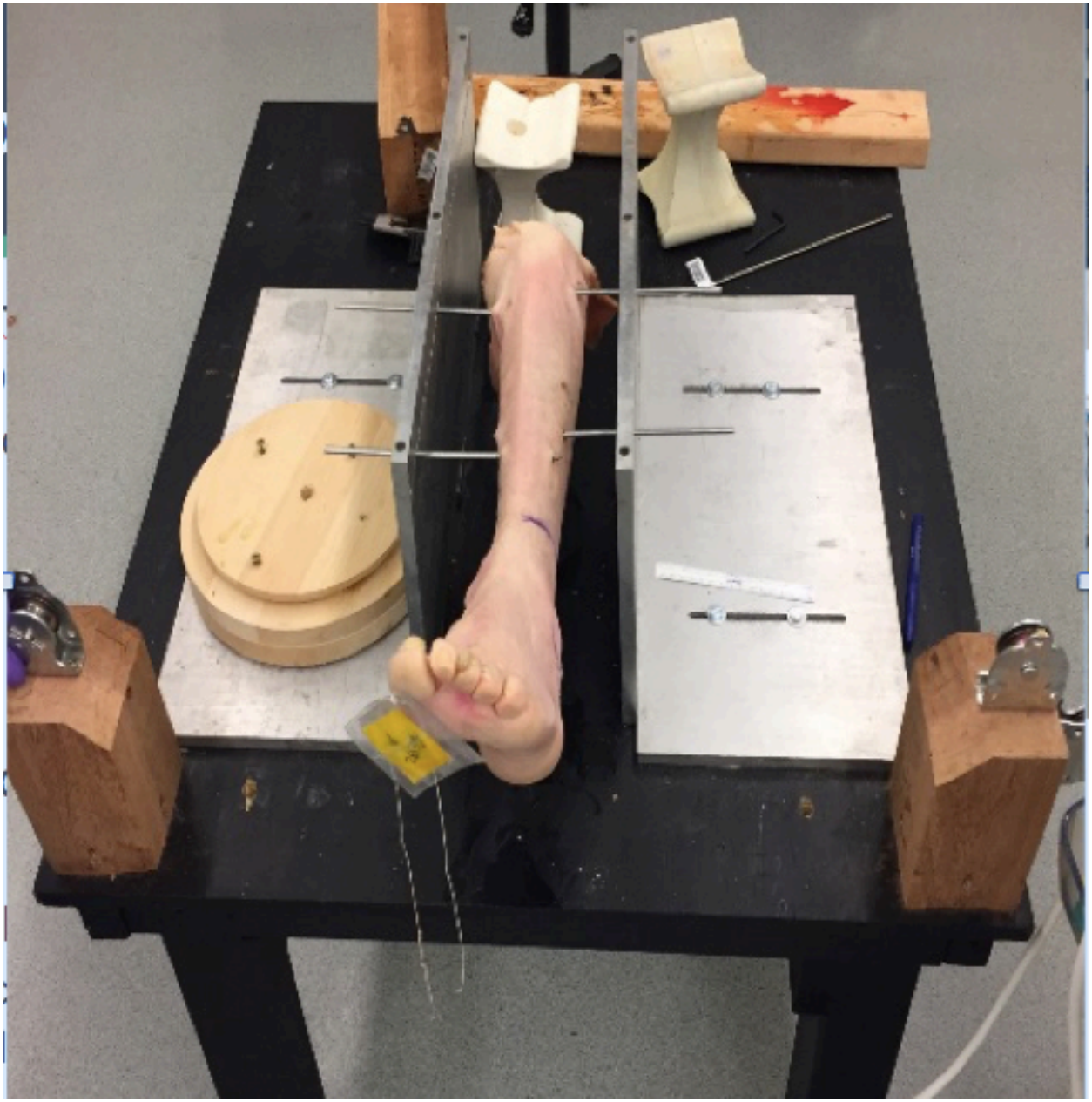

Figure 4.9. Specimen in ankle rig with four Steinman pins placed anterior to the fibula. (Photo credit: Addison Wood)

Figure 4.10. Polhemus sensor on tibia. The same set up was used for sensor two on the fibula as well. (Photo credit: Cara Fisher)

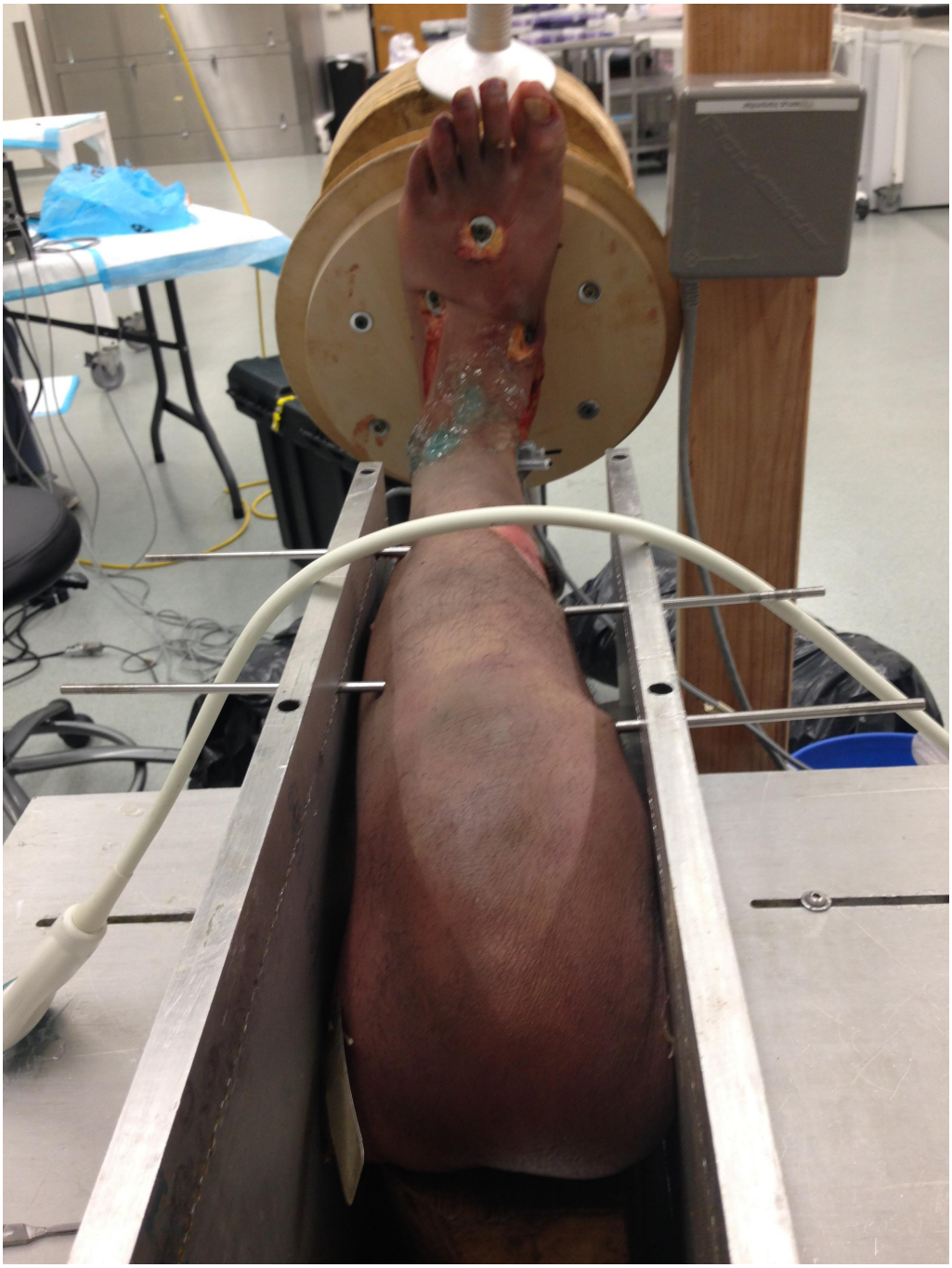

Figure 4.11. Proximal view of ankle in ankle rig and foot-mounting block. (Photo credit: Addison Wood)

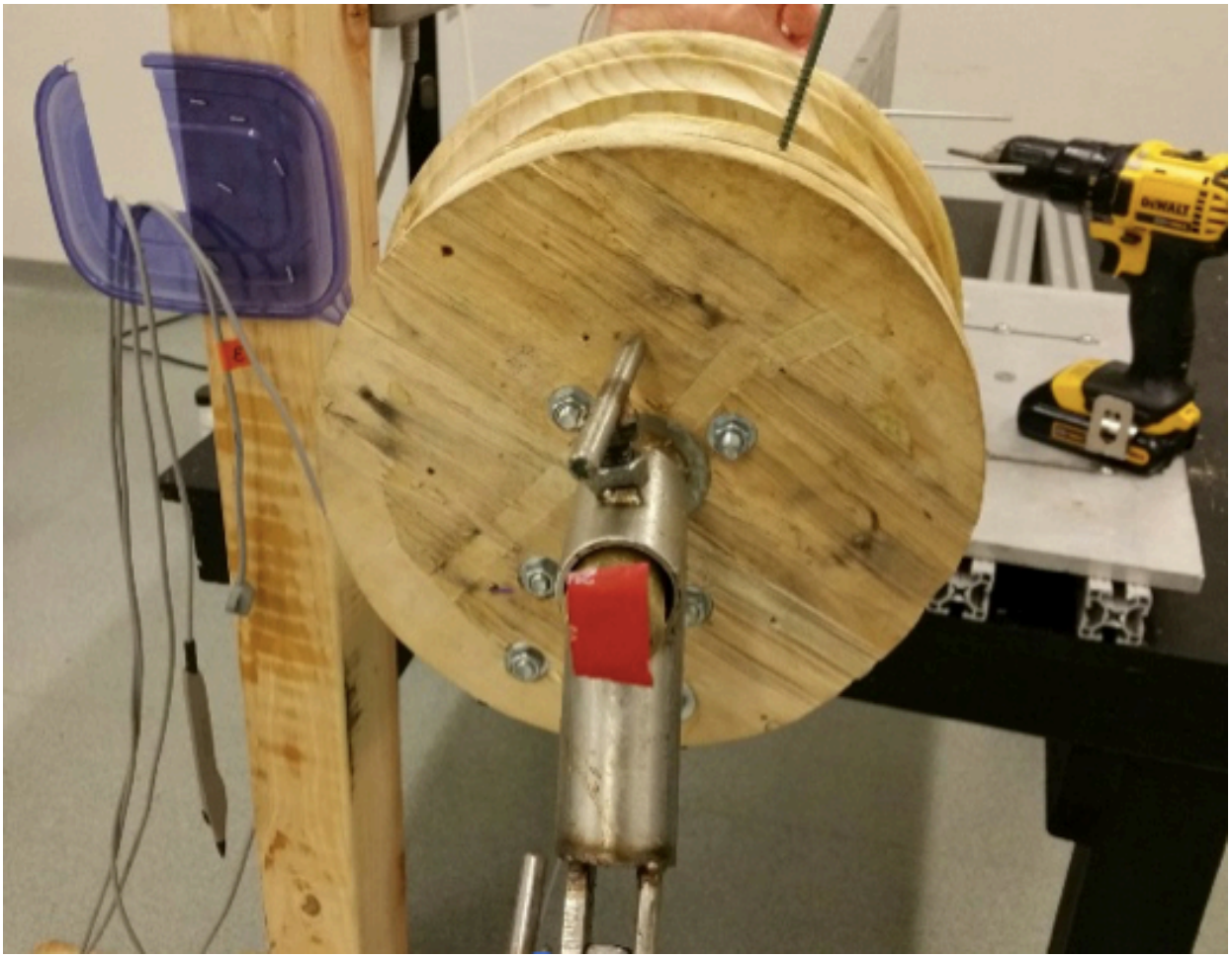

Figure 4.12. Red tape indicating location of third sensor on foot-mounting block, which is aligned with the 2nd digit and anterior border of the tibia. (Photo credit: Cara Fisher)

Initial Imaging

The c-arm was positioned in front of the table holding the ankle rig and the foot-mounting block was placed on the other side of the c-arm. It was positioned to give an anterior posterior (AP) view of the ankle (talocrural) joint (Figures 4.13- 4.15). Using the electromagnetic tracking system, the ankle was then positioned at a 90-degree angle. A static US image, with the probe positioned over the AITFL to visualize the tibiofibular clear space, and fluoroscope image were taken at this point. The ankle was then positioned at 15 degrees of dorsiflexion and static US and fluoroscopic images were taken again. Time to properly prepare a specimen, mount the foot into position, and take initial normal (baseline) images took 1-3 hours. I rarely performed more than two separate experiments in one day due to the extensive preparation process, especially if a specimen fractured early in the protocol.

Pre-experimental Soft Tissue Preparation

The specimen was then pre-stressed in each direction ten times to maximal range of motion to warm up the soft tissues. Pre-stressing joints is common in biomechanical in vitro research and as a method to reduce error.[11,44,68]

Figure 4.13. Placement of c-arm in relationship to the ankle rig and foot-mounting block. (Photo credit: Katelyn Johnson)

Figure 4.14. Ankle rig, foot-mounting block, and c-arm set up for right-sided ankle. (Photo credit: Katelyn Johnson)

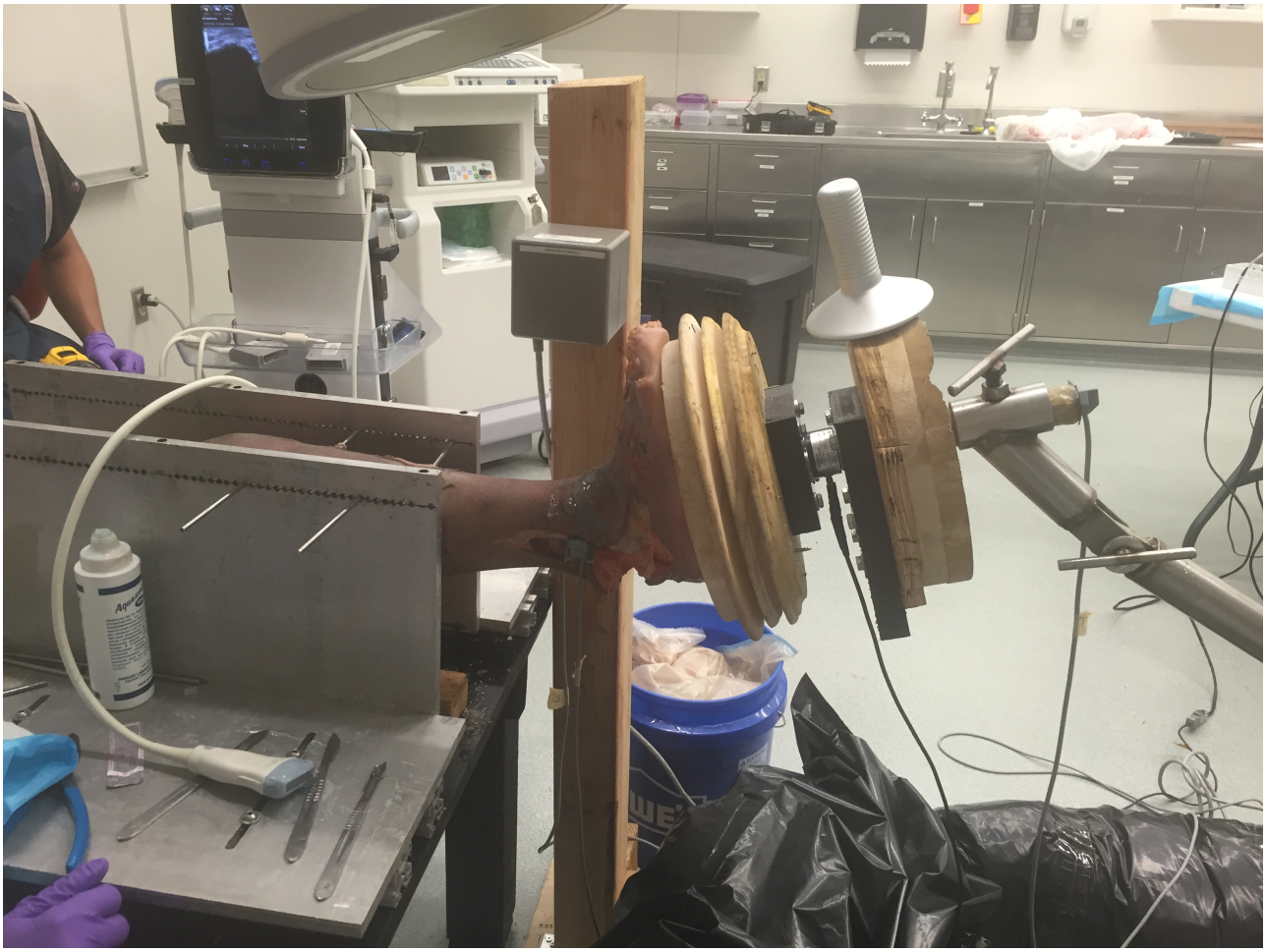

Figure 4.15. View of ankle rig and foot-mounting block in relationship to c-arm and sensor stand. (Photo credit: Katelyn Johnson)

4.4 Study Protocol

Rotational Stress Testing

The ankle was held in 15 degrees of dorsiflexion for all phases of external rotational stress testing, as this is the most common position of the ankle when a supination-external rotation (SER) injury occurs. Each trial of the experimental testing protocol required the primary examiner (Cara Fisher) and two research assistants. Each phase of injury had three trials. As the primary examiner, I handled the ultrasound probe and applied the rotational torque during each trial. One research assistant was responsible for starting and stopping the electromagnetic tracking and torque systems upon the command of the primary examiner. This research assistant was also responsible for calling out how many Newtons of torque were reached during each rotation trial to alert the primary examiner to cease force application. The second research assistant started and ended the recording of the ultrasound videos at the command of the primary examiner. The long process required everyone's continual attention and performance of his/her specific duties. When a trial was ready to be recorded, the ultrasound probe was placed directly over the AITFL for full visualization of the tibiofibular clear space during testing (Figure 4.16). I would call "Run torque." Once torque was started, I would count down "three, two, one." On "one", the dynamic ultrasound video recording was started and 10 Nm of torque was achieved by the primary examiner pulling on the wheel externally over a ten second period. Once the desired torque was achieved, I would slowly return the wheel to neutral and call "Stop." All ultrasound and torque recordings stopped at that time. If the ligaments in the ankle or the joint capsule started to tear during rotation, rotation was continued until peak torque was reached or the ankle failed completely. Failure could include fracture, complete tearing of all ankle ligaments, and/or tearing of the joint capsule.

A static AP fluoroscopic image was taken, followed by a dynamic fluoroscopic image taken at peak torque (Figure 4.17). Dynamic fluoroscopic images on damaged ankles were taken at the maximum amount of torque the ankle would reach in its damaged state. The research assistant running torque would call out how much torque was reached to alert the primary examiner to take the dynamic ultrasound image.

Each trial was repeated three times for each of the phases listed in Table 4.1. These phases follow the Lauge-Hansen SER injury pattern with incremental phases of 75% ligament injury between each stage.[45,46] Vertical ligaments were measured and sectioned from inferior to superior; horizontal ligaments were measured and sectioned from anterior to posterior (Figure 4.18). Typically, fractures associated with SER injuries go through the lateral malleolus in a posterior to inferior direction. Because it was necessary to have the electromagnetic sensor on the fibula stay attached to the distal portion of the fibula once it was fractured, I had to move the location of the simulated fracture in a proximal direction. The location of the fracture was identified by measuring 8 cm from the tip of the lateral malleolus, moving proximally along the fibula, to just past the fibular electromagnetic sensor and then creating the fracture by removing a 1 mm slice of bone from the fibula (Figures 4.19 and 4.20). These fibular fractures were created using a DeWalt XR cordless 20-volt max oscillating tool model number DCS355B.

Figure 4.16. Primary examiner locating tibiofibular clear space using US prior to starting a trial. (Photo credit: Armando Rosales)

Figure 4.17. A research assistant is seated at a table running torque and Polhemus. The primary examiner taking fluoroscopic images. (Photo credit: Armando Rosales)

Table 4.1. Phases of injury created during experiment and corresponding Lauge-Hansen supination-external rotation stage

Phase of Injury	Lauge-Hansen Supination-External Rotation Stage
1. Normal (baseline)	0
2. 75% of AITFL Cut	1
3. 100% of AITFL Cut	1
4. Fibula Fx - Cut 8 cm proximal	2
5. 75% PITFL Cut	3
6. 100% PITFL Cut	3
7. 75% Deltoid Cut	4
8. 100% Deltoid Cut	4

Figure 4.18. Measuring the AITFL in preparation for 75% sectioning. (Photo credit: Cara Fisher)

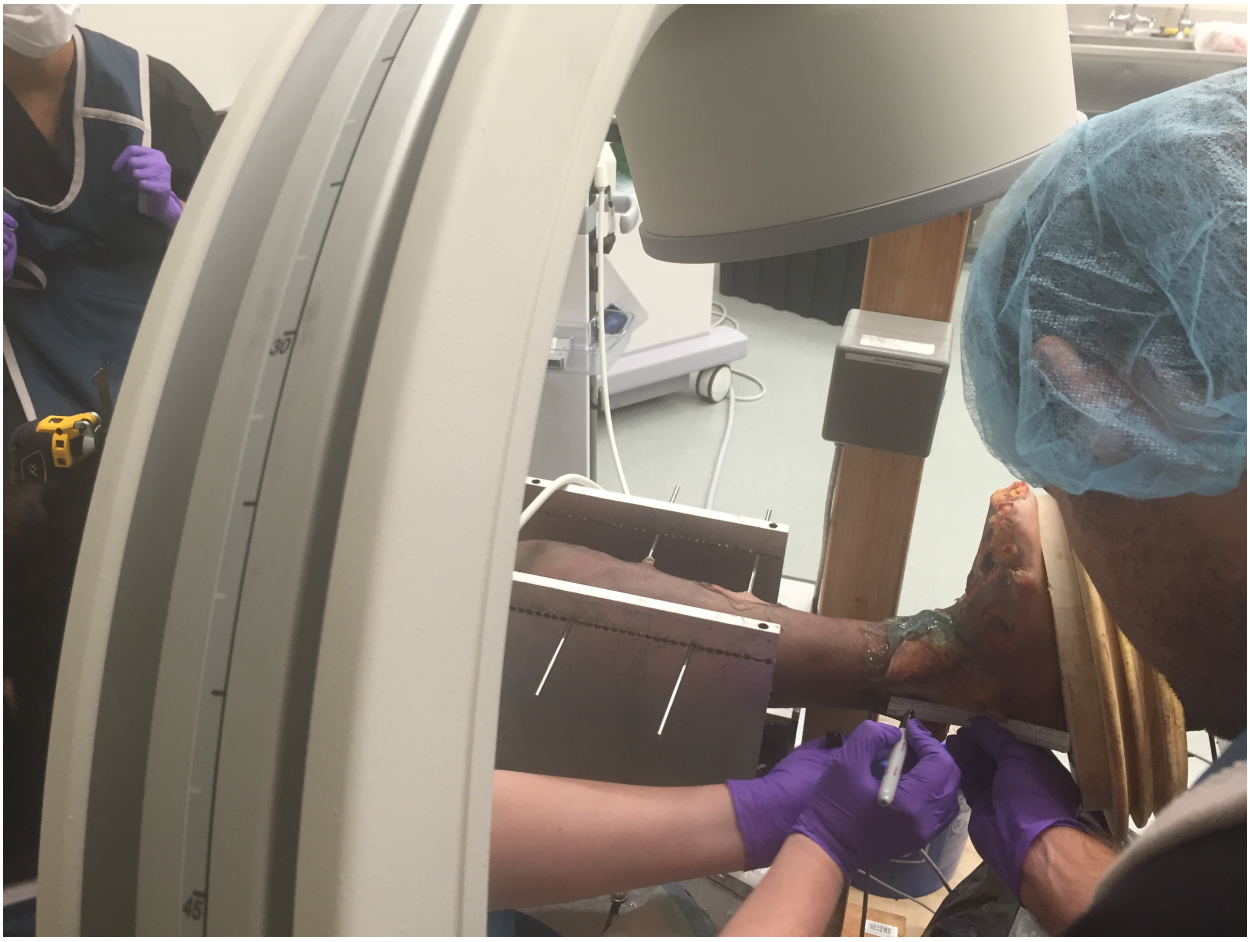

Figure 4.19. Primary examiner measuring 8cm proximal from tip of lateral malleolus to mark line for fibula fracture. (Photo credit: Katelyn Johnson)

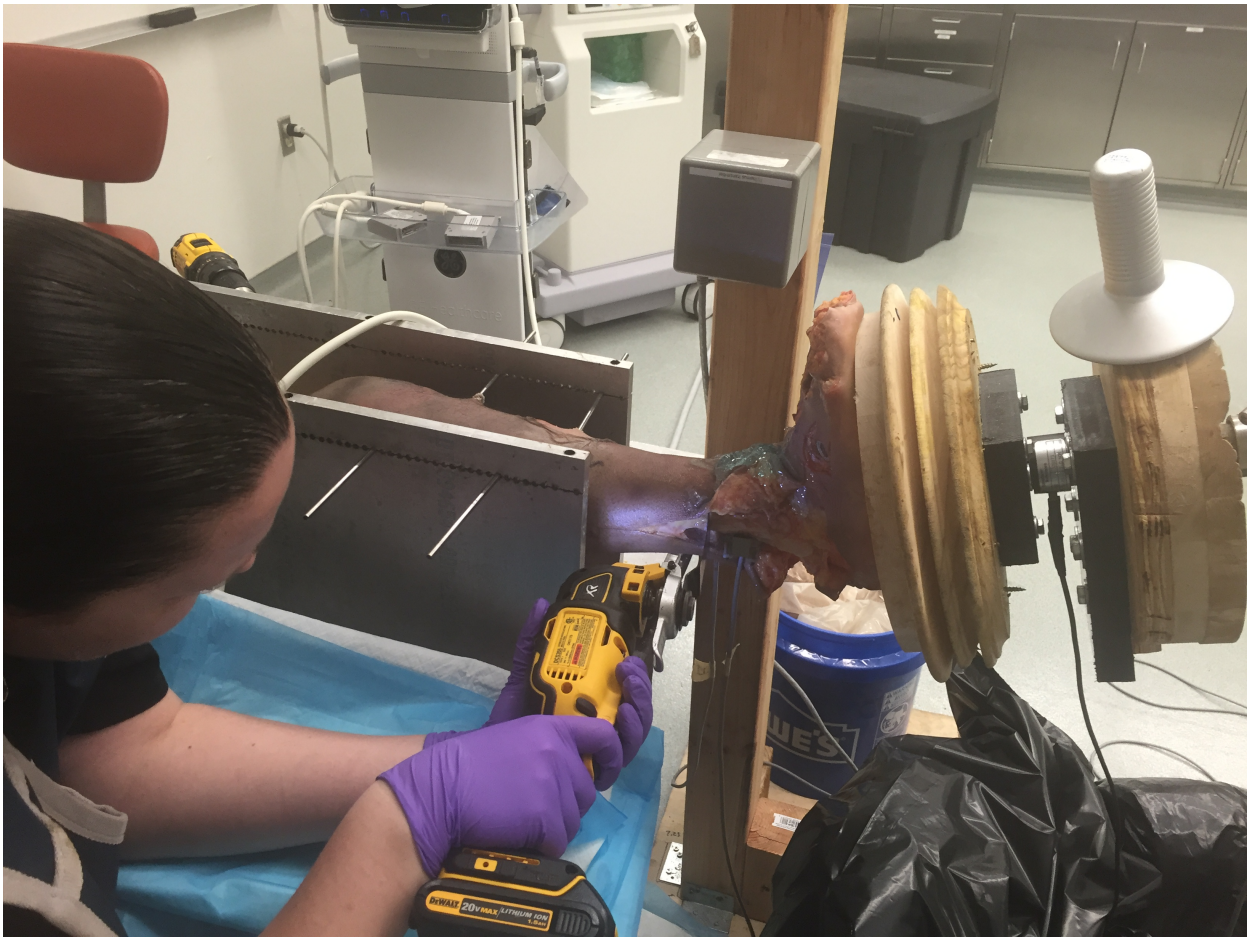

Figure 4.20. Primary examiner creating fibula fracture. (Photo credit: Katelyn Johnson)

Image Processing and Measurement Collection

All dynamic ultrasound videos were converted to static images with one image created for every half second of recorded video, yielding 30-40 images per video. Ideally, each ankle would withstand all eight phases, resulting in 24 videos per ankle. Not all ankles completed the entire protocol. The conversion of dynamic ultrasound video to static images resulted in approximately 7200 ultrasound images. Each static image was measured by three independent examiners, which resulted in more than 90 data points per phase. The tibiofibular clear space at peak torque was the data of interest, so I decided to use the torque data to find the exact point that peak torque (10 Nm) was reached for each trial and measure just those images that corresponded to that point. A representative figure, Figure 4.21, illustrates how the images corresponding to peak torque times were identified. Images corresponding to the point of peak torque and the same time point for the tibiofibular clear space were measured using ImageJ software (NIH, Bethesda MD). ImageJ was calibrated to these images using two different methods: a ball bearing for fluoroscopic images and the on-image ruler for ultrasound images. A ball bearing is round; the same diameter is maintained despite the angle of measurement. The ball bearing size was determined by taking the average of ten separate measurements using calipers (Figures 4.22 and 4.23). Three independent observers measured and recorded the tibiofibular clear space. Data for each phase was averaged. Each experiment consisted of eight phases and each phase consisted of three trials. Data for each trial was measured three times by three different observers resulting in nine measurements for every analyzed data point. Figures 4.24 and 4.25 show where on the ultrasound and c-arm images the tibiofibular clear space was measured.

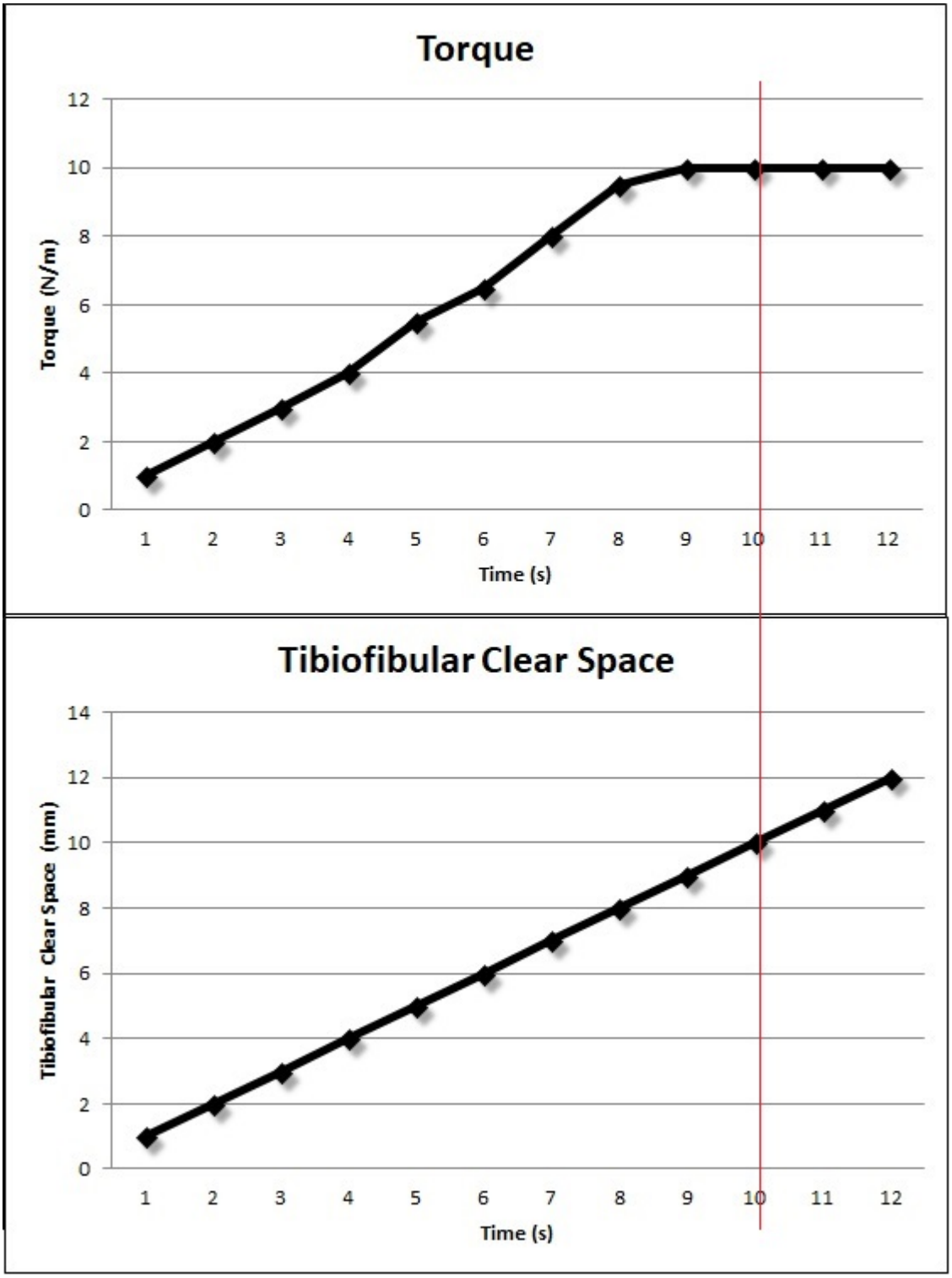

Figure 4.21. Example of how peak torque and corresponding data point was found. Torque – increase in torque measured as Newton meter (Nm) over time the force is steadily increased. Tibiofibular clear space – measured in mm at the 10 second mark. Red vertical line denotes corresponding measurement data points.

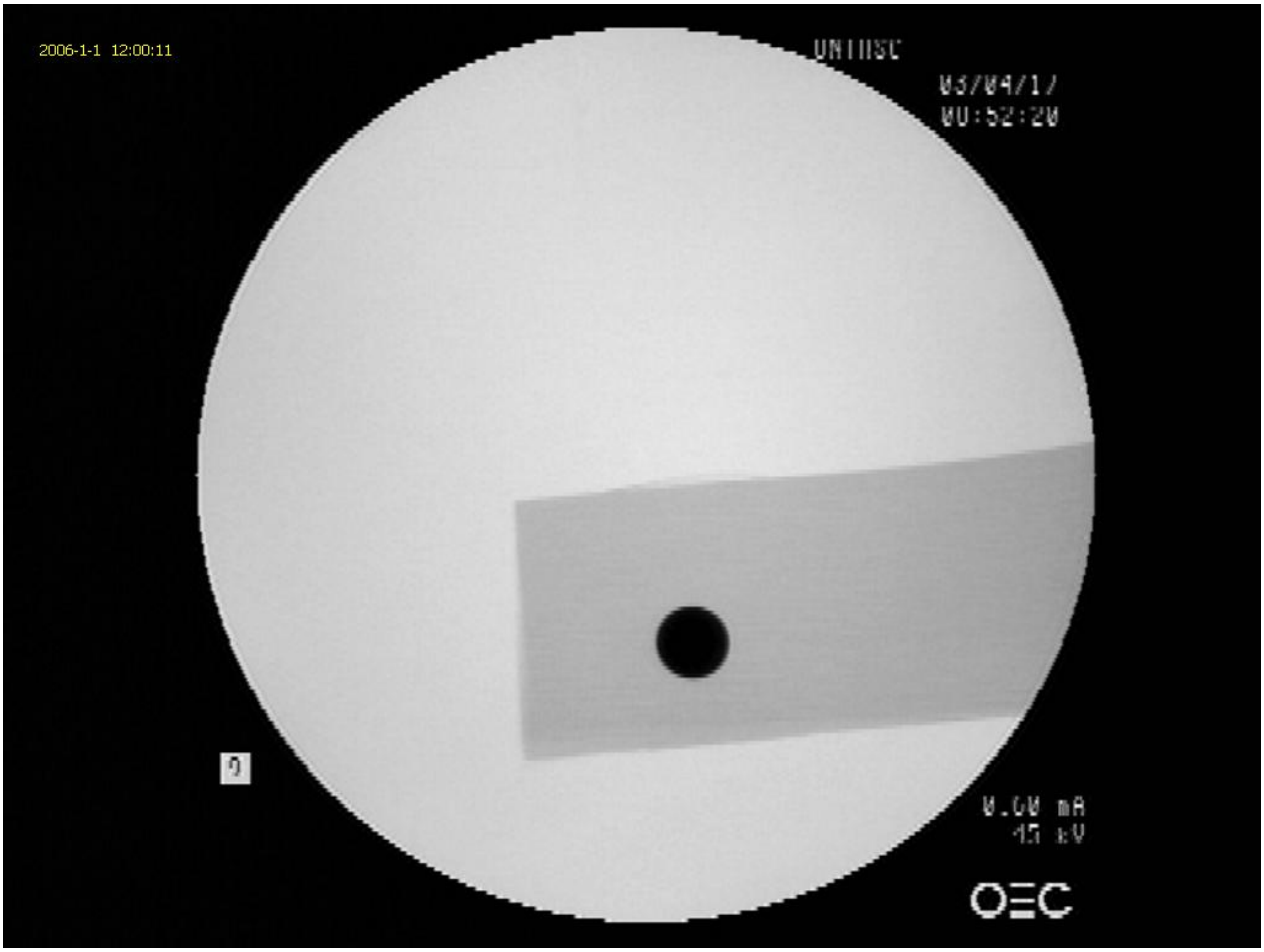

Figure 4.22. Ball bearing image used to calibrate ImageJ. This calibration was used to measure fluoroscopic c-arm images.

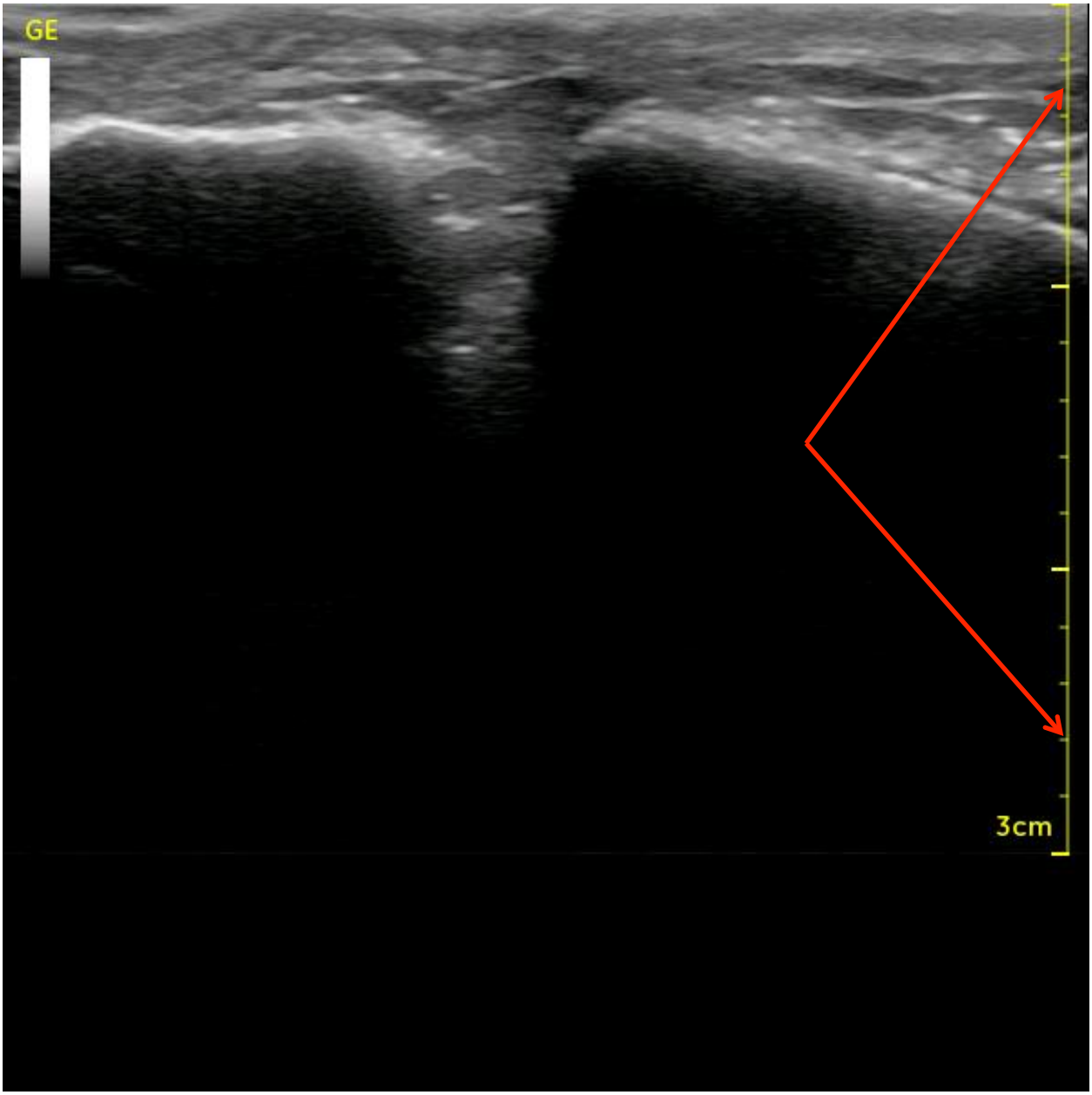

Figure 4.23. Image showing US on-screen calibration ruler, indicated by arrows, that was used for ImageJ.

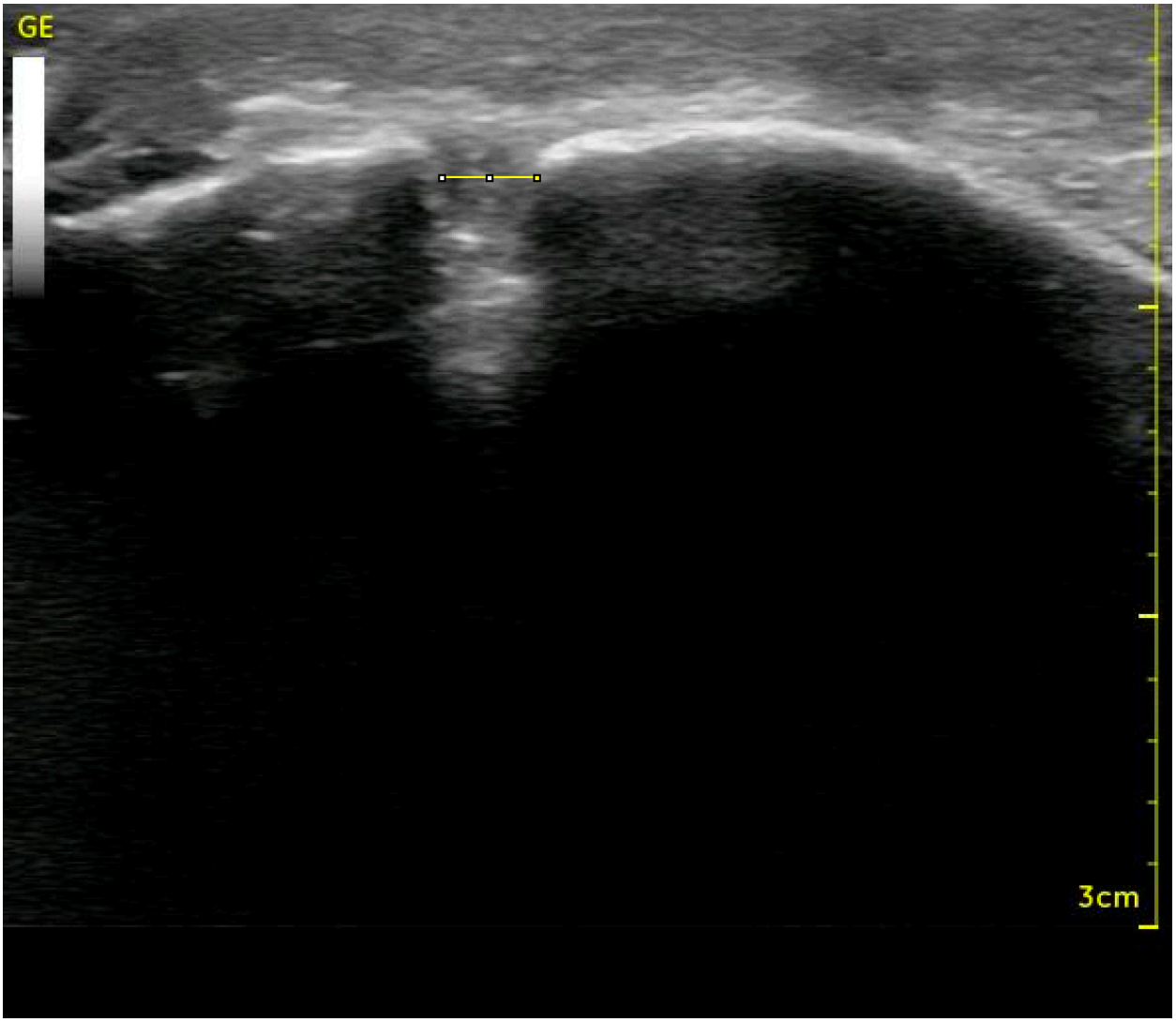

Figure 4.24. Yellow line indicates where the tibiofibular clear space was measured on ultrasound images.

Figure 4.24. Yellow line indicates where the tibiofibular clear space was measured on fluoroscopic c-arm images.

4.5 Data Analysis

Since three observers collected tibiofibular clear space measurements, an interobserver analysis was first performed using the Bland-Altman method.[69-71] This statistical method compares the measurements of Observer 1 to Observer 2, Observer 1 to Observer 3, and Observer 2 to Observer 3, in a pairwise fashion. The 95% confidence interval for the mean difference between observers was used to assess interobserver error, with a null hypothesis of the mean difference between observers being 0.0 mm.

Tukey's range tests were used to screen for potential outliers among the tibiofibular clear space values. The effect of outliers was reduced using Log10 transformation rather than outright removal, as there were few distinguishable outliers in the measurements. A two-way repeated measures ANOVA was then conducted, with Log10 tibiofibular clear space employed as the dependent variable, and trial and phase as the two independent variables. Importantly, as stress examination at each phase of injury was repeated three times (trials), the use of two-way repeated measures ANOVA permitted assessment of the interaction effect between trial and phase on tibiofibular clear space dimensions. A Tukey-Kramer post hoc tests were subsequently employed to identify which specific trials and/or phases exhibited significant differences in tibiofibular clear space measurements.

The Bland-Altman method[69-71] was also used to compare the results of US and fluoroscopic modalities, with the 95% confidence interval utilized to evaluate agreement between the two imaging modalities. The null hypothesis of a mean difference of 0.0 mm between modalities was again employed.

CHAPTER 5

RESULTS

This chapter covers the results from the analyses described in Chapter 4. Interobserver error is discussed first, followed by a discussion of ultrasound tibiofibular clear space measurement results. This is followed by a discussion on the fluoroscopic c-arm data.

5.1 Introduction

Nine of the eleven specimens withstood the complete study protocol and were included in the study. Two specimens, 06971R and 069102R, had early fibula fractures through the tracking sensor screw holes on the fibula and were excluded from the study. Given that the Lauge-Hansen classification includes deltoid ligament injury at stage 4 (see Table 4.1), this study was intended to include examination of a partial and complete deltoid ligament injury as the last phase of injury in the study. However, this portion of the study was excluded due to the failure of the majority of the specimens to make it to this phase of the protocol.

5.2 Interobserver Error (Bland-Altman Analyses)

A summary of interobserver analyses using the Bland-Altman method for the ultrasound (US) tibiofibular clear space measurements amongst observers is provided in Table 5.1, with

corresponding figures presented in the Appendix (Figures A.1–A.18). The results of the pairwise comparisons indicated the tibiofibular clear space measurements of Observer 2 and Observer 3 were exceedingly similar, with an average difference of only 0.16 mm between the two observers. Conversely, the tibiofibular clear space measurements of Observer 1 were found to be consistently higher than both Observer 2 (2.5 mm) and Observer 3 (2.4 mm). Despite this tendency for Observer 1 to overestimate tibiofibular clear space dimensions compared to the other two observers, the measurements of Observer 1 were found to be internally consistent (i.e., Observer 1 overestimated Observer 2 and 3 by similar amounts at each experimental phase). Thus, the measurements of Observer 1 were still included in the calculation of the overall mean value, with the understanding that all mean measurements were similarly influenced by Observer 1's values. Accordingly, all mean values included in the subsequent two-way repeated measures ANOVA (Table 5.2) represent the geometric mean of all three observers.

Table 5.1. Summary of Bland-Altman analyses of average difference in tibiofibular clear space measurements. AITFL – anterior inferior tibiofibular ligament, PITFL – posterior inferior tibiofibular ligament.

Injury Phase	Observer 1 vs. Observer 2	Observer 1 vs. Observer 3	Observer 2 vs. Observer 3
Normal	3.64	2.32	-1.32
75AITFL	2.47	1.90	-0.40
100AITFL	3.06	2.88	-0.22
Fibular Fracture (Fx)	2.96	2.79	-0.17
75PITFL	1.83	2.43	0.58
100PITFL	1.18	1.77	0.59
Mean Average (Std. Dev.)	2.52 (0.89)	2.35 (0.45)	-0.16 (0.71)

5.3 Ultrasound Tibiofibular Clear Space Measurements

Tibiofibular clear space measurements for the three trials are presented in Table 5.2. Results of the two-way repeated measures ANOVA are presented in Table 5.3. No significant differences were found between the three trials ($F = 0.4$, $p = 0.67$), indicating that the different trials within each phase of the experiment did not return significantly different values (e.g., earlier trial rotations of the ankle did not influence the clear space dimensions of the later trials). Conversely, significant differences were found between the different phases of the experiment ($F = 6.80$, $p = 0.0001$). Importantly, no significant interaction effect was found between trial and phase ($F = 0.39$, $p = 0.94$), demonstrating that significant differences found among the phases were not influenced by differences among trials.

Tukey-Kramer post hoc test results for differences among the phases are provided in Table 5.4. Although no significant difference was found between the Normal and 75AITFL phases, significant differences were found between the Normal phase and all other later phases of the experiment (100AITFL, Fibula Fx, 75PITFL, 100PITFL). Additionally, none of the later experimental phases was found to be significantly different from each other.

Figure 5.1 provides visualization of mean tibiofibular clear space values for each phase of the experiment. From this figure a general trend of increasing tibiofibular clear space dimensions at each phase of the experiment is readily apparent. Moreover, a rapid increase in clear space dimensions from Normal to a 100% tear of the AITFL is visible, followed by more minimal increases in clear space values from fibula fracture (Fibula Fx) through 100% PITFL.

Table 5.2. Mean tibiofibular clear space ultrasound measurements (mm) for 10 specimens from all three observers, for three trials for each phase. X – denotes that this specimen failed prior to this phase and it was not used in the two-way repeated measures ANOVA.

Ankle	Normal	75 AITFL	100AITFL	Fibula Fx	75PITFL	100PITFL
65499L – Trial 1	3.1	3.9	7.2	6.4	6.2	5.7
65499L – Trial 2	3.3	5.9	5.8	4.9	7.1	6.3
65499L – Trial 3	5.5	4.6	6.3	6.8	6.4	6.5
67416L – Trial 1	4.4	5.9	5.7	6.2	7.5	7
67416L – Trial 2	4.3	5	6.2	6.1	6.6	6.4
67416L – Trial 3	5.1	5.6	6.6	7.9	6.3	5.6
69071L – Trial 1	3.3	5.3	7.9	6.4	6.6	6.3
69071L – Trial 2	5.4	4.8	6.4	5.8	5.9	5.8
69071L – Trial 3	3.3	6.5	7	5.8	7.1	5.8
69084L – Trial 1	4.9	3.5	5.2	7.4	6.8	8.5
69084L – Trial 2	4.8	3.6	5.8	5.2	8.6	5.5
69084L – Trial 3	5.2	5.1	5.3	6.9	5.1	6.2
69084R – Trial 1	8.2	5.5	4.5	7.3	5.5	6
69084R – Trial 2	7.2	5.9	5	5.5	4.8	5.2
69084R – Trial 3	7.3	6.1	5	5.8	5.3	5.9
69091R – Trial 1	6.3	7	5.7	7.1	5.8	6.5
69091R – Trial 2	2.3	6	4.2	7	5.1	6.8
69091R – Trial 3	3.8	4.5	7.4	6.5	4.7	6.8
69100L – Trial 1	4.8	8.1	7.8	5.8	8.2	7.8
69100L – Trial 2	7.6	6.3	6.9	6	6.6	7.1
69100L – Trial 3	6.1	7.4	5.9	5.3	5.9	8
69100R – Trial 1	2.4	4.5	4.9	8	6	5.8
69100R – Trial 2	3.3	4.5	7.3	11	7.8	7
69100R – Trial 3	3	5.4	6.8	6.7	7.9	7.5
69102L – Trial 1	4.8	6.7	6.4	6.2	7.4	8.2
69102L – Trial 2	5.5	5.8	5.6	5.1	8.3	8.2
69102L – Trial 3	4.1	4.5	6.2	7.1	7	7.5
69102R – Trial 1	5.5	4.7	6.4	5.6	7.6	X
69102R – Trial 2	5	5.6	5.5	6.8	6.7	X
69102R – Trial 3	3.1	5.8	5.1	5	6.5	X
Geometric Mean	**4.5**	**5.4**	**6.0**	**6.4**	**6.5**	**6.6**

Table 5.3. Summary of Two-way Repeated Measures ANOVA results.

Source Term	DF	F-Ratio	Regular *P*-value	Geisser Greenhouse Epsilon *P*-value	Huynh Feldt Epsilon *P*-value
Trial	2	0.40	0.6794	0.6105	0.6369
Phase	5	6.80	**0.0001***	**0.0066**	**0.0023**
Trial & Phase Interaction Effect	10	0.39	0.9454	0.8064	0.9208

P-values significant at alpha = 0.05 in **Bold**

Table 5.4. Summary of Tukey-Kramer Multiple Comparison Test results for pairwise comparisons between the experimental phases.

Phase	Count	Mean	Different From Phases
Normal	27	-0.3435	100AITFL, Fibula Fx, 75PITFL, 100PITFL
75AITFL	27	-0.2703	
100AITFL	27	-0.2194	Normal
Fibula Fx	27	-0.1916	Normal
75PITFL	27	-0.1905	Normal
100PITFL	27	-0.1803	Normal

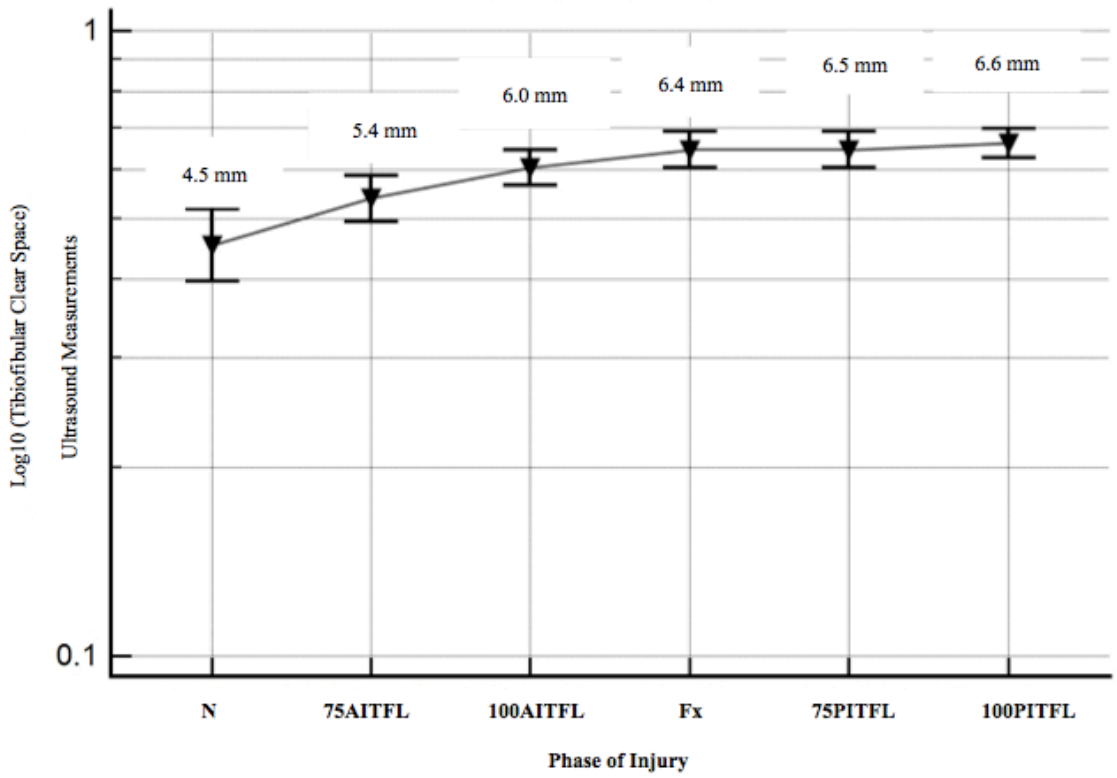

Figure 5.1. Mean ultrasound tibiofibular clear space measurements at 10 Nm of external rotational torque for each of the experimental phases. 95% CI for error bars.

5.4 Fluoroscopic Tibiofibular Clear Space Measurements

Fluoroscopic tibiofibular clear space data was collected from both static and dynamic images at the end of each of the three ultrasound trials. The same three independent Observers also measured these images. Bland-Altman plots were then used to compare mean US and fluoroscopic tibiofibular clear space measurements are presented in Figures 5.2–5.7. Results indicate substantial differences between the two methods, with the 95% confidence intervals failing to encompass 0.0 mm during any of the post-Normal injury phases between the two imaging modalities. Further evaluation of tibiofibular clear space measurements found fluoroscopic values to be discordant with realistic measurements found with direct measurement using a ruler and US imaging. Figure 5.8 demonstrates the unrealistic relationship of decreasing tibiofibular clear space with increasing levels of injury found with fluoroscopy. Therefore, all fluoroscopic data was considered aberrant and was excluded from further study. This was disappointing as it represented a significant amount of data lost and didn't allow for comparison of ultrasound and fluoroscopic methods of diagnosis.

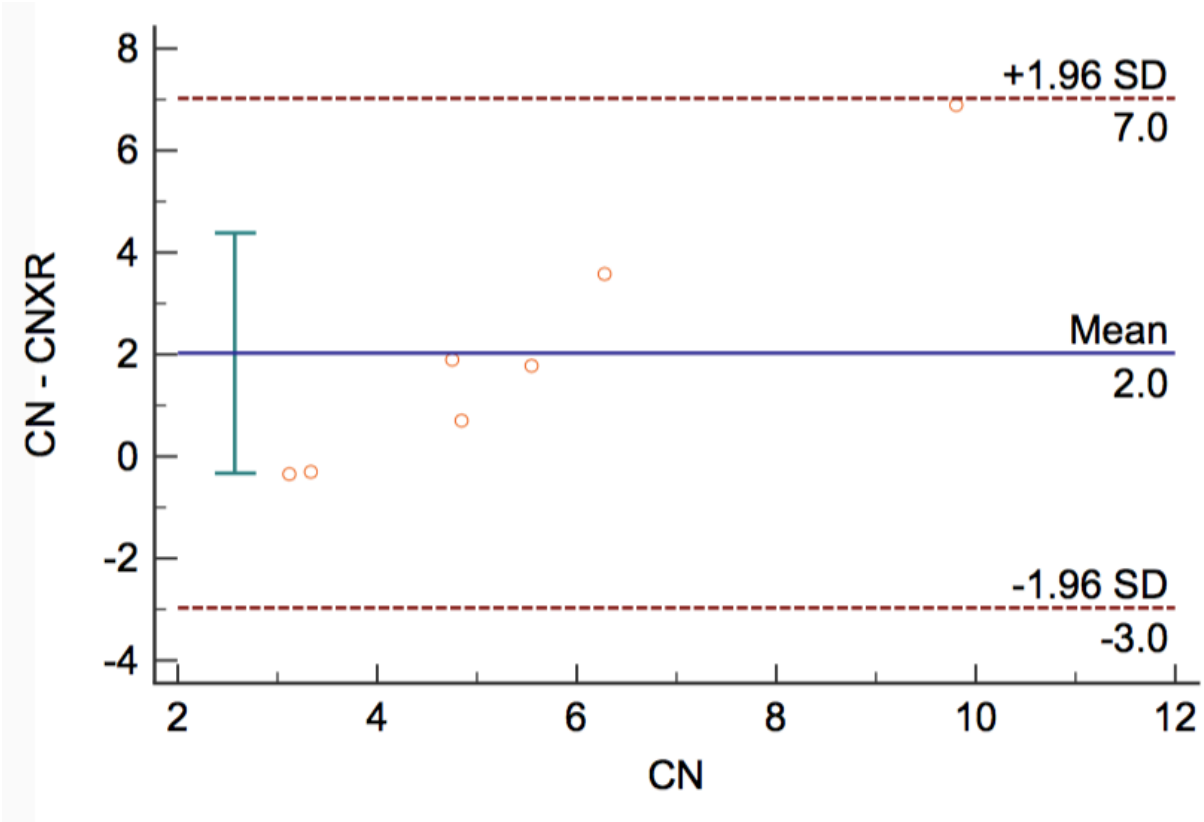

Figure 5.2. Bland-Altman plot for comparison of mean US and fluoroscope measurements in the normal phase. CN – combined normal ultrasound; CNXR – combined normal fluoroscope. Note that the 95% confidence interval (green whiskers) does encompass a mean difference of 0.0mm, indicating agreement between measurement methods.

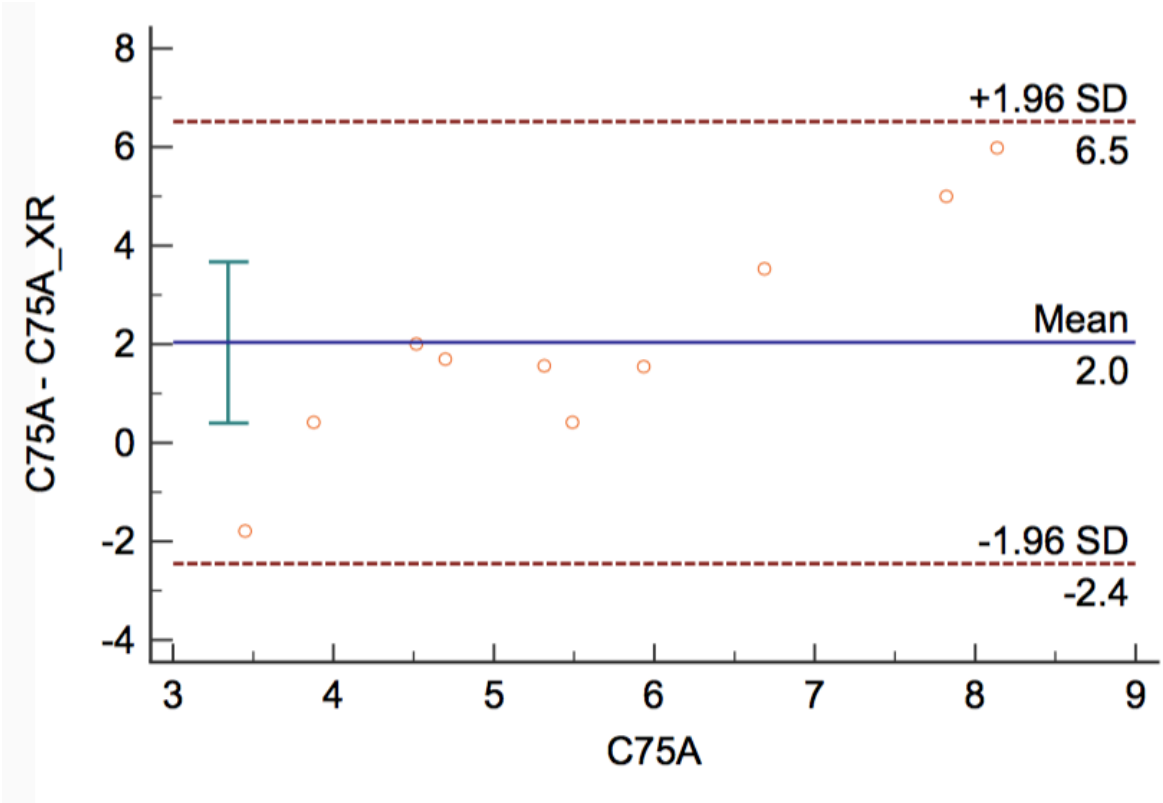

Figure 5.3. Bland-Altman plot for comparison of mean US and fluoroscope measurements in the 75AITFL phase. C75A – combined 75AITFL ultrasound; C75A_XR – combined 75AITFL fluoroscope. Note that the 95% confidence interval (green whiskers) does not encompass a mean difference of 0.0mm, indicating discordance between measurement methods.

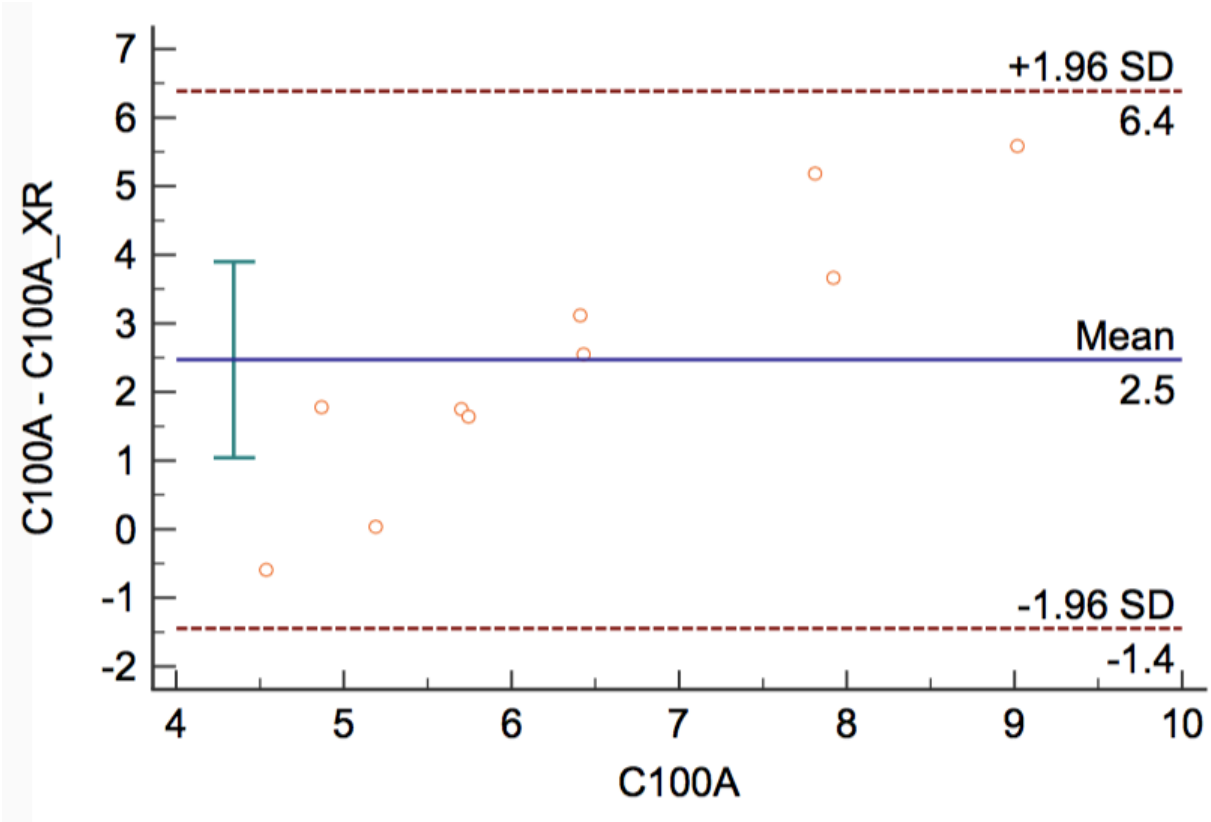

Figure 5.4. Bland-Altman plot for comparison of mean US and fluoroscope measurements in the 100AITFL phase. C100A – combined 100AITFL ultrasound; C100A_XR – combined 100AITFL fluoroscope. Note that the 95% confidence interval (green whiskers) does not encompass a mean difference of 0.0mm, indicating discordance between measurement methods.

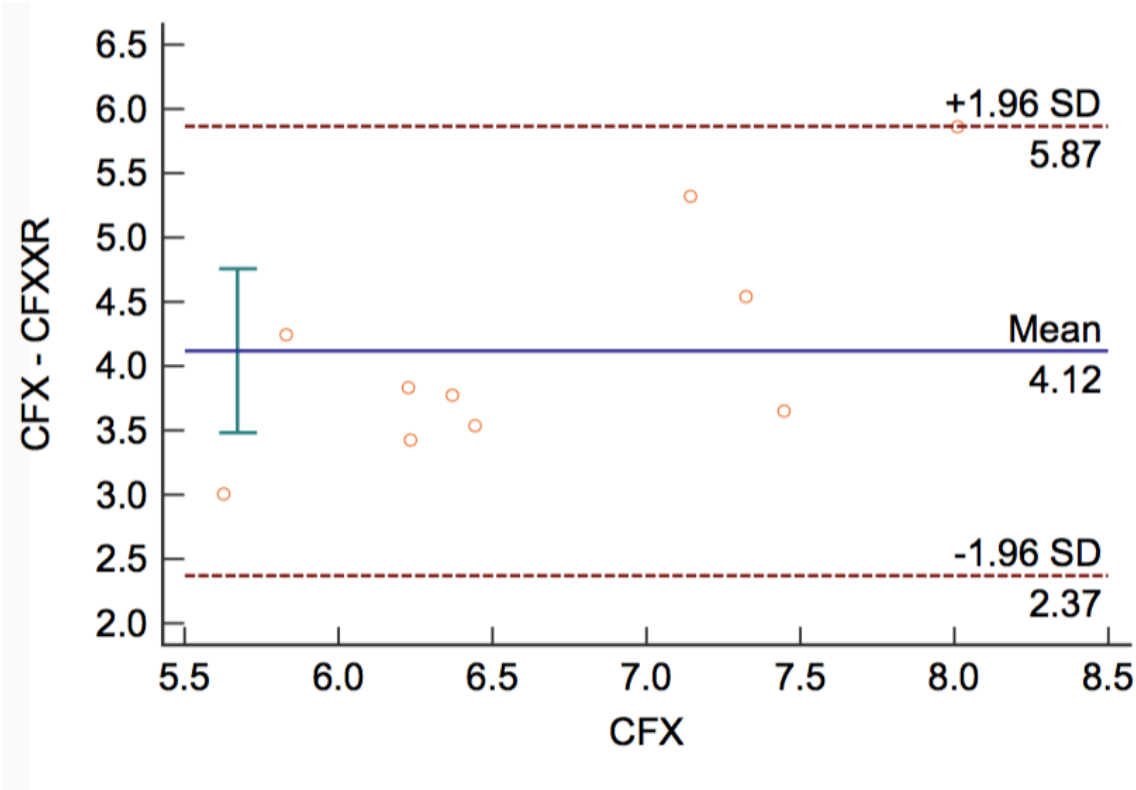

Figure 5.5. Bland-Altman plot for comparison of mean US and fluoroscope measurements in the Fibula Fx phase. CFX – combined fracture ultrasound; CFXXR – combined fracture fluoroscope. Note that the 95% confidence interval (green whiskers) does not encompass a mean difference of 0.0mm, indicating discordance between measurement methods.

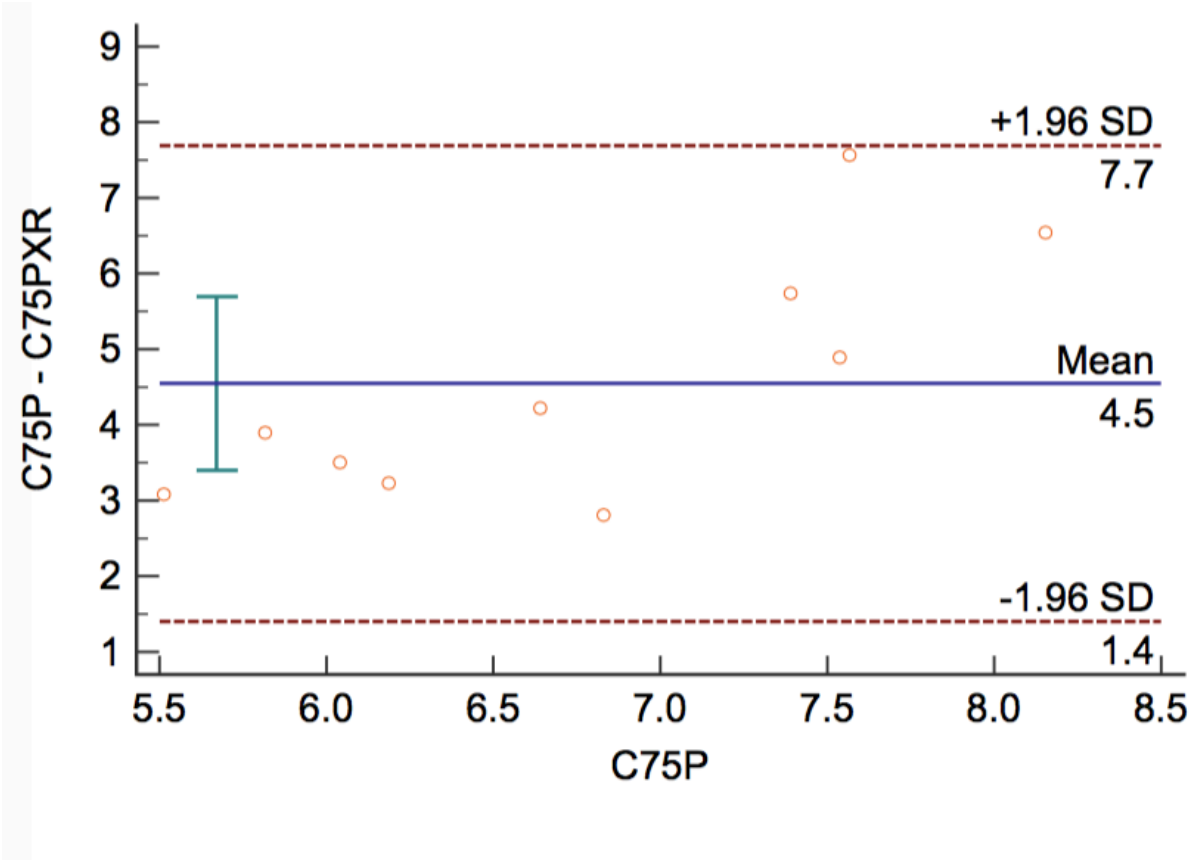

Figure 5.6. Bland-Altman plot for comparison of mean US and fluoroscope measurements in the 75PITFL phase. C75P – combined 75PITFL ultrasound; C75PXR – combined 75PITFL fluoroscope. Note that the 95% confidence interval (green whiskers) does not encompass a mean difference of 0.0mm, indicating discordance between measurement methods.

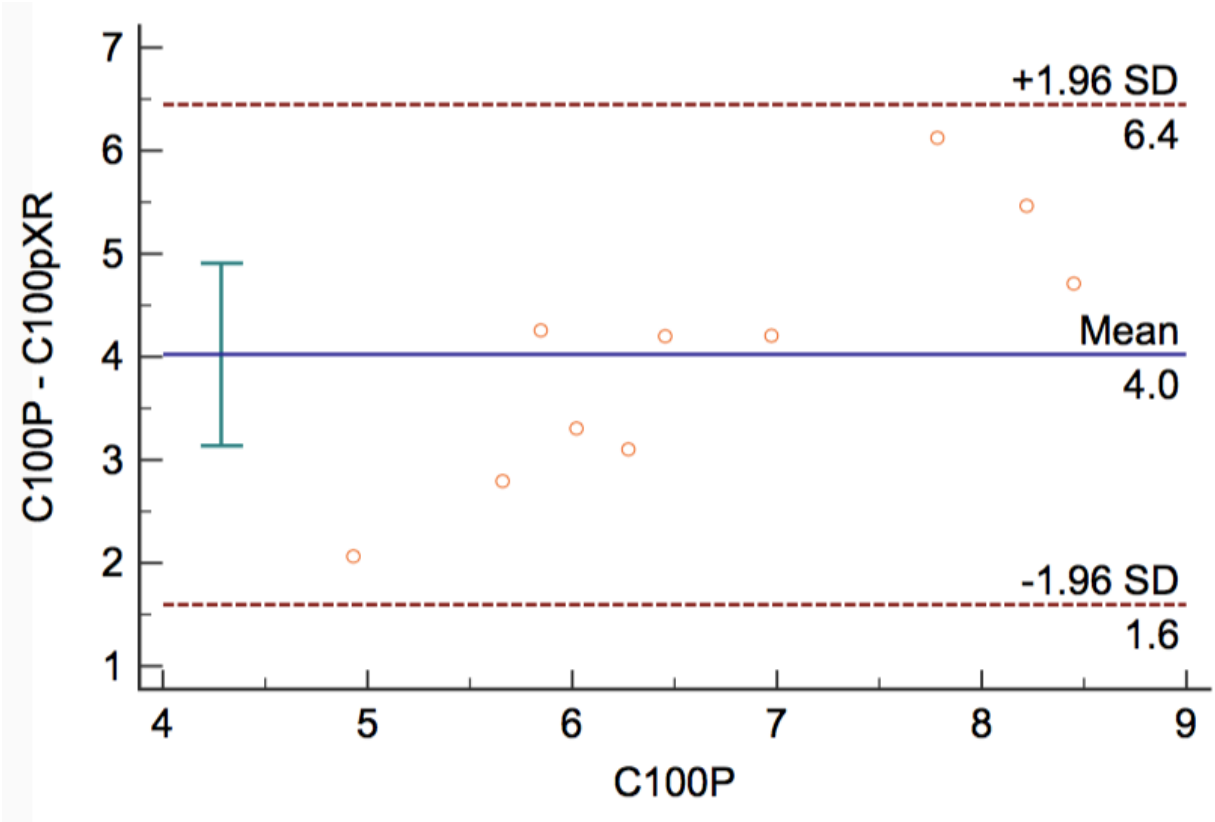

Figure 5.7. Bland-Altman plot for comparison of mean US and fluoroscope measurements in the 100PITFL phase. C100P – combined 100PITFL ultrasound; C100PXR – combined 100PITFL fluoroscope. Note that the 95% confidence interval (green whiskers) does not encompass a mean difference of 0.0mm, indicating discordance between measurement methods.

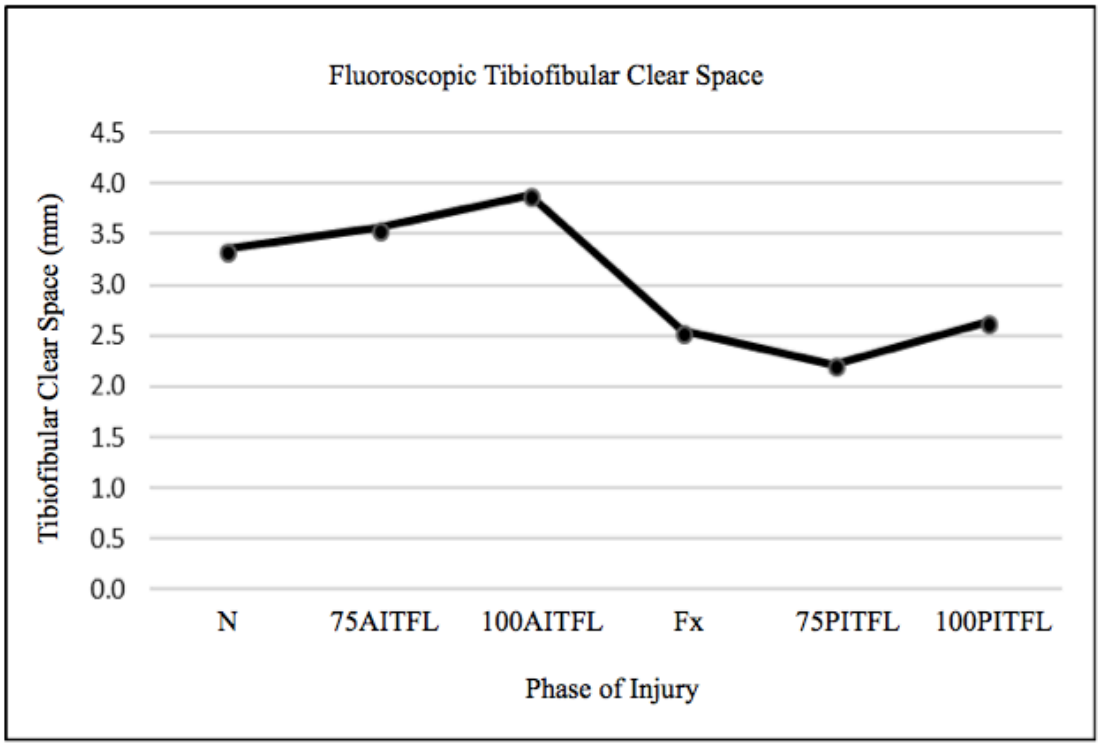

Figure 5.8. Mean fluoroscopic tibiofibular clear space measurements at 10 Nm of external rotational torque for each of the experimental phases. Note the paradoxical decrease in tibiofibular clear space as injury level progresses.

CHAPTER 6

DISCUSSION

The impetus for this research study was to familiarize physicians and technicians with ultrasound (US) diagnosis of syndesmotic injuries and increase the support for the use of US to detect subtle injuries. Diagnosis of syndesmotic injuries depends on clinical suspicion and imaging to make a definitive diagnosis, but are still often missed.[1] Imaging focuses on measurements of the tibiofibular overlap, tibiofibular clear space, and the medial clear space. However, these measurements look for relatively small changes in length of less than 5 mm which is easily affected by examination method and examiner.[63] Dynamic ultrasound examination allows detailed tracking of the tibia and fibula (Figure 6.1) during stress and may be more inclined to pick up subtle changes in clear space found in mild stage 1 supination-external rotation (SER) injuries. Clinically, plain film non-stress and stress radiographs are most commonly used for assessment of syndesmosis integrity, as they are low-cost and widely available with well-trained technicians (Figure 6.2). Based upon epidemiological data and clinician experience, dynamic ultrasound evaluation of the ankle syndesmosis is also widely available and is inexpensive, but underutilized.[63] Ultrasound evaluation of the syndesmosis is currently not used on a widespread basis at many institutions due to a lack of providers and technicians with sufficient expertise and efficiency with the technology for this specific

purpose.[41] This study demonstrates that US is capable of detecting complete and incomplete SER injuries at stages 1-4, supporting expanded use of dynamic US examination for subtle SER type syndesmosis injuries in clinical settings.

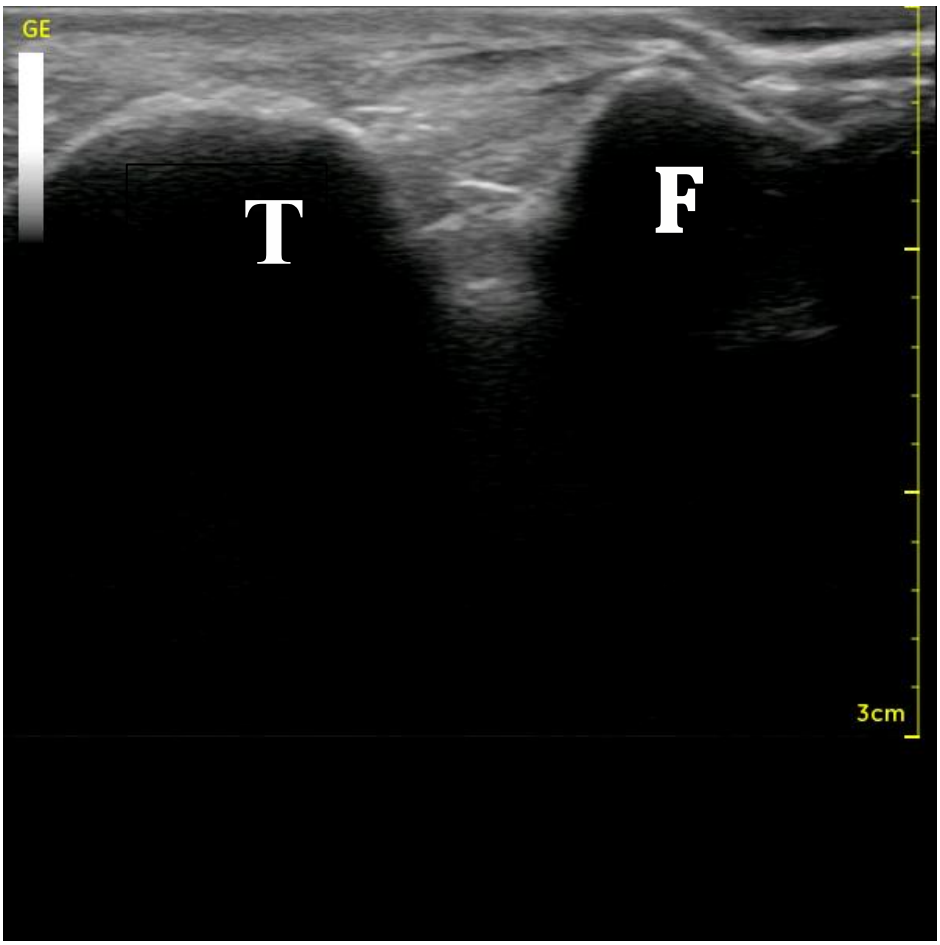

Figure 6.1. Ultrasound image of intact syndesmosis in neutral position (T – tibia, F- fibula).

Figure 6.2. Fluoroscopic image of intact syndesmosis in neutral position.

While capable of identifying most SER type syndesmosis injuries, dynamic US examination was unable to detect a difference between the uninjured ankle and the 75% anterior inferior tibiofibular ligament (AITFL) injury state during this study (Figures 5.1 and 6.3), thus failing to support Hypothesis 1 that dynamic ultrasound evaluation can detect all stages of SER injury. This was likely due to the combination of the partially intact AITFL, interosseous ligament (IOL), and posterior inferior tibiofibular ligament (PITFL) withstanding the 10 Nm stress of examination without the tibiofibular clear space exceeding 6 mm. Thus it appears that a partially intact AITFL remains biomechanically stable enough to prevent an overt diagnosis of a syndesmosis injury using ultrasound. The fact that an AITFL with only 25% of its fibers intact was able to maintain ankle stability during this study may suggest that patients with partial

AITFL injuries remain capable of bearing weight, potentially making simple activity restrictions for non-operative management a viable treatment option for this level of injury. This hypothesis would need further study, as this model did not test the repetitive stress encountered with physiological movement.

In contrast, a complete stage 1 injury with 100% of AITFL torn was identified with dynamic US, with the tibiofibular clear space attaining a width of 6 mm (approximately 1.5 mm larger than the uninjured state). This reinforces the standard 6 mm tibiofibular clear space cut off for diagnosing a syndesmosis injury[63]. The addition of a fibula fracture with a stage 2 SER injury increased tibiofibular clear space width from the stage 1 injury, although somewhat minimally, from 6.0 to 6.4 mm. These results may indicate that, due to the AITFL being the major restraint to external rotation of the fibula motion, completely severing the AITFL reduces ankle stability so substantially that further injury had little additional effect in the ability of the ankle to resist an external rotational force.[44] This assertion appears supported by the fact that clear space widening appeared to plateau during stage 3-4 injuries. Here it is also important to note that, in later stages of injury, it became increasingly difficult to clearly identify the tibiofibular clear space due to the position of the bone in a highly unstable ankle. This was a limitation in the study, but at the same time highlights an important diagnostic clinical pearl. Once the ankle becomes grossly unstable, it becomes important to stress the ankle after fixation of the fibula, medial malleolus, deltoid ligament, posterior malleolus, or the PITFL, as injuries from SER stages 2-4 can hide an injured AITFL and can continue to give the patient instability if not repaired. An untreated syndesmosis injury allows diastasis of the tibiofibular joint giving the talus more freedom of movement and will translate or rotate more than the intact state.[11] This decreases tibiotalar contact area, which

can lead to higher contact pressures.[12] Failure to diagnose a syndesmotic injury is not rare and can lead to longer recovery times, early onset osteoarthritis, and poor outcomes.[1,2]

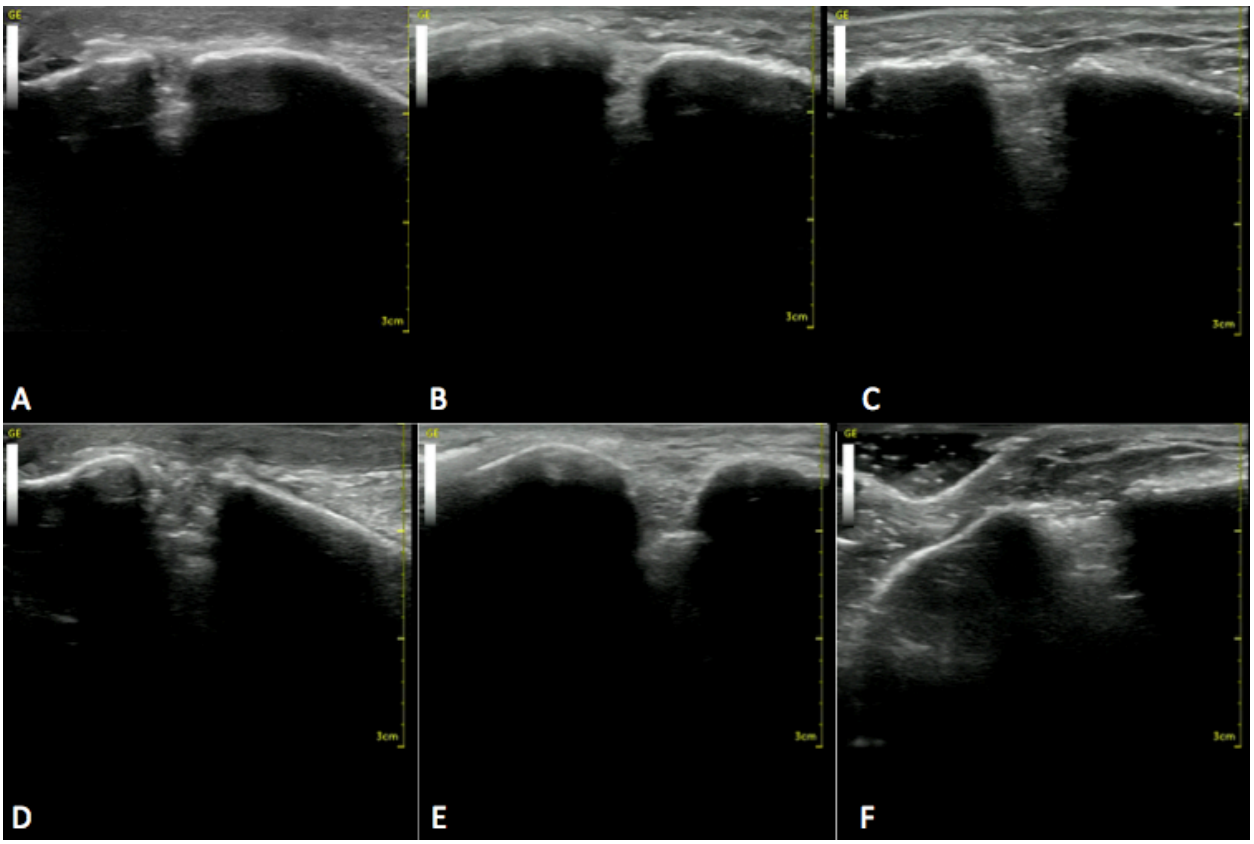

Figure 6.3. Ultrasound imaging of the tibiofibular clear space at 70N of external rotational torque. A – Normal phase; B – 75AITFL phase; C – 100AITFL phase; D – Fibula Fx phase; E -75PITFL phase; F – 100PITFL phase.

Stress examination using ultrasound or fluoroscopy increases the value of the base radiological test by measuring tibiofibular and medial clear spaces while syndesmotic ligaments are under tension.[2,61,63,64] Fluoroscopic data was collected during this study, but accurate results were unable to be obtained due to equipment positioning during experimentation that was unavoidable. The fluoroscopy arm was malrotated during experimentation due to the requirement that the examiner maintain proper positioning of the ultrasound probe and torque on the ankle combined with structural limitations and constraints of the ankle rig and foot-mounting block.

This prevented accurate fluoroscopy alignment with the ankle. Because of this I was not able to evaluate Specific Aim 2: determine the minimum level of syndesmotic injury detectable by stress fluoroscopy examination of the tibiofibular clear space or test hypothesis 2: stress fluoroscopy maintains diagnostic fidelity at SER injury stage 2 and above. In plain film radiography and fluoroscopy, the position of the leg in relation to the beam can significantly affect clear space measurements as can the amount of force being applied to the ankle.[62] In addition, the tibiofibular clear space boney contours represented on radiographs and fluoroscopy may not accurately reflect multiplanar movement of the fibula in injured states.[2] Takao et al. found arthroscopy to be 100% accurate in identifying syndesmotic injuries in patients when compared to plain film radiography which had accuracies of 48% and 64% in AP and mortise views respectively.[72] These findings reflect the limitations of fixed, single plane imaging to identify complex geometric anatomical changes. Larger changes in anatomical alignment are more likely visible on planar imaging such as those found in severe stage 3-4 SER injuries. Electromagnetic sensor placement also interfered with accurate measuring on several specimens. In short, due to the complexity and space constraints of the experiment, alignment between the fluoroscopy machine and the ankle mortise were unable to be achieved (Figures 6.4 and 6.5). Additionally, the experiment planned to include data from a 75% and 100% deltoid ligament injury. Data was collected during these phases; however, it was apparent to all observers that inadequate imaging, ultrasound and fluoroscopic, was obtained while applying torque to the ankle due to the complete instability of the ankle. The ankle was so unstable at these stages of injury that the US probe was unable to see both the fibula and tibia at the same time. Observers noted the fibula and tibia were rotated and translated too far from the viewing plane of the US probe, therefore making measurements impossible as there were little to no visible landmarks apparent on imaging

obtained via ultrasound (Figures 6.6 and 6.7). This is important to note, as clinically, practitioners may have difficulty examining a highly unstable stage 4 SER ankle injury using ultrasound.

Figure 6.4. Fluoroscopic mortise view of Normal (baseline) phase.

Figure 6.5. Fluoroscopic mortise view of 100AITFL phase.

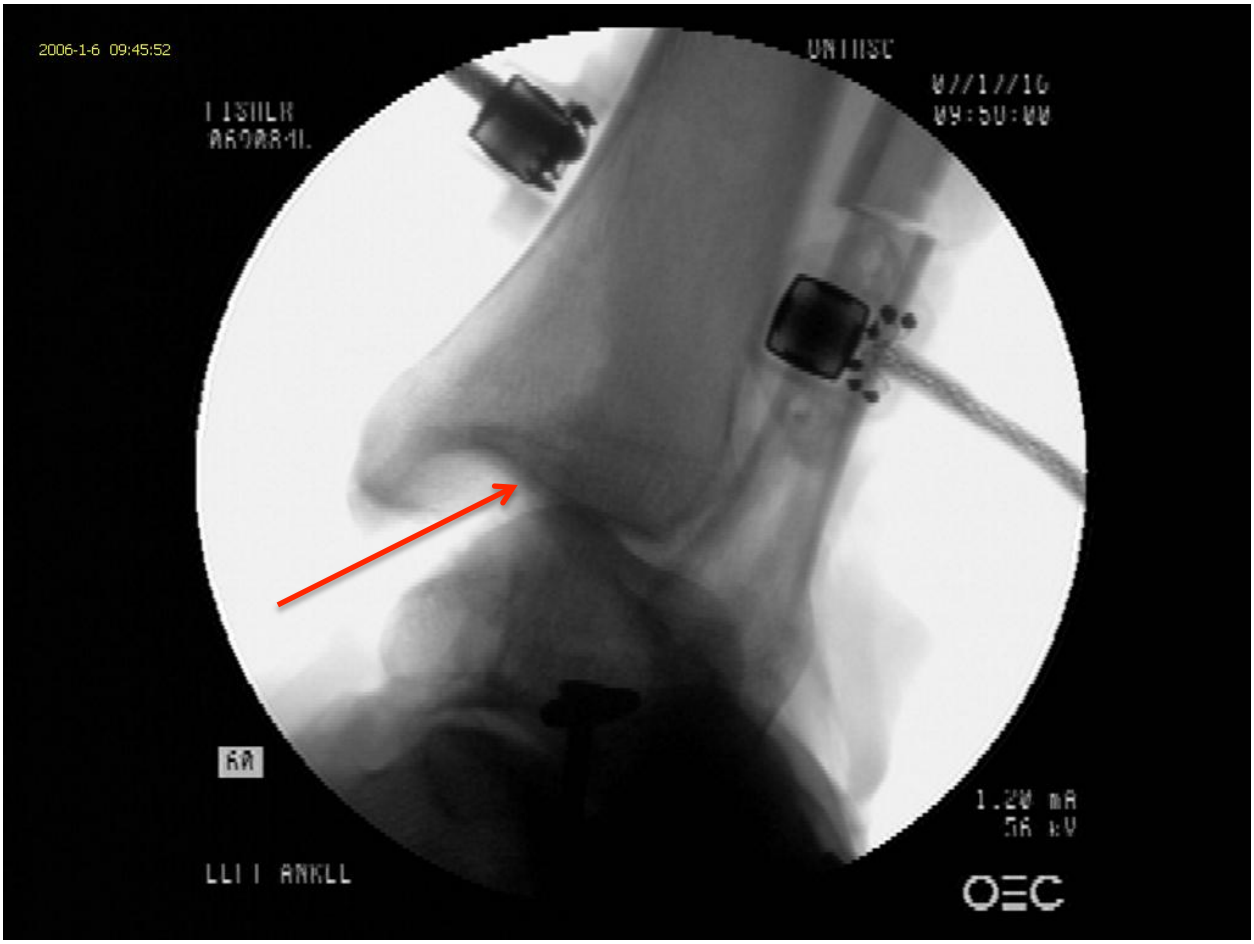

Figure 6.6. Fluoroscopic mortise view of 100Deltoid phase. Note the displacement of the tibial plafond (arrow) off the dome of the talus. The distal fibular fragment is also rotated thus making tibiofibular clear space measurements difficult and unreliable.

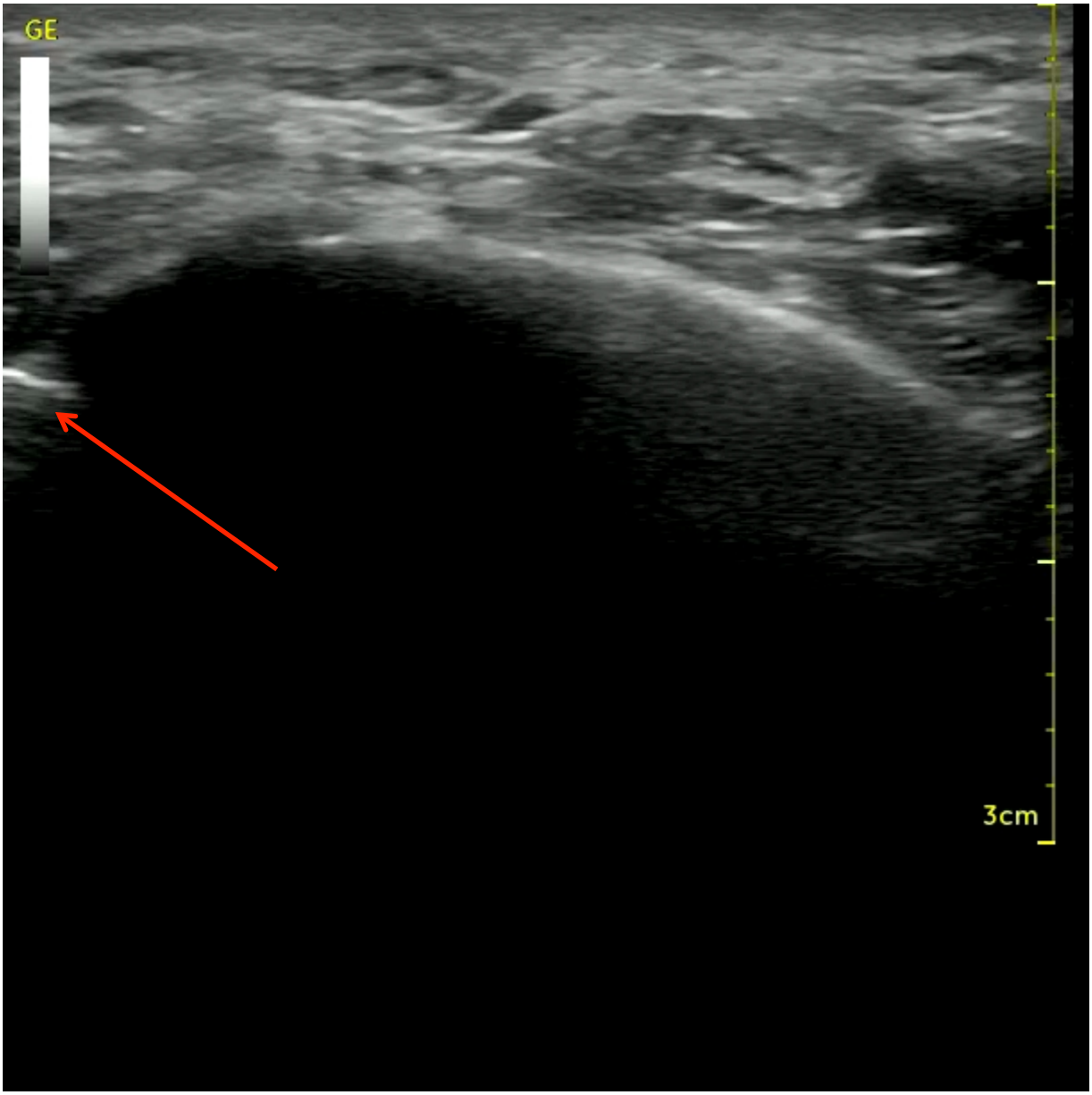

Figure 6.7. Ultrasound image at 100Deltoid phase. The tibiofibular clear space (arrow) is largely off screen. Without the landmark of the tibia, making reliable measurement of the tibiofibular clear space impossible.

Dynamic stress ultrasound evaluation of the ankle syndesmosis has most recently been reported to by Mei-Dan et al., to have a sensitivity and specificity of 100%, but the study had a small sample size.[61] An older study using less advanced ultrasound technology and comparing results to MRI reported a sensitivity of 66% and a specificity of 91% for AITFL injuries.[60] At the present time, ultrasound evaluation is underutilized, but is inexpensive and time efficient.[63] Stress fluoroscopy was found to be unreliable for detecting syndesmosis injuries and reduction with rotationally displaced syndesmosis injuries.[2] Most patients with a suspected syndesmosis injury receive provocative testing and plain film radiographic evaluation first before proceeding to stress examination or advanced imaging (MRI, CT). The considerations for cost, personal preference, radiation dose, and necessity of the test are made prior to proceeding to advanced imaging and stress testing, as there are no agreed upon diagnostic algorithms. This study provides data that indicates dynamic US evaluation can be relied upon for detection of syndesmosis disruptions of complete stage 1 injuries and above which may prevent the need for advanced imaging. This study was the first of its kind to show the ability to detect significant changes in tibiofibular clear space at each level of injury in a cadaveric model. Our data also indicates that a partial AITFL tear may go undiagnosed when relying upon clear space measurements alone with US. These findings should be kept in mind for physicians and technicians when evaluating the ankle syndesmosis through dynamic US evaluation.

There were several limitations to this study. The fresh frozen cadaveric material had a mean age that is older than the prototypical demographic for syndesmosis injury. Additionally, the specimens did not have muscle forces acting upon them or undergo a physiologic movement, which may influence tibiofibular clear space by either increasing or decreasing the stability of the ankle syndesmosis. The ankle rig and foot-mounting block were designed to simulate the

clinical stress test that would be performed by a clinician but did not attempt to simulate physiological loading of the ankle joint. Therefore, the study does not accurately reflect the forces found at the ankle during gait or physiological situations and only represents a characterization of the syndesmosis during diagnostic evaluation. These factors may have affected the ability to detect changes in clear space measurement, but are common limitations amongst in vitro simulations of the syndesmosis.[11,44,66,73-75] There were three independent measurements made by each independent observer for each set of imaging performed by the primary examiner to lessen the effect of examiner bias which is known to affect tibiofibular clear space measurements with US. Furthermore, findings of this cadaveric study need to be followed by controlled trial studies. However, these experiments are expensive and would require a large sample size of participants in order to obtain similar data specific to each level of injury as was performed with cadaveric specimens. The generalizability of this study is limited as only the supination-external rotation ankle Lauge-Hansen injury pattern was examined and there are many other injury patterns that are possible and may affect the diagnostic success of dynamic stress US examination. This dynamic ultrasound study initially included a fluoroscopic evaluation of the ankle syndesmosis.

Accurate fluoroscopic evaluation of the syndesmosis was unfeasible in this experiment, as rotation of the fluoroscopy machine could not reliably be controlled for each specimen. Each specimen needed to have radiographic evaluation with a specific viewing angle that was specific to the alignment of the specimen in the ankle rig, the orientation of the syndesmosis, and allowed for the controlled application and measurement of torque without interfering with dynamic US evaluation. Consistent achievement of these criteria could not be met with the experimental apparatus utilized in this study.

In addition, the fluoroscopic results for tibiofibular clear space measurements were found to have a large standard deviation with many results being anatomically impossible. Because of the inability to position the c-arm correctly, it is important to not that we are not saying that fluoroscopy is not as effective at diagnosing SER injuries as ultrasound since we were not able to test our second specific aim. Therefore, the study focused on dynamic US diagnosis of syndesmosis injuries at partial and complete stages of injury from 1 to 3. The stage 4 injury, which includes a deltoid injury, was not analyzed due to the grossly unstable nature of the injury causing large variations in tibiofibular clear space measurement. Female specimens were excluded due to most cadaveric specimen are of older age and female specimens have a much higher likelihood of having poor bone quality due to osteoporosis.[67] Only male specimens were included to lessen the probability of ankle fracture with application of force. This limitation is likely without any great affect as there are no studies showing a definite difference between male and female syndesmosis anatomy.[44,62,64,76] This study sought to characterize the ability of dynamic US stress evaluation to diagnose partial and complete syndesmosis injury, but this was not a clinical study. Sensitivity and specificity were reported for this cadaveric study, but this did not involve patients nor was the study structured specifically for this purpose. However, a strength of the study was the ability to directly verify the type and quality of the injury. Clinical diagnostic sensitivity and specificity studies use other imaging as controls, which do not have the distinct advantage of being able to directly visualize the injury. Clinically performing an external rotational stress test of the syndesmosis may be pain limited as many patients would not be able to tolerate a large torque due to injury acuity. This may change the amount of torque an examiner would be able to apply to a patient's ankle and thereby influence the ability of US to detect a

tibiofibular clear space indicating a syndesmosis injury. This makes the highly controlled manner in which torque was applied a strength and weakness of the study.

Ramsey et al., described a 42% decrease in tibiotalar contact area with as little as 1 mm of talar shift due to a syndesmosis injury.[12] Further validating these results was a study done by Lloyd et al., in 2006 when they conducted their own research on tibiotalar contact area and talar shift.[77] The decreased tibiotalar contact surface area leads to higher contact pressures, which may accelerate progression of osteoarthritis in the ankle joint. This leads to pain and decreased function, which is completely preventable with prompt diagnosis and treatment. In addition, malreduction has been found to range as high as 25-52% after syndesmosis fixation; which can lead to the same sequelae as a missed diagnosis.[1] Malreduction of the syndesmosis can occur for three different reasons: malreduction of one or both malleoli; osseous or soft-tissue interposition; and malreduction of the fibula into the incisura.[78] Identification of malreduction and the presence of syndesmosis injury are similar and any improvement in imaging assessment may very well improve both evaluation of injury and treatment. Stress ultrasound evaluation also provides a unique method for providing visualization of syndesmosis fixation intra-operatively. This may allow the surgeon to evaluate their work prior to closing the surgical wound to allow for adjustments to fixation as needed. Overall, dynamic ultrasound stress evaluation of the ankle syndesmosis may be more cost effective, improve diagnostic accuracy, and decrease radiation exposure over traditional imaging techniques. However, most physicians do not rely on a single test for diagnosis and more advanced imaging options are typically used when occult injuries are considered. Arthroscopy has the highest sensitivity and specificity of close to 100%, but is invasive and costly.[72] Radiological evaluation through MRI, CT, and plain radiographs provide the next level of evaluation (in descending order of sensitivity/specificity).[2,54,62,64]

This study was the first of its kind to show the ability to detect significant changes in tibiofibular clear space at each level of injury in a cadaveric model. The data also indicates that a partial AITFL tear may go undiagnosed when relying upon clear space measurements alone with US. The sensitivity and specificity were 80.5% and 83.3% respectively, although this was not a clinical study designed to capture clinically accurate data with respect to sensitivity and specificity. This includes partial and complete injuries to the ankle syndesmosis. A partial (75%) AITFL injury would not be expected to show tibiofibular clear space widening and was treated as such during calculations of sensitivity and specificity. The sensitivity and specificity are lower than those reported for prior studies which is likely due to the difference in study design as this was an in vitro study. The results of this study do show improved accuracy over previously reported radiographic studies for sensitivity and specificity. However, this is not a conclusive result, as the two diagnostic modalities were not directly compared using the same specimen. The results of this study do confirm that dynamic US evaluation of the syndesmosis is valid and able to detect syndesmosis injuries. These findings should be kept in mind for physicians and technicians when evaluating the ankle syndesmosis through dynamic US evaluation. Dynamic external rotational stress evaluation using ultrasound was able to detect stage 1 Lauge-Hansen SER injuries with statistical significance and corroborates criteria for diagnosing a syndesmosis injury at ≥ 6.0 mm of tibiofibular clear space widening. These findings should build confidence with physicians and technicians in using US on a more widespread basis, as our findings are novel. Prior clinical and biomechanical studies have only shown the sensitivity and specificity of US diagnosis of syndesmosis injuries without much regard to severity of injury. These findings should serve as a basis for expanding the role of dynamic US evaluation of the syndesmosis for providers and technicians.

CHAPTER 7

CONCLUSIONS AND FUTURE STUDIES

The work encompassed by this dissertation includes a wide breadth of knowledge that is fundamental to teaching health professions students and anatomical research of the foot and ankle. The role of a health professions faculty member is to lay groundwork knowledge and then build upon that knowledge with increasing complexity and depth through associations with real world applications. When it comes to anatomical science, this is especially true. It is not enough to teach the foundation of anatomy with structure and function, as knowledge solely in this format would be soon forgotten and poorly prepare a student for the realities of their future profession. The kinesthetic feel of dissection deepens a student's anatomical library and makes it real to them. To further this approach, I sought to deepen my own knowledge through research of the foot and ankle with a sub-focus on diagnostic ultrasound. This will enable me to provide an additional layer of real world application and association to foundational anatomical knowledge health profession students are required to learn.

Clinical diagnosis of syndesmosis injuries is difficult to do on a consistent basis. There are multiple imaging modalities, provocative tests, and injury patterns that are meant to guide a clinician in achieving the correct diagnosis. Many clinicians rely on technicians to accurately

image the syndesmosis through radiographs or ultrasound which introduces some unreliability of these tests due to examiner bias. This study may bring more confidence to physicians to perform their own evaluation using ultrasound (US) and increase the reliability of the test and the diagnosis. Dynamic ultrasound evaluation of the ankle syndesmosis is a valid method for diagnosis with a cut off greater than 6mm of tibiofibular clear space indicating a significant syndesmosis injury according to the data presented within. The sensitivity and specificity of dynamic US in this study were both greater than 80% using three independent examiners in a highly controlled environment for identifying significant syndesmotic injuries. Additionally, examiners may wish to include a torque-measuring device to their diagnostic algorithm to ensure consistent stress of the syndesmosis. The results of this dissertation should provide confidence to clinicians of the functionality and validity of dynamic stress ultrasound evaluation of the syndesmosis. Through widespread application of the techniques described, fewer misdiagnoses can be made while reducing radiation exposure and cost. Dynamic stress evaluation of the ankle syndesmosis is a valid method for diagnosis of syndesmotic injuries through the measurement of the tibiofibular clear space.

Future Studies

The focus of the work in this dissertation is on dynamic stress evaluation of ankle syndesmosis injuries. Because this study involved cadavers and not patients, the logical next step is to design a clinical study that would involve living patients. IRB approval would be required prior to beginning a study such as this. A large sample size would also be required in order to replicate the data from the different phases of injury we created in our cadaveric study. Studies beyond the clinical study will lead into post fixation evaluation. One of the more difficult and subjective aspects of syndesmosis fixation is evaluating the overall reduction and stability of the

joint after fixation has occurred. In the next series of experiments utilizing cadaveric specimens, I will evaluate the syndesmosis before and after fixation has occurred with computed tomography as a control. This data should provide convincing evidence for both ultrasound diagnosis of injury as well as adequacy of reduction of the syndesmosis. Currently, physicians rely upon feel and fluoroscopic imaging for evaluation of adequacy of reduction/fixation. The use of ultrasound could allow fine tuning of fixation as you can stress the ankle under continuous observation to increase or decrease the tibiofibular clear space. Fluoroscopic imaging has limits due to radiation dosage that makes it prohibitive to continually record images. Since ultrasound evaluation easily overcomes this hurdle, many physicians may find the method advantageous. The method for measuring the joint space could be applied to other joints as well. For instance, many surgical sports procedures on the knee could be closely evaluated intraoperatively with high accuracy. An interesting study in the future could use ultrasound to evaluate medial collateral ligament (MCL) integrity using medial knee joint space measurement pre-operatively, intraoperatively, and post operatively from reconstruction. The data would allow physicians to measure the contralateral side and attempt to recreate joint space found in the uninjured knee and allow a more thorough intraoperative evaluation. The technology could be utilized for other joints throughout the body as well to measure spacing between joint surfaces for more accurate reconstruction or diagnosis. Many practitioners in the healthcare field diagnose and treat syndesmotic ankle injures. With supportive data from a clinical study, I would like to start a training program in our BioSkills Lab to teach physical therapists, orthopedic surgeons, athletic trainers, and sports medicine doctors how to use ultrasound to diagnose different levels of syndesmotic injury. This information would allow the practitioner to make an immediate diagnosis and plan the proper treatment.

APPENDIX

BLAND-ALTMAN RESULTS

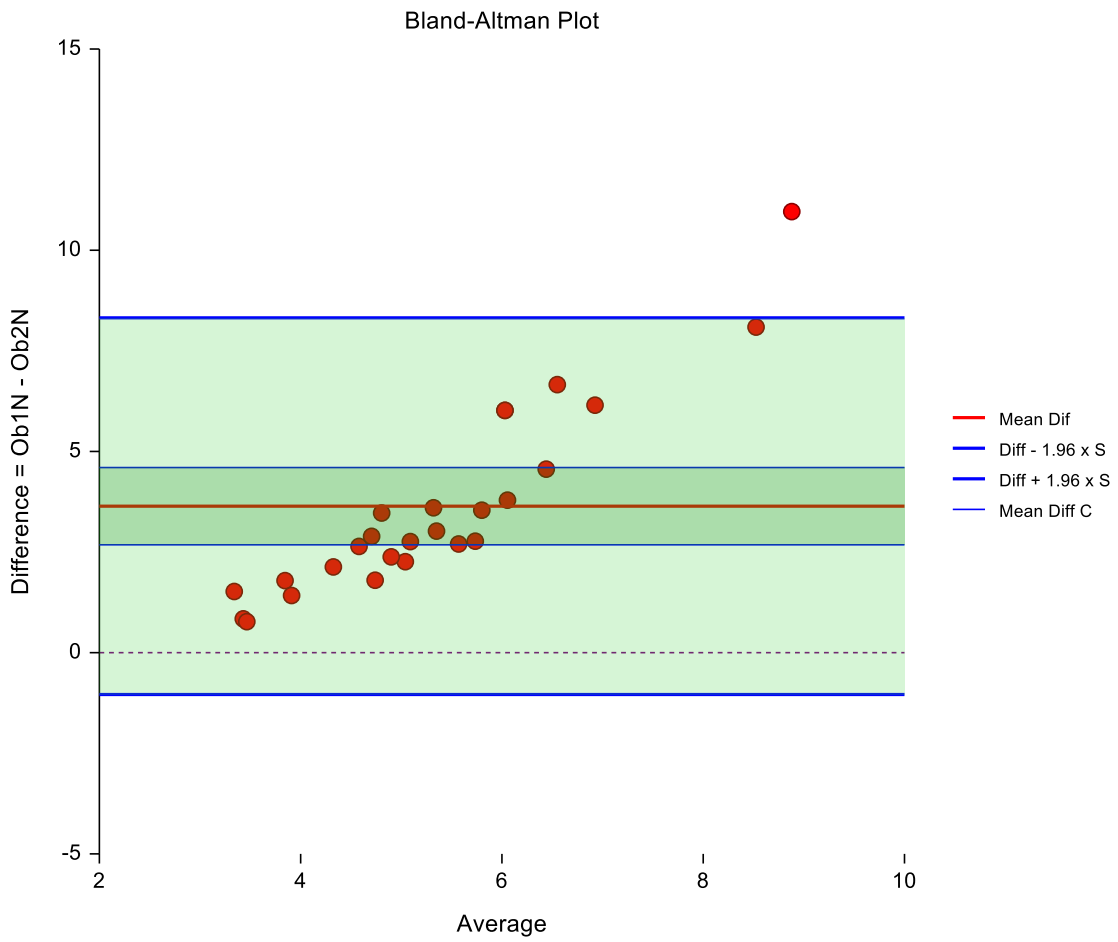

Figure A.1. Bland-Altman plot comparing Observer 1 (Ob1) to Observer 2 (Ob2) for Normal (N) phase. Average = tibiofibular clear space measurements. Note that the 95% CI (dark green area) does not encompass a mean difference of 0.0 mm. The measurements between these two observers are not repeatable. These average differences can be found summarized in **Table 5.1**.

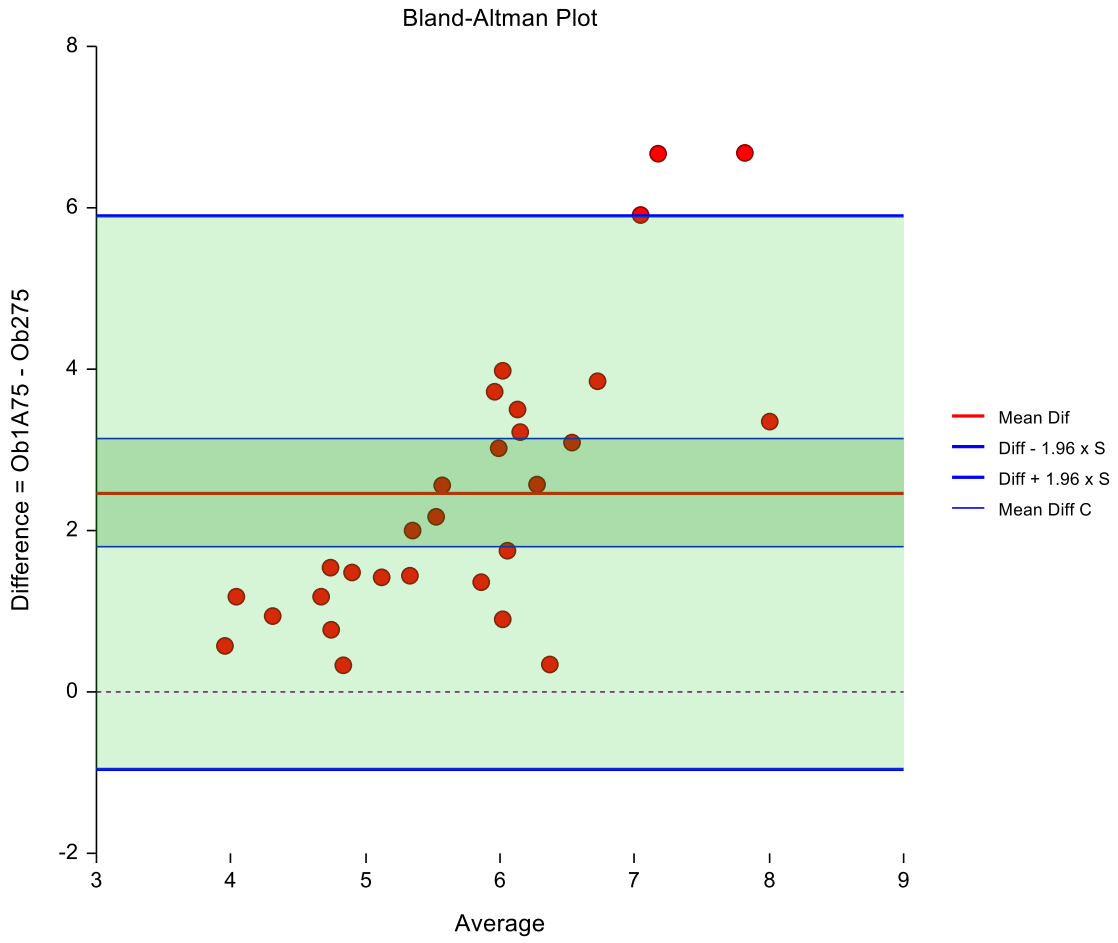

Figure A.2. Bland-Altman plot comparing Observer 1 (Ob1) to Observer 2 (Ob2) for 75AITFL (A75) phase. Average = tibiofibular clear space measurements. Note that the 95% CI (dark green area) does not encompass a mean difference of 0.0 mm. The measurements between these two observers are not repeatable. These average differences can be found summarized in **Table 5.1**.

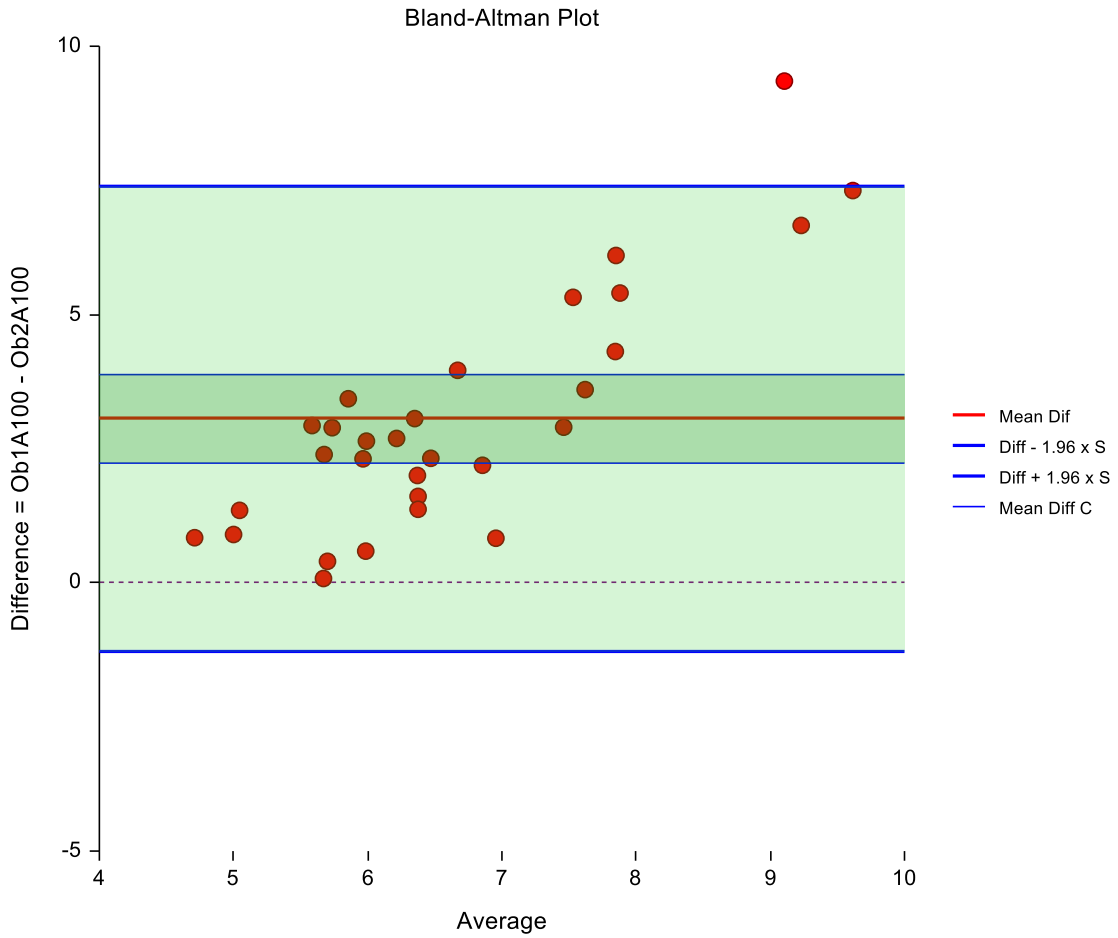

Figure A.3. Bland-Altman plot comparing Observer 1 (Ob1) to Observer 2 (Ob2) for 100AITFL (A100) phase. Average = tibiofibular clear space measurements. Note that the 95% CI (dark green area) does not encompass a mean difference of 0.0 mm. The measurements between these two observers are not repeatable. These average differences can be found summarized in **Table 5.1**.

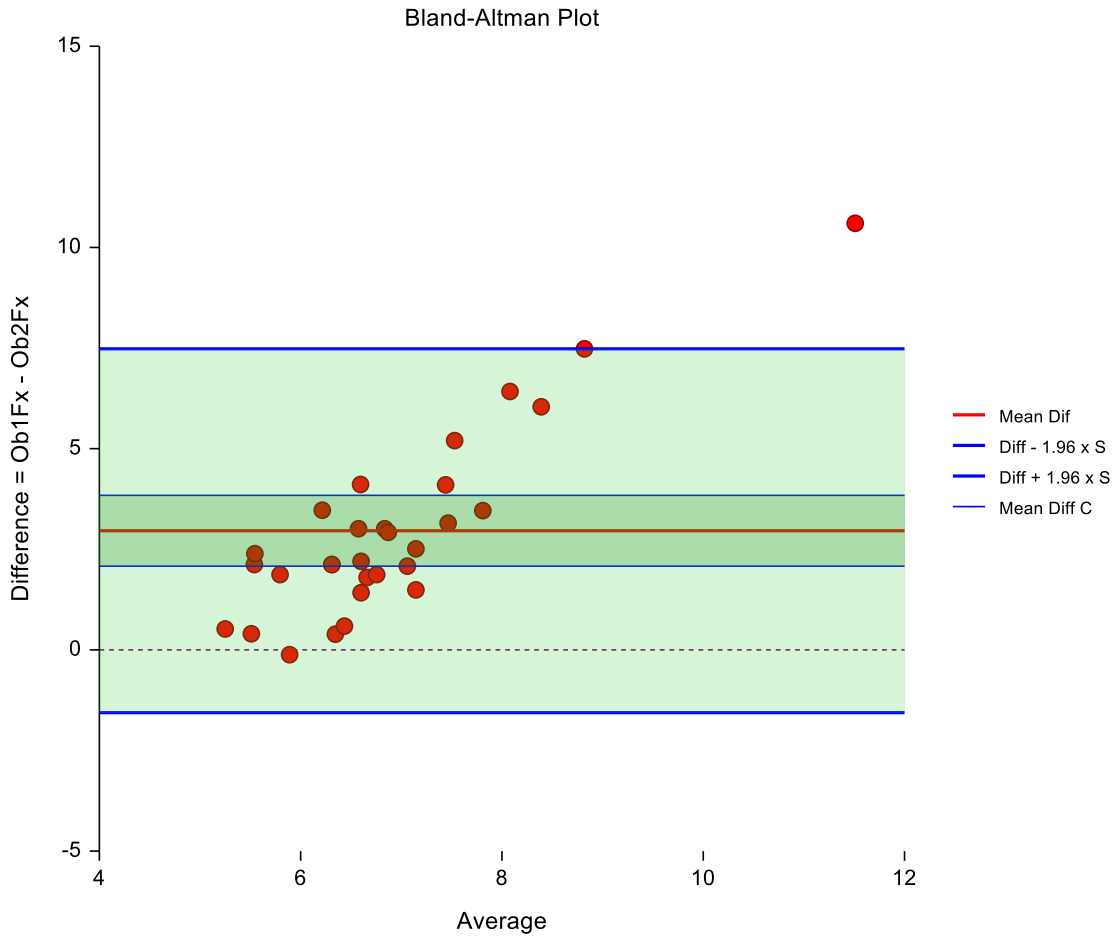

Figure A.4. Bland-Altman plot comparing Observer 1 (Ob1) to Observer 2 (Ob2) for Fibular fracture (Fx) phase. Average = tibiofibular clear space measurements. Note that the 95% CI (dark green area) does not encompass a mean difference of 0.0 mm. The measurements between these two observers are not repeatable. These average differences can be found summarized in **Table 5.1**.

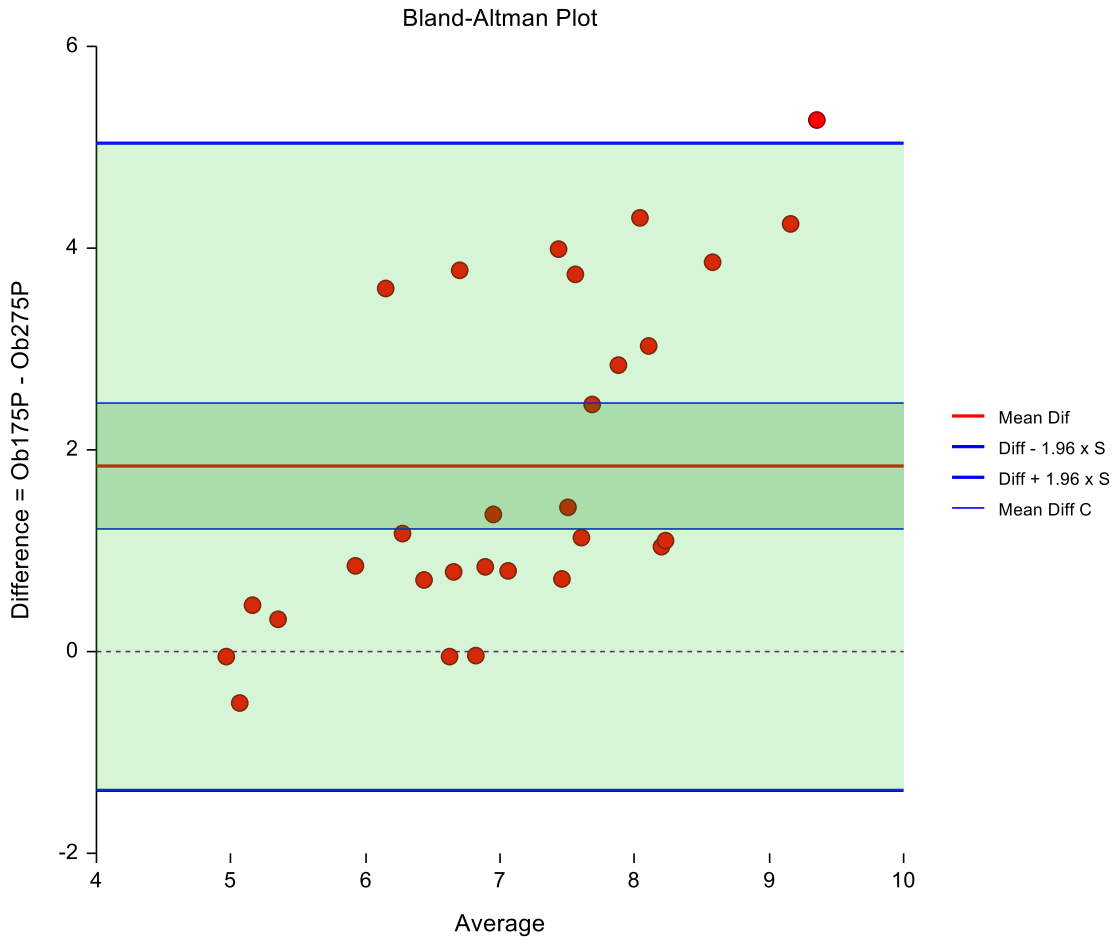

Figure A.5. Bland-Altman plot comparing Observer 1 (Ob1) to Observer 2 (Ob2) for 75PITFL (75P) phase. Average = tibiofibular clear space measurements. Note that the 95% CI (dark green area) does not encompass a mean difference of 0.0 mm. The measurements between these two observers are not repeatable. These average differences can be found summarized in **Table 5.1**.

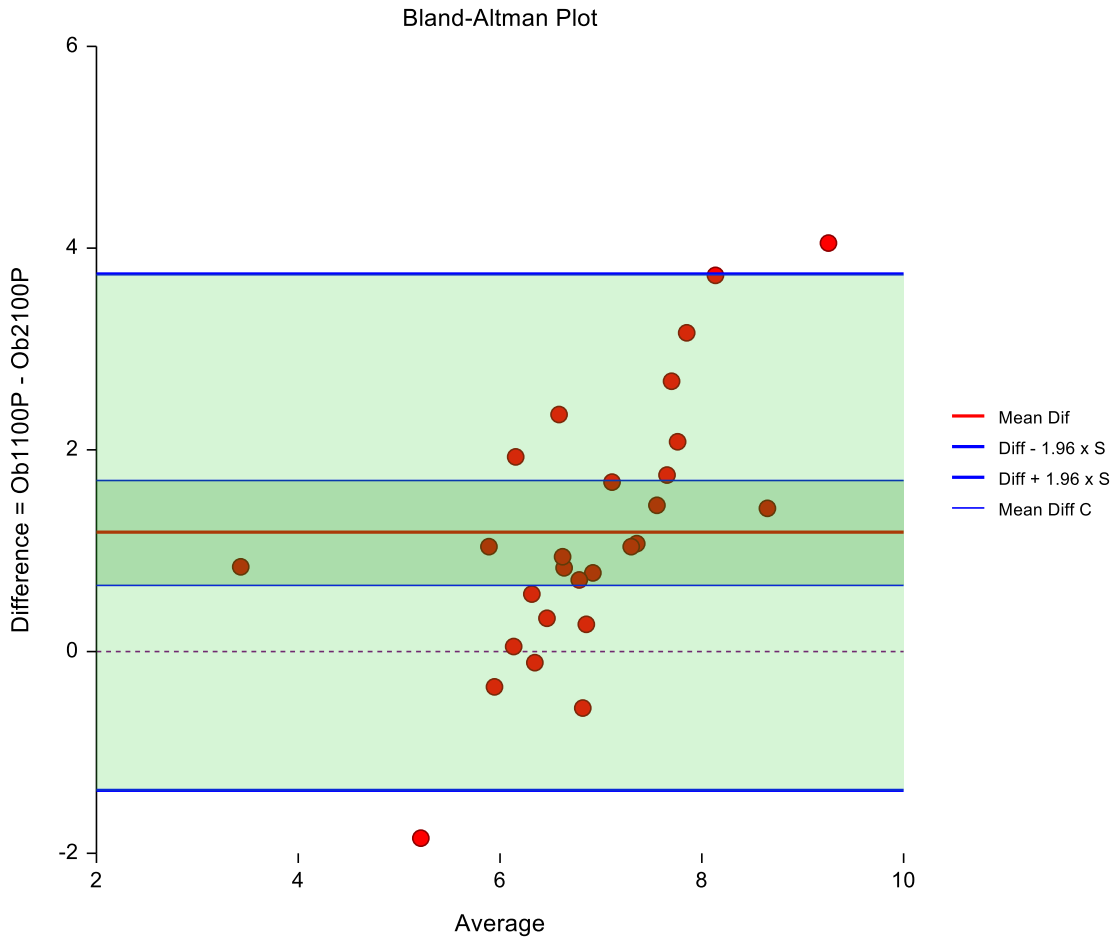

Figure A.6. Bland-Altman plot comparing Observer 1 (Ob1) to Observer 2 (Ob2) for 100PITFL (100P) phase. Average = tibiofibular clear space measurements. Note that the 95% CI (dark green area) does not encompass a mean difference of 0.0 mm. The measurements between these two observers are not repeatable. These average differences can be found summarized in **Table 5.1**.

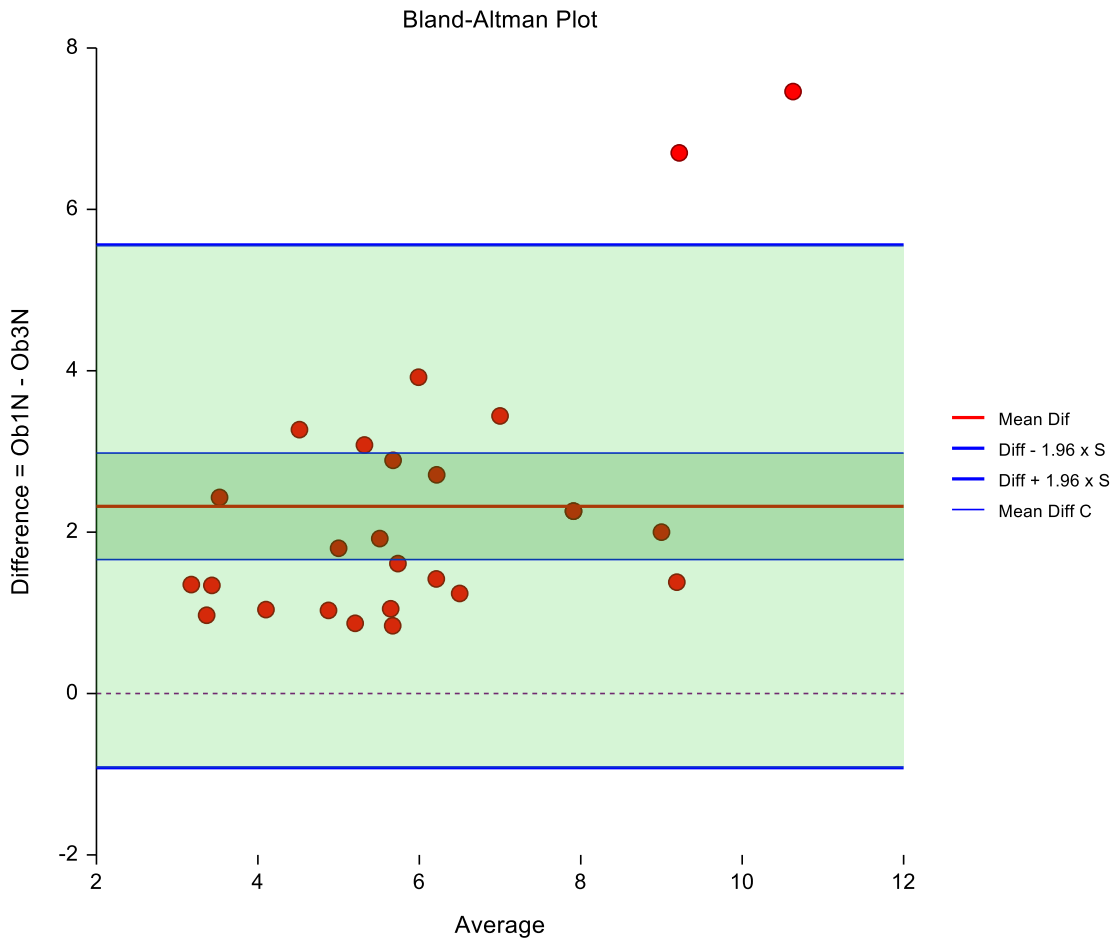

Figure A.7. Bland-Altman plot comparing Observer 1 (Ob1) to Observer 3 (Ob3) for Normal (N) phase. Average = tibiofibular clear space measurements. Note that the 95% CI (dark green area) does not encompass a mean difference of 0.0 mm. The measurements between these two observers are not repeatable. These average differences can be found summarized in **Table 5.1**.

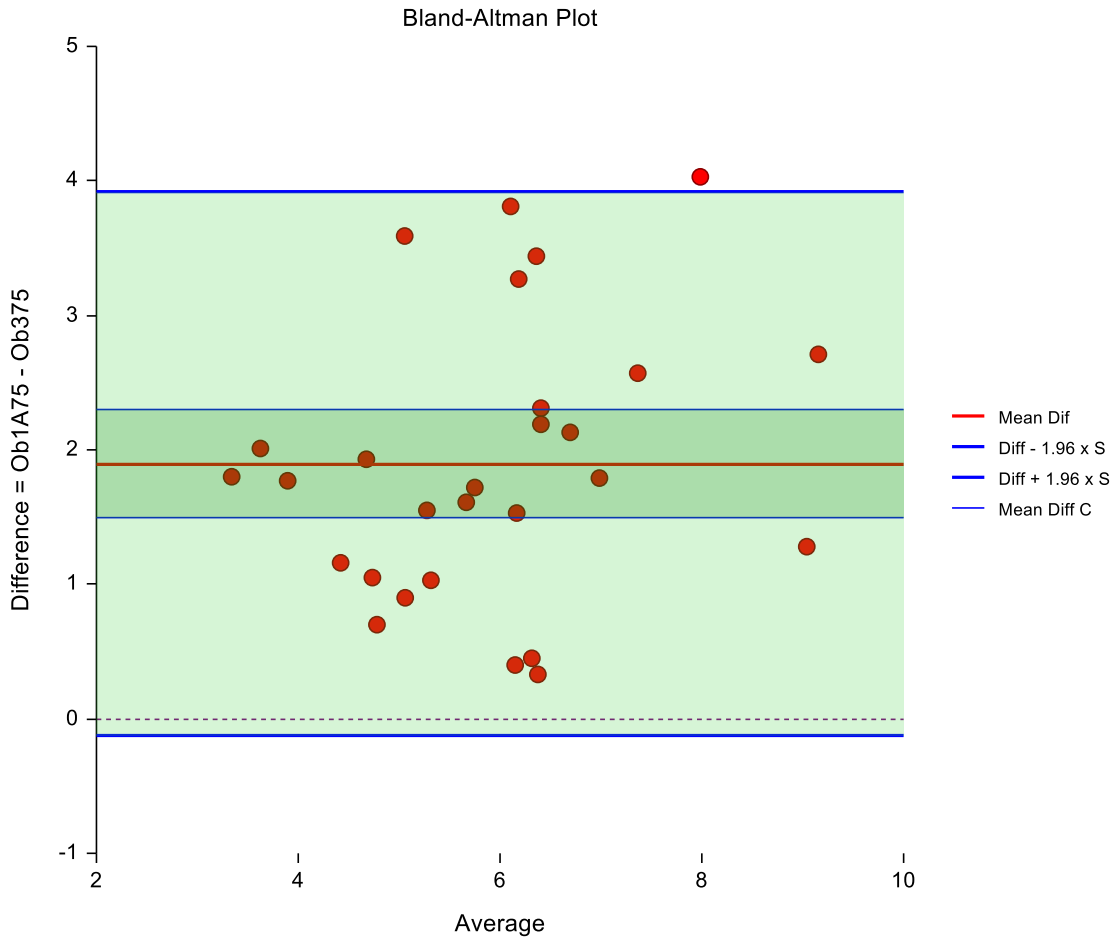

Figure A.8. Bland-Altman plot comparing Observer 1 (Ob1) to Observer 3 (Ob3) for 75AITFL (A75) phase. Average = tibiofibular clear space measurements. Note that the 95% CI (dark green area) does not encompass a mean difference of 0.0 mm. The measurements between these two observers are not repeatable. These average differences can be found summarized in **Table 5.1**.

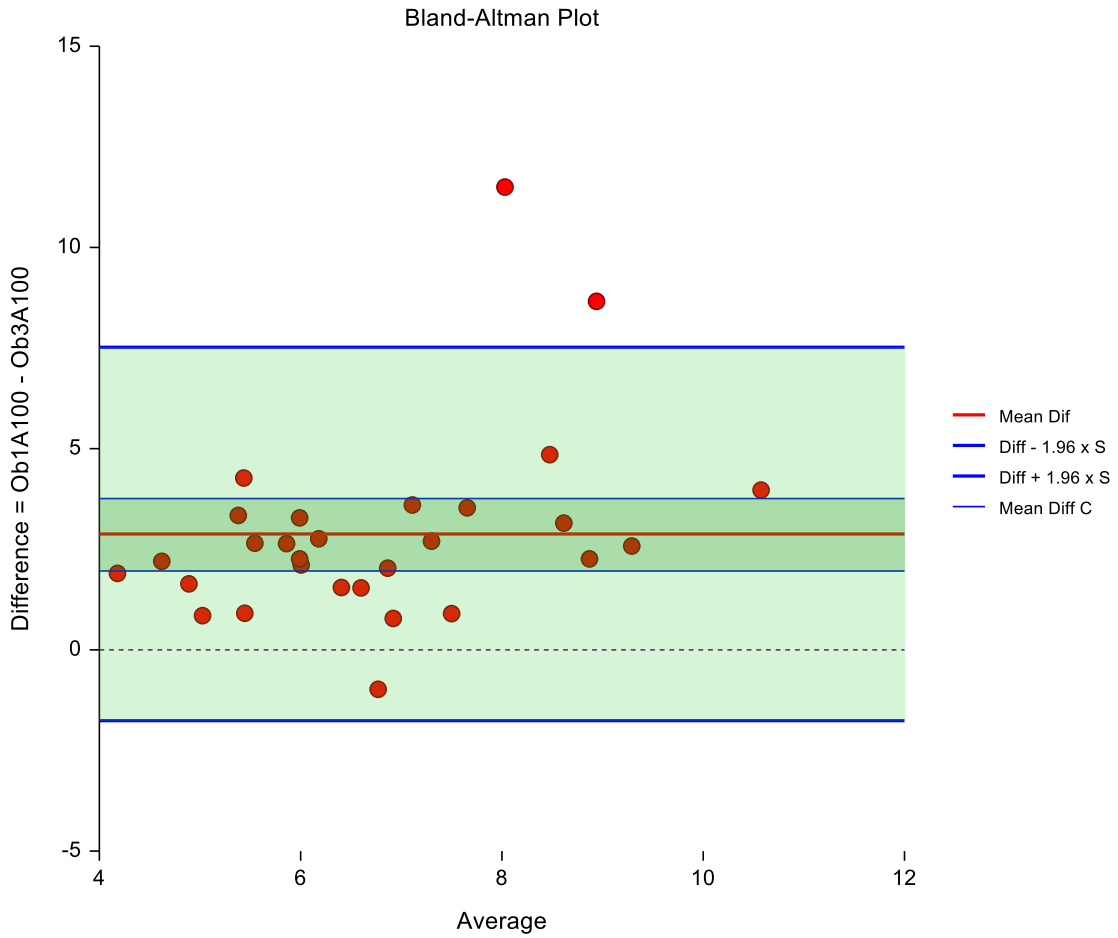

Figure A.9. Bland-Altman plot comparing Observer 1 (Ob1) to Observer 3 (Ob3) for 100AITFL (A100) phase. Average = tibiofibular clear space measurements. Note that the 95% CI (dark green area) does not encompass a mean difference of 0.0 mm. The measurements between these two observers are not repeatable. These average differences can be found summarized in **Table 5.1**.

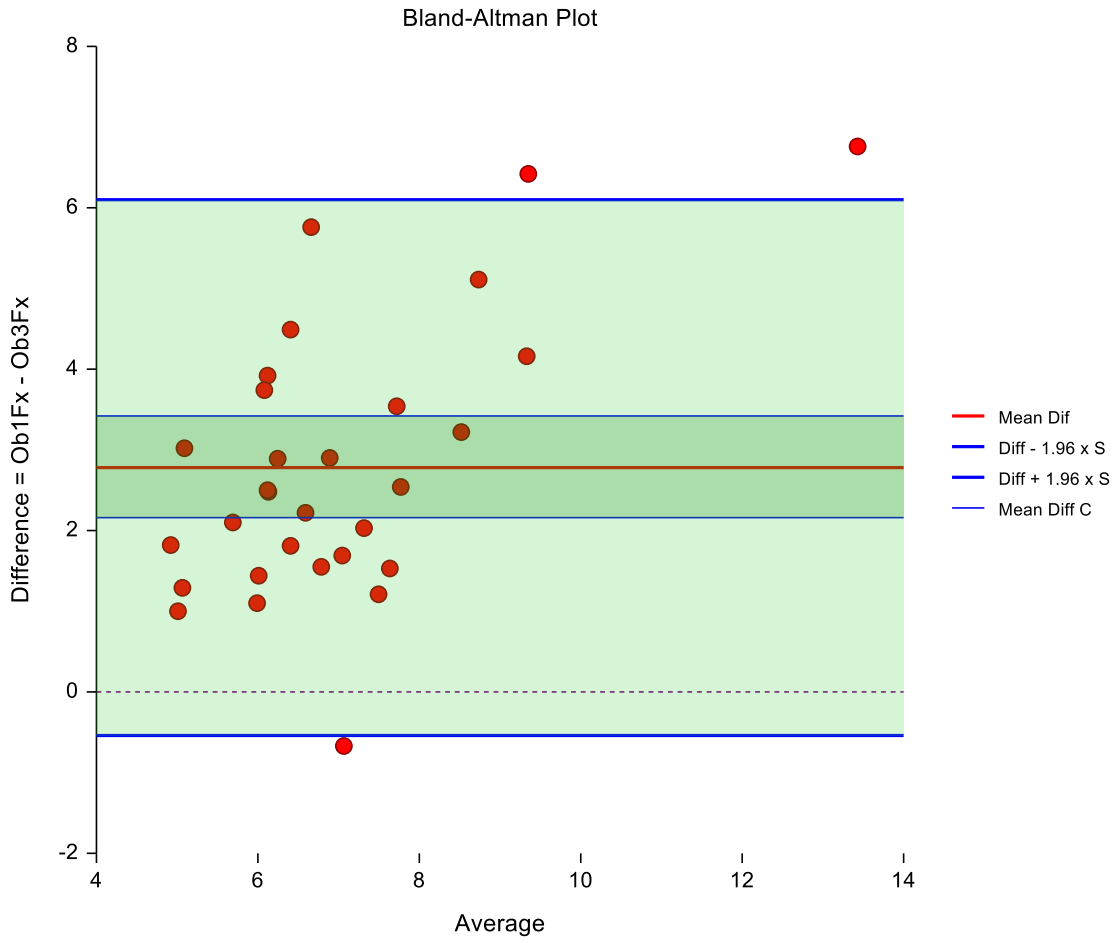

Figure A.10. Bland-Altman plot comparing Observer 1 (Ob1) to Observer 3 (Ob3) for Fibula fracture (Fx) phase. Average = tibiofibular clear space measurements. Note that the 95% CI (dark green area) does not encompass a mean difference of 0.0 mm. The measurements between these two observers are not repeatable. These average differences can be found summarized in **Table 5.1**.

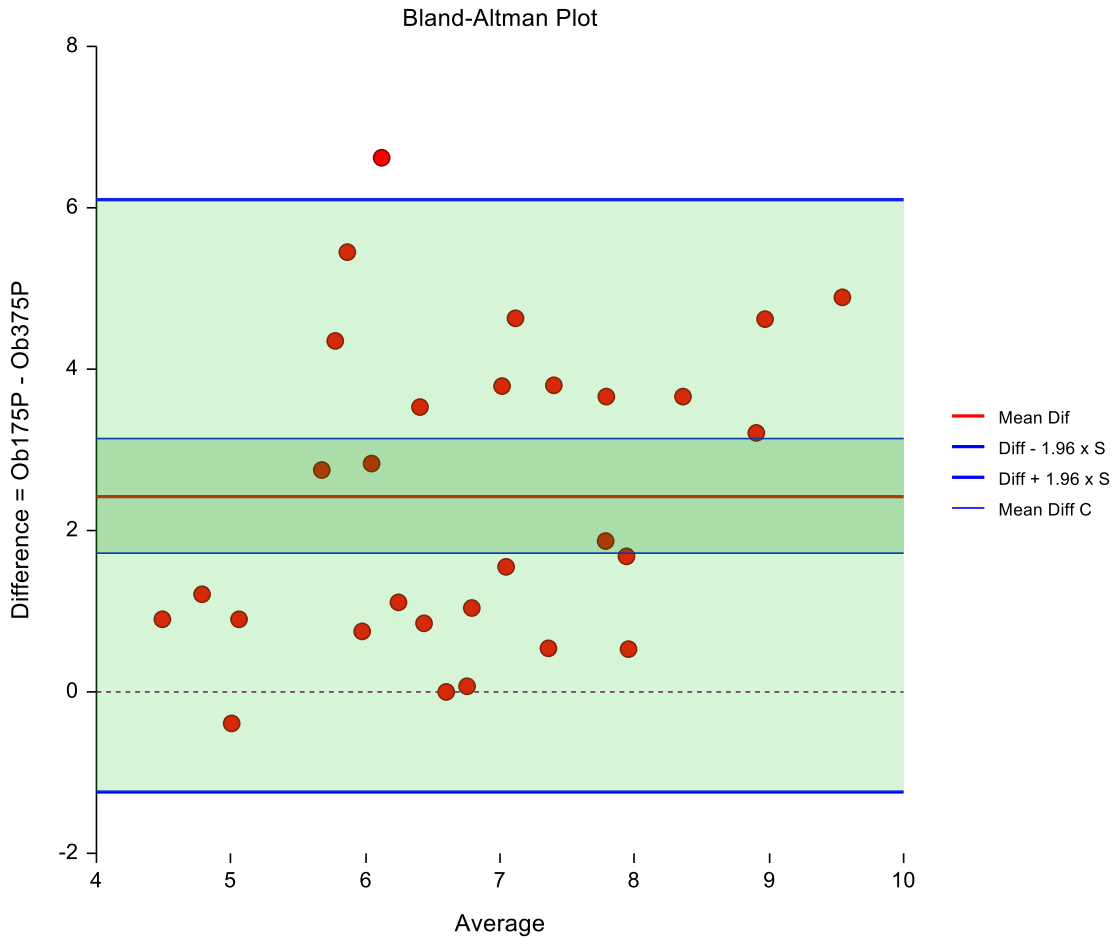

Figure A.11. Bland-Altman plot comparing Observer 1 (Ob1) to Observer 3 (Ob3) for 75PITFL (75P) phase. Average = tibiofibular clear space measurements. Note that the 95% CI (dark green area) does not encompass a mean difference of 0.0 mm. The measurements between these two observers are not repeatable. These average differences can be found summarized in **Table 5.1**.

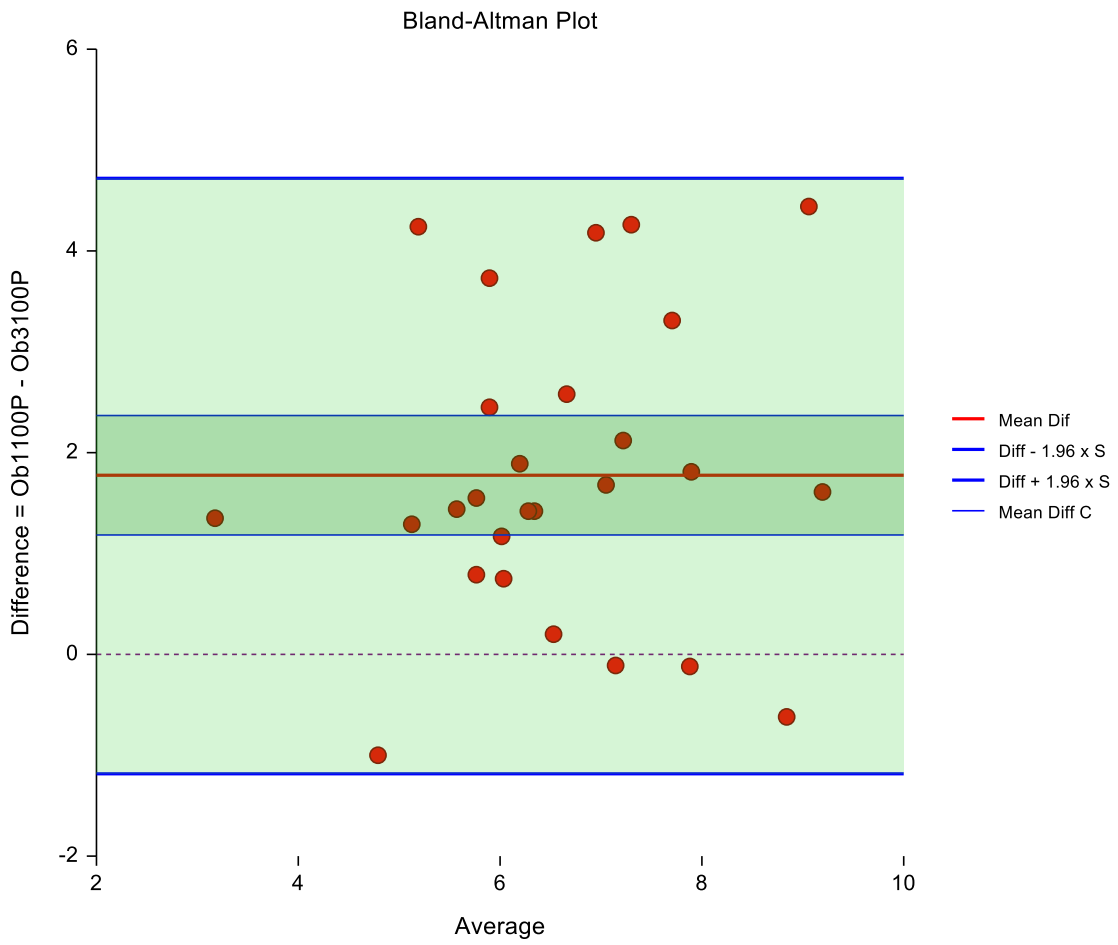

Figure A.12. Bland-Altman plot comparing Observer 1 (Ob1) to Observer 3 (Ob3) for100PITFL (100P) phase. Average = tibiofibular clear space measurements. Note that the 95% CI (dark green area) does not encompass a mean difference of 0.0 mm. The measurements between these two observers are not repeatable. These average differences can be found summarized in **Table 5.1**.

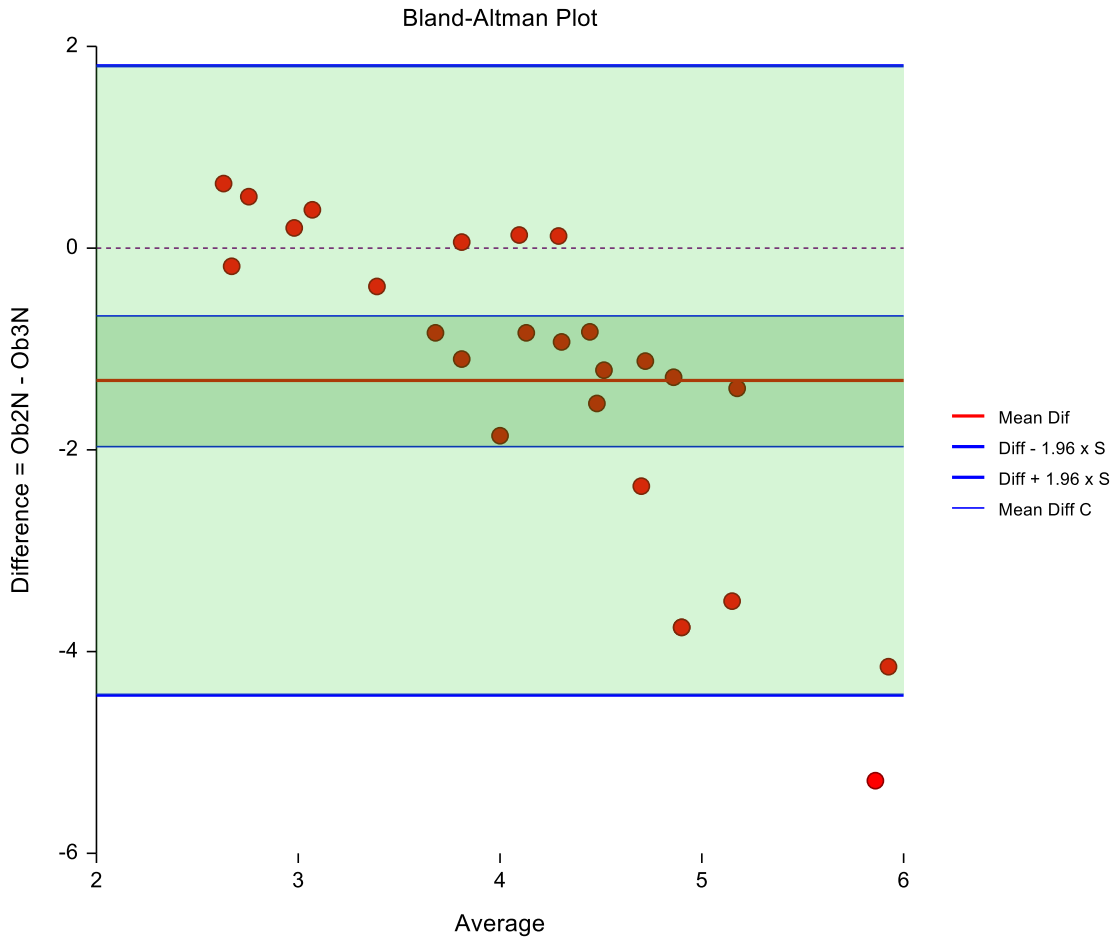

Figure A.13. Bland-Altman plot comparing Observer 2 (Ob2) to Observer 3 (Ob3) for Normal (N) phase. Average = tibiofibular clear space measurements. Note that the 95% CI (dark green area) does not encompass a mean difference of 0.0 mm. The measurements between these two observers are not repeatable. These average differences can be found summarized in **Table 5.1**.

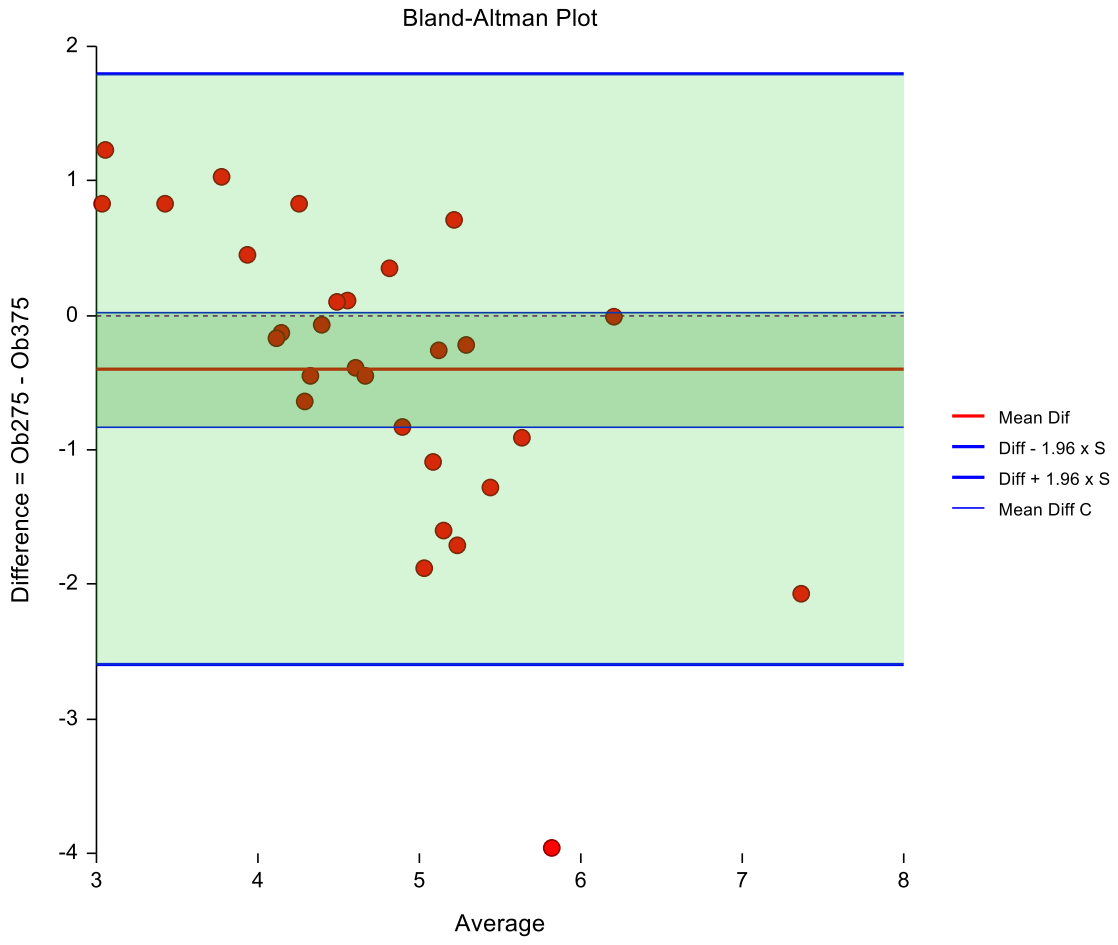

Figure A.14. Bland-Altman plot comparing Observer 2 (Ob2) to Observer 3 (Ob3) for 75AITFL (A75) phase. Average = tibiofibular clear space measurements. Note that the 95% CI (dark green area) does not encompass a mean difference of 0.0 mm. The measurements between these two observers are not repeatable. These average differences can be found summarized in **Table 5.1**.

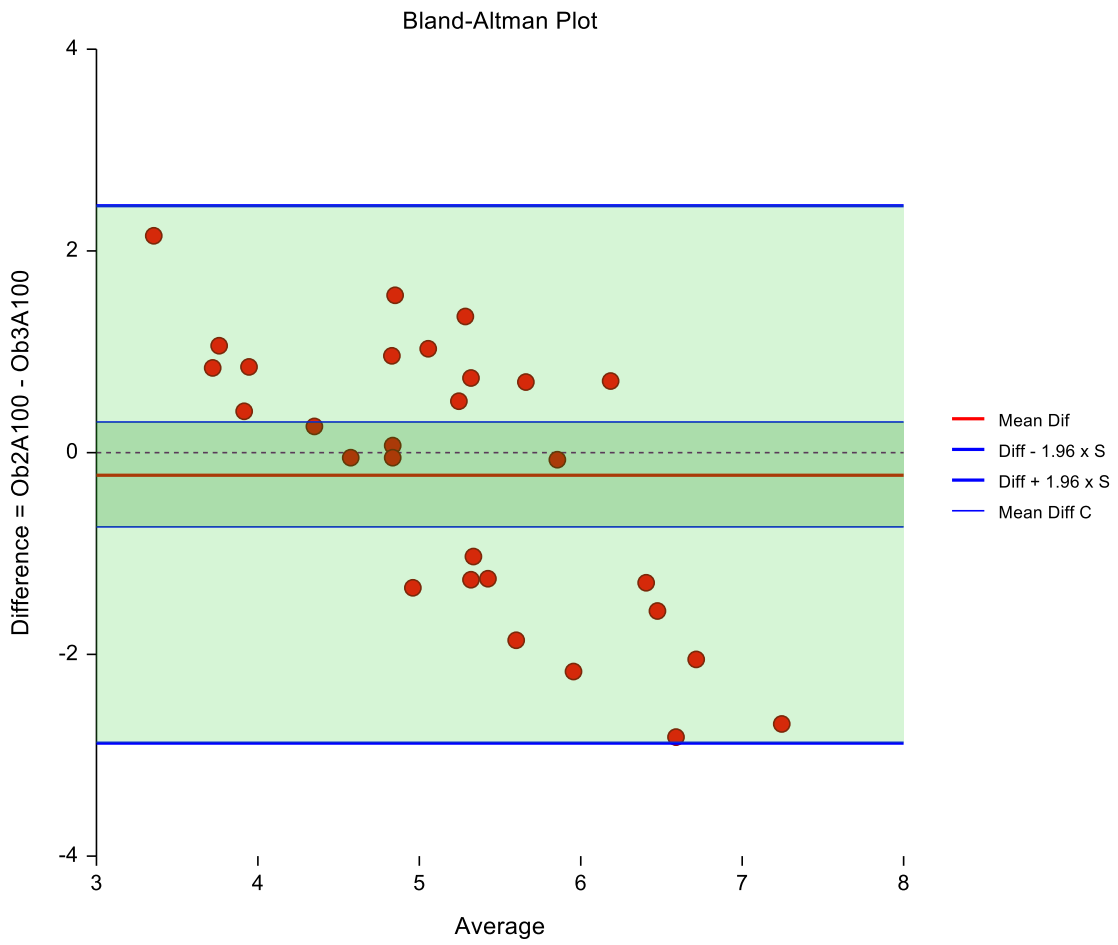

Figure A.15. Bland-Altman plot comparing Observer 2 (Ob2) to Observer 3 (Ob3) for 100AITFL (A100) phase. Average = tibiofibular clear space measurements. Note that the 95% CI (dark green area) encompasses a mean difference of 0.0 mm. The measurements between these two observers are repeatable. These average differences can be found summarized in **Table 5.1**.

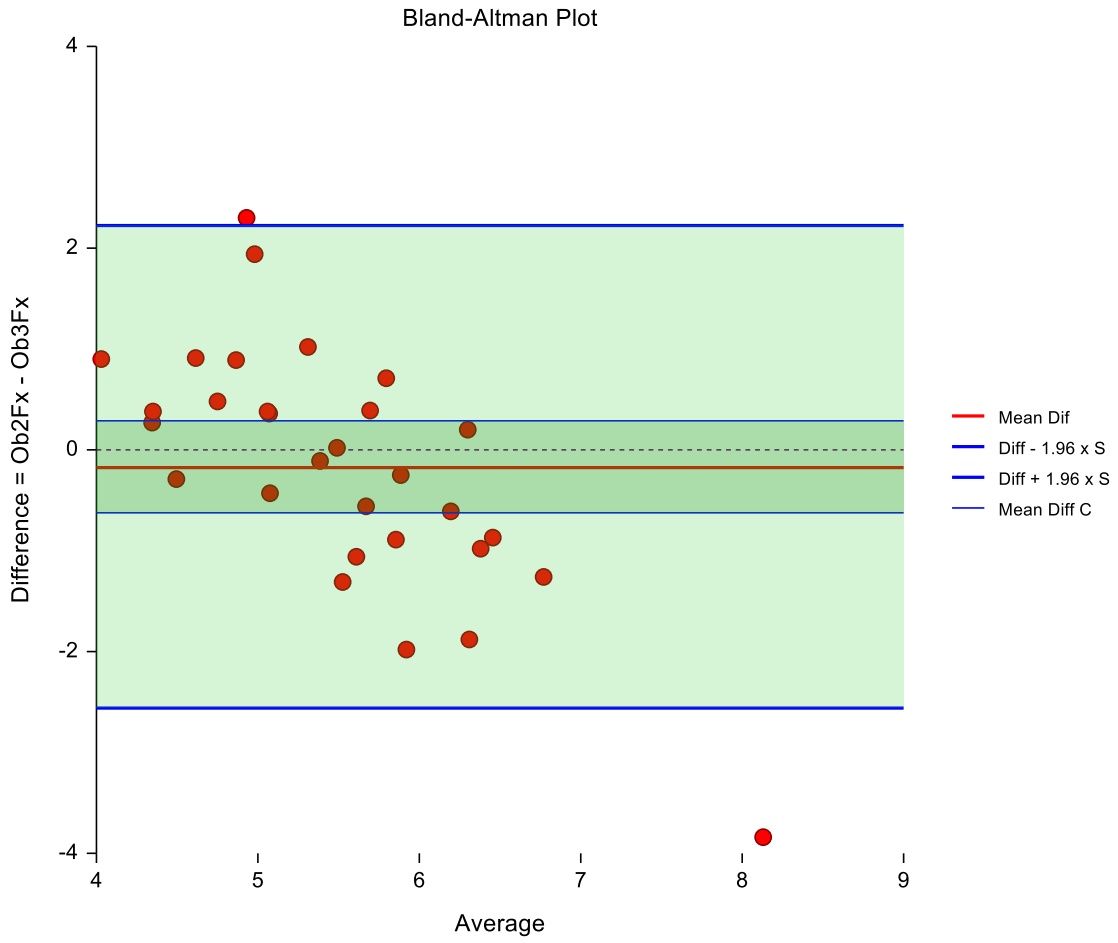

Figure A.16. Bland-Altman plot comparing Observer 2 (Ob2) to Observer 3 (Ob3) for Fibular fracture (FX) phase. Average = tibiofibular clear space measurements. Note that the 95% CI (dark green area) encompasses a mean difference of 0.0 mm. The measurements between these two observers are repeatable. These average differences can be found summarized in **Table 5.1**.

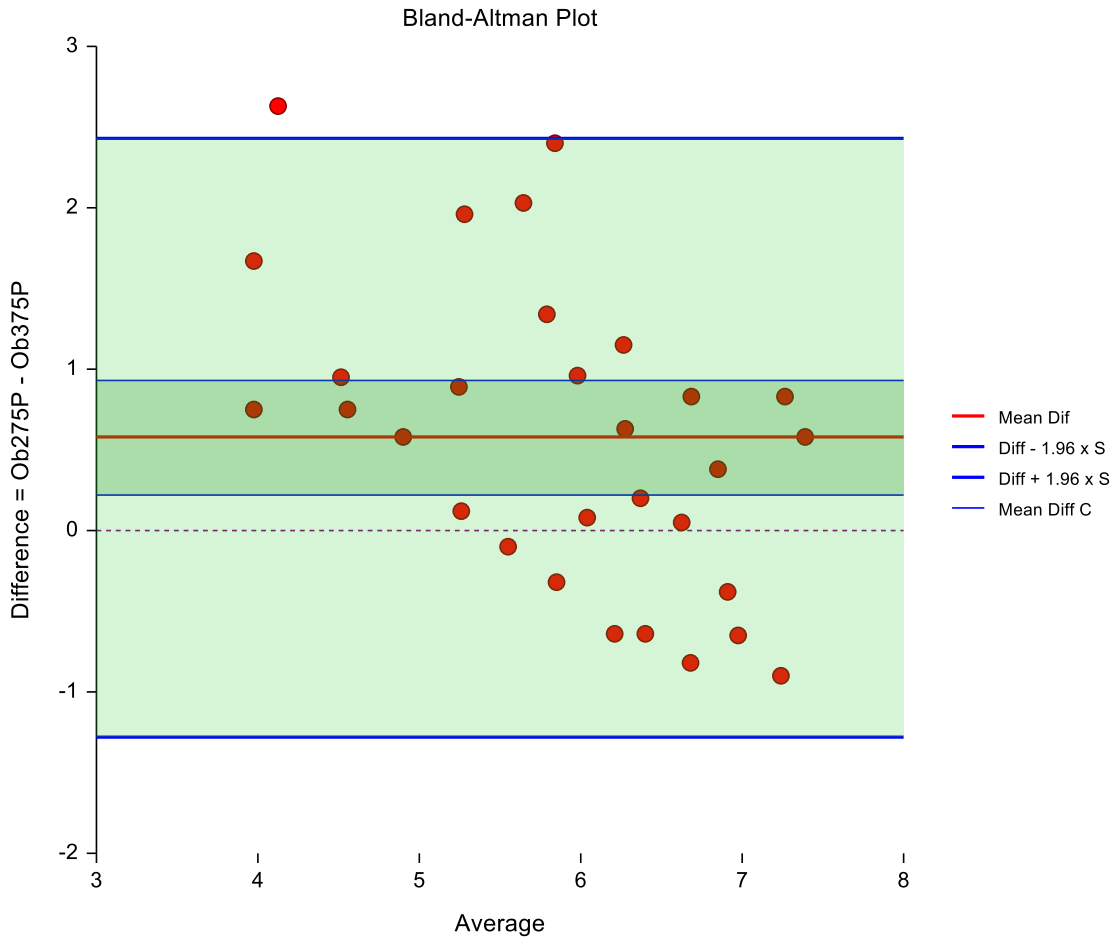

Figure A.17. Bland-Altman plot comparing Observer 2 (Ob2) to Observer 3 (Ob3) for 75PITFL (75P) phase. Average = tibiofibular clear space measurements. Note that the 95% CI (dark green area) does not encompass a mean difference of 0.0 mm. The measurements between these two observers are not repeatable. These average differences can be found summarized in **Table 5.1**.

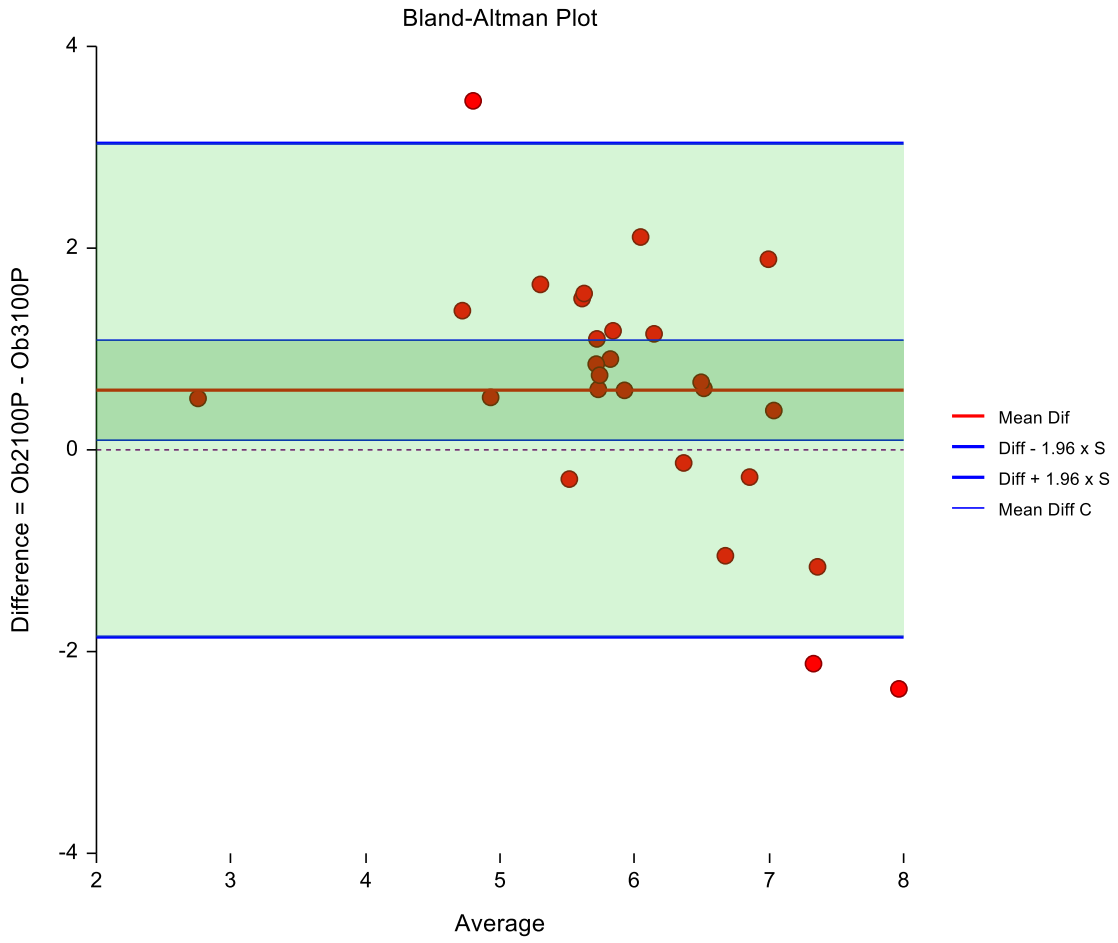

Figure A.18. Bland-Altman plot comparing Observer 2 (Ob2) to Observer 3 (Ob3) for 100PITFL (100P) phase. Average = tibiofibular clear space measurements. Note that the 95% CI (dark green area) does not encompass a mean difference of 0.0 mm. The measurements between these two observers are not repeatable. These average differences can be found summarized in **Table 5.1**.

REFERENCES

1. Van Heest TJ, Lafferty PM. Injuries to the ankle syndesmosis. *J Bone Joint Surg Am.* 2014;96(7):603-613.

2. Marmor M, Hansen E, Han HK, Buckley J, Matityahu A. Limitations of standard fluoroscopy in detecting rotational malreduction of the syndesmosis in an ankle fracture model. *Foot Ankle Int.* 2011;32(6):616-622.

3. Saltzman CL, Salamon ML, Blanchard GM, et al. Epidemiology of ankle arthritis: report of a consecutive series of 639 patients from a tertiary orthopaedic center. *Iowa Orthop J.* 2005;25:44-46.

4. Levangie PK, Norkin CC, Levangie PK. *Joint structure and function : a comprehensive analysis.* 5th ed. Philadelphia: F.A. Davis Co.; 2011.

5. Hollinshead WH. *Textbook of anatomy.* 3d ed. Hagerstown, Md.,: Medical Dept.; 1974.

6. Takebe K, Nakagawa A, Minami H, Kanazawa H, Hirohata K. Role of the fibula in weight-bearing. *Clin Orthop Relat Res.* 1984(184):289-292.

7. Funk JR, Rudd RW, Kerrigan JR, Crandall JR. The line of action in the tibia during axial compression of the leg. *J Biomech.* 2007;40(10):2277-2282.

8. Moore KL, Dalley AF, Agur AMR. *Clinically oriented anatomy.* 7th ed. Philadelphia: Wolters Kluwer/Lippincott Williams & Wilkins Health; 2014.

9. Beumer A, van Hemert WL, Niesing R, et al. Radiographic measurement of the distal tibiofibular syndesmosis has limited use. *Clin Orthop Relat Res.* 2004(423):227-234.

10. Bartonicek J. Anatomy of the tibiofibular syndesmosis and its clinical relevance. *Surg Radiol Anat.* 2003;25(5-6):379-386.

11. Hunt KJ, Goeb Y, Behn AW, Criswell B, Chou L. Ankle Joint Contact Loads and Displacement With Progressive Syndesmotic Injury. *Foot Ankle Int.* 2015;36(9):1095-1103.

12. Ramsey PL, Hamilton W. Changes in tibiotalar area of contact caused by lateral talar shift. *J Bone Joint Surg Am.* 1976;58(3):356-357.

13. Hatch GF, Labib SA, Rolf RH, Hutton WC. Role of the peroneal tendons and superior peroneal retinaculum as static stabilizers of the ankle. *J Surg Orthop Adv.* 2007;16(4):187-191.

14. Klein P, Mattys S, Rooze M. Moment arm length variations of selected muscles acting on talocrural and subtalar joints during movement: an in vitro study. *J Biomech.* 1996;29(1):21-30.

15. McKeon KE, Wright RW, Johnson JE, McCormick JJ, Klein SE. Vascular anatomy of the tibiofibular syndesmosis. *J Bone Joint Surg Am.* 2012;94(10):931-938.

16. Standring S. *Gray's anatomy : the anatomical basis of clinical practice.* Forty-first edition. ed. New York: Elsevier Limited; 2016.

17. Di Gregorio R, Parenti-Castelli V, O'Connor JJ, Leardini A. Mathematical models of passive motion at the human ankle joint by equivalent spatial parallel mechanisms. *Med Biol Eng Comput.* 2007;45(3):305-313.

18. Fujii T, Kitaoka HB, Luo ZP, Kura H, An KN. Analysis of ankle-hindfoot stability in multiple planes: an in vitro study. *Foot Ankle Int.* 2005;26(8):633-637.

19. Bozkurt M, Doral MN. Anatomic factors and biomechanics in ankle instability. *Foot Ankle Clin.* 2006;11(3):451-463.

20. Cromeens BP, Kirchhoff CA, Patterson RM, et al. An attachment-based description of the medial collateral and spring ligament complexes. *Foot Ankle Int.* 2015;36(6):710-721.

21. McCollum GA, van den Bekerom MP, Kerkhoffs GM, Calder JD, van Dijk CN. Syndesmosis and deltoid ligament injuries in the athlete. *Knee Surg Sports Traumatol Arthrosc.* 2013;21(6):1328-1337.

22. Mentzel M, Fleischmann W, Bauer G, Kinzl L. Ankle joint denervation. Part 1: Anatomy - the sensory innervation of the ankle joint. *Foot and Ankle Surgery.*5(1):15-20.

23. Erdemir A, Hamel AJ, Fauth AR, Piazza SJ, Sharkey NA. Dynamic loading of the plantar aponeurosis in walking. *J Bone Joint Surg Am.* 2004;86-A(3):546-552.

24. Wang CL, Cheng CK, Chen CW, Lu CM, Hang YS, Liu TK. Contact areas and pressure distributions in the subtalar joint. *J Biomech.* 1995;28(3):269-279.

25. Bunning PS, Barnett CH. A Comparison of Adult and Foetal Talocalcaneal Articulations. *J Anat.* 1965;99:71-76.

26. Harper MC. The lateral ligamentous support of the subtalar joint. *Foot Ankle.* 1991;11(6):354-358.

27. Stephens MM, Sammarco GJ. The stabilizing role of the lateral ligament complex around the ankle and subtalar joints. *Foot Ankle.* 1992;13(3):130-136.

28. Ward KA, Soames RW. Morphology of the plantar calcaneocuboid ligaments. *Foot Ankle Int.* 1997;18(10):649-653.

29. Cromeens B, Patterson R, Sheedlo H, et al. Association of hindfoot ligament tears and osteochondral lesions. *Foot Ankle Int.* 2011;32(12):1164-1174.

30. Sammarco VJ. The talonavicular and calcaneocuboid joints: anatomy, biomechanics, and clinical management of the transverse tarsal joint. *Foot Ankle Clin.* 2004;9(1):127-145.

31. Hicks JH. The mechanics of the foot. II. The plantar aponeurosis and the arch. *J Anat.* 1954;88(1):25-30.

32. Thordarson DB, Schmotzer H, Chon J, Peters J. Dynamic support of the human longitudinal arch. A biomechanical evaluation. *Clin Orthop Relat Res.* 1995(316):165-172.

33. Headlee DL, Leonard JL, Hart JM, Ingersoll CD, Hertel J. Fatigue of the plantar intrinsic foot muscles increases navicular drop. *J Electromyogr Kinesiol.* 2008;18(3):420-425.

34. Fiolkowski P, Brunt D, Bishop M, Woo R, Horodyski M. Intrinsic pedal musculature support of the medial longitudinal arch: an electromyography study. *J Foot Ankle Surg.* 2003;42(6):327-333.

35. Schappert SM, Rechtsteiner EA. Ambulatory medical care utilization estimates for 2007. *Vital Health Stat 13.* 2011(169):1-38.

36. Waterman BR, Owens BD, Davey S, Zacchilli MA, Belmont PJ, Jr. The epidemiology of ankle sprains in the United States. *J Bone Joint Surg Am.* 2010;92(13):2279-2284.

37. Lambers K, Ootes D, Ring D. Incidence of patients with lower extremity injuries presenting to US emergency departments by anatomic region, disease category, and age. *Clin Orthop Relat Res.* 2012;470(1):284-290.

38. Court-Brown CM, Caesar B. Epidemiology of adult fractures: A review. *Injury.* 2006;37(8):691-697.

39. van Staa TP, Dennison EM, Leufkens HG, Cooper C. Epidemiology of fractures in England and Wales. *Bone.* 2001;29(6):517-522.

40. Osborne MD, Rizzo TD, Jr. Prevention and treatment of ankle sprain in athletes. *Sports Med.* 2003;33(15):1145-1150.

41. Soboroff SH, Pappius EM, Komaroff AL. Benefits, risks, and costs of alternative approaches to the evaluation and treatment of severe ankle sprain. *Clin Orthop Relat Res.* 1984(183):160-168.

42. Bielska IA, Wang X, Lee R, Johnson AP. The health economics of ankle and foot sprains and fractures: A systematic review of English-language published papers. Part 2: The direct and indirect costs of injury. *Foot (Edinb).* 2017.

43. Ogilvie-Harris DJ, Reed SC, Hedman TP. Disruption of the ankle syndesmosis: biomechanical study of the ligamentous restraints. *Arthroscopy.* 1994;10(5):558-560.

44. Clanton TO, Williams BT, Backus JD, et al. Biomechanical Analysis of the Individual Ligament Contributions to Syndesmotic Stability. *Foot Ankle Int.* 2017;38(1):66-75.

45. Lauge-Hansen N. Fractures of the ankle. III. Genetic roentgenologic diagnosis of fractures of the ankle. *Am J Roentgenol Radium Ther Nucl Med.* 1954;71(3):456-471.

46. Lauge-Hansen N. Fractures of the ankle. II. Combined experimental-surgical and experimental-roentgenologic investigations. *Arch Surg.* 1950;60(5):957-985.

47. Taylor B. Orthobullets. https://www.orthobullets.com/trauma/1047/ankle-fractures.

48. Gardner MJ, Demetrakopoulos D, Briggs SM, Helfet DL, Lorich DG. The ability of the Lauge-Hansen classification to predict ligament injury and mechanism in ankle fractures: an MRI study. *J Orthop Trauma.* 2006;20(4):267-272.

49. Mulligan EP. Evaluation and management of ankle syndesmosis injuries. *Phys Ther Sport.* 2011;12(2):57-69.

50. Fites B, Kunes J, Madaleno J, Silvestri P, Johnson DL. Latent syndesmosis injuries in athletes. *Orthopedics.* 2006;29(2):124-127.

51. Miller CD, Shelton WR, Barrett GR, Savoie FH, Dukes AD. Deltoid and syndesmosis ligament injury of the ankle without fracture. *Am J Sports Med.* 1995;23(6):746-750.

52. Karl EL, Wrazidlo W. [Fresh rupture of the syndesmosis of the proximal ankle joint. Clinical significance and arthrographic diagnosis]. *Unfallchirurg.* 1987;90(2):92-96.

53. Frick H. [The isolated tear of the tibio-fibular syndesmosis-mechanism, clinical observations, diagnosis and therapy (author's transl)]. *Unfallheilkunde.* 1978;81(8):542-545.

54. Sman AD, Hiller CE, Rae K, et al. Diagnostic accuracy of clinical tests for ankle syndesmosis injury. *Br J Sports Med.* 2015;49(5):323-329.

55. Nussbaum ED, Hosea TM, Sieler SD, Incremona BR, Kessler DE. Prospective evaluation of syndesmotic ankle sprains without diastasis. *Am J Sports Med.* 2001;29(1):31-35.

56. Cotton FJ. *Dislocations and joint-fractures.* 2d ed. Philadelphia ; London: W.B. Saunders company; 1924.

57. Candal-Couto JJ, Burrow D, Bromage S, Briggs PJ. Instability of the tibio-fibular syndesmosis: have we been pulling in the wrong direction? *Injury.* 2004;35(8):814-818.

58. Scheyerer MJ, Helfet DL, Wirth S, Werner CM. Diagnostics in suspicion of ankle syndesmotic injury. *Am J Orthop (Belle Mead NJ).* 2011;40(4):192-197.

59. Alonso A, Khoury L, Adams R. Clinical tests for ankle syndesmosis injury: reliability and prediction of return to function. *J Orthop Sports Phys Ther.* 1998;27(4):276-284.

60. Milz P, Milz S, Steinborn M, Mittlmeier T, Putz R, Reiser M. Lateral ankle ligaments and tibiofibular syndesmosis. 13-MHz high-frequency sonography and MRI compared in 20 patients. *Acta Orthop Scand.* 1998;69(1):51-55.

61. Mei-Dan O, Kots E, Barchilon V, Massarwe S, Nyska M, Mann G. A dynamic ultrasound examination for the diagnosis of ankle syndesmotic injury in professional athletes: a preliminary study. *Am J Sports Med.* 2009;37(5):1009-1016.

62. Croft S, Furey A, Stone C, Moores C, Wilson R. Radiographic evaluation of the ankle syndesmosis. *Can J Surg.* 2015;58(1):58-62.

63. Mei-Dan O, Carmont M, Laver L, et al. Standardization of the functional syndesmosis widening by dynamic U.S examination. *BMC Sports Sci Med Rehabil.* 2013;5:9.

64. Beumer A, Valstar ER, Garling EH, et al. External rotation stress imaging in syndesmotic injuries of the ankle: comparison of lateral radiography and radiostereometry in a cadaveric model. *Acta Orthop Scand.* 2003;74(2):201-205.

65. Xenos JS, Hopkinson WJ, Mulligan ME, Olson EJ, Popovic NA. The tibiofibular syndesmosis. Evaluation of the ligamentous structures, methods of fixation, and radiographic assessment. *J Bone Joint Surg Am.* 1995;77(6):847-856.

66. LaMothe JM, Baxter JR, Murphy C, Gilbert S, DeSandis B, Drakos MC. Three-Dimensional Analysis of Fibular Motion After Fixation of Syndesmotic Injuries With a Screw or Suture-Button Construct. *Foot Ankle Int.* 2016;37(12):1350-1356.

67. Friedman SM, Mendelson DA. Epidemiology of fragility fractures. *Clin Geriatr Med.* 2014;30(2):175-181.

68. Mow VC, Huiskes R. *Basic orthopaedic biomechanics & mechano-biology.* 3rd ed. Philadelphia, PA: Lippincott Williams & Wilkins; 2005.

69. Bland JM, Altman DG. Statistical methods for assessing agreement between two methods of clinical measurement. *Lancet.* 1986;1(8476):307-310.

70. Bland JM, Altman DG. Comparing methods of measurement: why plotting difference against standard method is misleading. *Lancet.* 1995;346(8982):1085-1087.

71. Bland JM, Altman DG. Measuring agreement in method comparison studies. *Stat Methods Med Res.* 1999;8(2):135-160.

72. Takao M, Ochi M, Naito K, et al. Arthroscopic diagnosis of tibiofibular syndesmosis disruption. *Arthroscopy.* 2001;17(8):836-843.

73. Clanton TO, Whitlow SR, Williams BT, et al. Biomechanical Comparison of 3 Current Ankle Syndesmosis Repair Techniques. *Foot Ankle Int.* 2017;38(2):200-207.

74. Schottel PC, Baxter J, Gilbert S, Garner MR, Lorich DG. Anatomic Ligament Repair Restores Ankle and Syndesmotic Rotational Stability as Much as Syndesmotic Screw Fixation. *J Orthop Trauma.* 2016;30(2):e36-40.

75. Wang C, Yang J, Wang S, et al. Three-dimensional motions of distal syndesmosis during walking. *J Orthop Surg Res.* 2015;10:166.

76. Qamar F, Kadakia A, Venkateswaran B. An anatomical way of treating ankle syndesmotic injuries. *J Foot Ankle Surg.* 2011;50(6):762-765.

77. Lloyd J, Elsayed S, Hariharan K, Tanaka H. Revisiting the concept of talar shift in ankle fractures. *Foot Ankle Int.* 2006;27(10):793-796.

78. Herscovici D, Jr., Anglen JO, Archdeacon M, Cannada L, Scaduto JM. Avoiding complications in the treatment of pronation-external rotation ankle fractures, syndesmotic injuries, and talar neck fractures. *J Bone Joint Surg Am.* 2008;90(4):898-908.